COSMOGENIC NUCLIDE DATING OF OLD, HIGH PLUVIAL SHORELINES IN THE WESTERN GREAT BASIN

Gabrielle Kurth

Submitted in partial fulfillment of a Master of Science Degree in Hydrology
Department of Earth and Environmental Science
New Mexico Institute of Mining and Technology
May, 2003

ABSTRACT

Evidence of the most recent highstand cycle of Lake Lahontan and associated paleolakes persists throughout the western Great Basin and has been studied intensively for over 100 years. In contrast, little is known about the longer-term history of the basin. Many workers agree that lake filling events were somehow related to glacial periods, when amounts of precipitation and stream runoff into lakes were higher. Two competing hypotheses have been put forth to explain the response of the western Great Basin to the forcing of Pleistocene climate changes. One is that there were large basin-filling events during oxygen isotope stages (OIS) 16, 6, and 2 with a long period of aridity after OIS 16. The second is that the basin responded in a predictable manner to global climate cycles by filling during these glacials as well as the other glacial periods in the sequence. This study tests these hypotheses by dating paleoshorelines in the western Great Basin.

Dating ancient shorelines in the western Great Basin allows for a better understanding of both the timing and the magnitudes of lake-filling events. Geomorphic and soil properties suggest that the ages of several shorelines above the latest Pleistocene level increase as a function of elevation. Shoreline deposits at three sites in western Nevada were sampled for cosmogenic nuclide (^{36}Cl) dating to test this apparent increase. Chlorine-36 results from sites near Walker Lake, in Newark

Valley, and around Columbus Salt Marsh in Nevada corroborate the geomorphic and soil evidence. Furthermore, ^{36}Cl results suggest that Lake Lahontan filled to nearly the same level during OIS 2 and 4; the results also suggest large filling events occurred during OIS 6, 8, and possibly 12 or 16. From these results, we can conclude that the Lahontan Basin filled more frequently and to higher levels than previously thought and that preserved shorelines show an apparent decrease in maximum lake levels with time.

ACKNOWLEDGEMENTS

I have enjoyed working with Fred Phillips and I appreciate his support over the course of this project. His knowledge and enthusiasm for this research has greatly benefited the outcome of this work. I also appreciate the help I received from Marith Reheis; her patient explanations of arid-region soils and geomorphology were invaluable to me. Both Fred and Marith made the fieldwork for this project enjoyable and a wonderful learning experience. Joanna Redwine's knowledge of Newark Valley geology was an invaluable help to me, as were the geologic maps that she constructed. Finally, I wish to thank the members of my committee, Eric Small and Bruce Harrison, for their helpful suggestions on earlier drafts of this thesis. Financial support for this project came from National Science Foundation grant EAR-0001063.

TABLE OF CONTENTS

LIST OF TABLES

LIST OF FIGURES

This thesis is accepted on behalf of the
Faculty of the Institute by the following committee:

Advisor

Andrew Caplis for Peter Mosley

5 May 03
Date

I release this document to the New Mexico Institute of Mining and Technology.

Student's Signature

5 May 2003
Date

1. Introduction

1.1 Location and description

The Great Basin is an internally drained expanse that covers most of Nevada and western Utah with edges reaching into California, Idaho, and Oregon. With an area of over 500,00 km^2, it makes up the largest part of the Basin and Range physiographic province, a province characterized by fault-block horsts and grabens. It is bounded by the Sierra Nevada to the west and the Wasatch Mountains to the east. The Snake River Plain and part of the Columbia Plateau mark the northern border while the 35^{th} parallel north roughly defines the southern border.

The Great Basin consists of over 160 primarily north-south-trending mountain ranges, which separate over 150 intermontane basins. Some of these features are visible in Figure 1.1. This horst-and-graben setting formed due to intraplate extensional tectonics beginning in mid-Miocene time. High heat flow, a thin crust, and normal faults trending primarily NNE characterize the structural geology of the region. Topographically, the Great Basin is highest in the center and lower around its boundaries. More specifically, it is highest in northeast and east-central Nevada, where basin floor altitudes range between 1,150 m to about 1,400 m. The southern and southeastern reaches of the basin have the lowest basin floors, with altitudes about 600 m and lower.

Lacustrine geomorphic features are present throughout the western Great Basin. Many of these features have been studied for over 100 years (Russell, 1885) and a number of studies have addressed the climate changes necessary to create lakes in this region (Russell, 1885; Hubbs, 1948; Reheis, 1999). At their maximum extent, about 120 pluvial lakes were present in the Great Basin. The largest of these were Lake Bonneville in Utah and Lake Lahontan (Figure 1.1) in western Nevada. Remnants of these and other Great Basin lakes have been studied to answer questions regarding the region's response to climate changes. The lacustrine chronology of Lake Lahontan and two nearby lakes, Newark (Newark Valley) and Columbus (Columbus Salt Marsh) (shown in Figures 1.1 and 1.2), in the western Great Basin are the focuses this thesis with the major goals of: (1) determining the chronology and magnitudes of lake-filling events and (2) understanding their relationship to Pleistocene climate changes.

1.2 Previous studies

Although the Great Basin climate is principally semiarid to arid today, evidence of large Pleistocene lakes (spits, bars, terraces, and wave-cut cliffs) persists throughout the region in almost all the closed or formerly closed basins. Russell (1885) was one of the first to notice and document this evidence in the western Great Basin. In his work, he integrated stratigraphy, geomorphology, water chemistry, and tufa morphology. He differentiated between normal lakes, or those that overflow, and enclosed lakes, or those that do not have an outlet. He noted that normal lakes are found in humid regions whereas closed lakes develop in arid regions and are sensitive

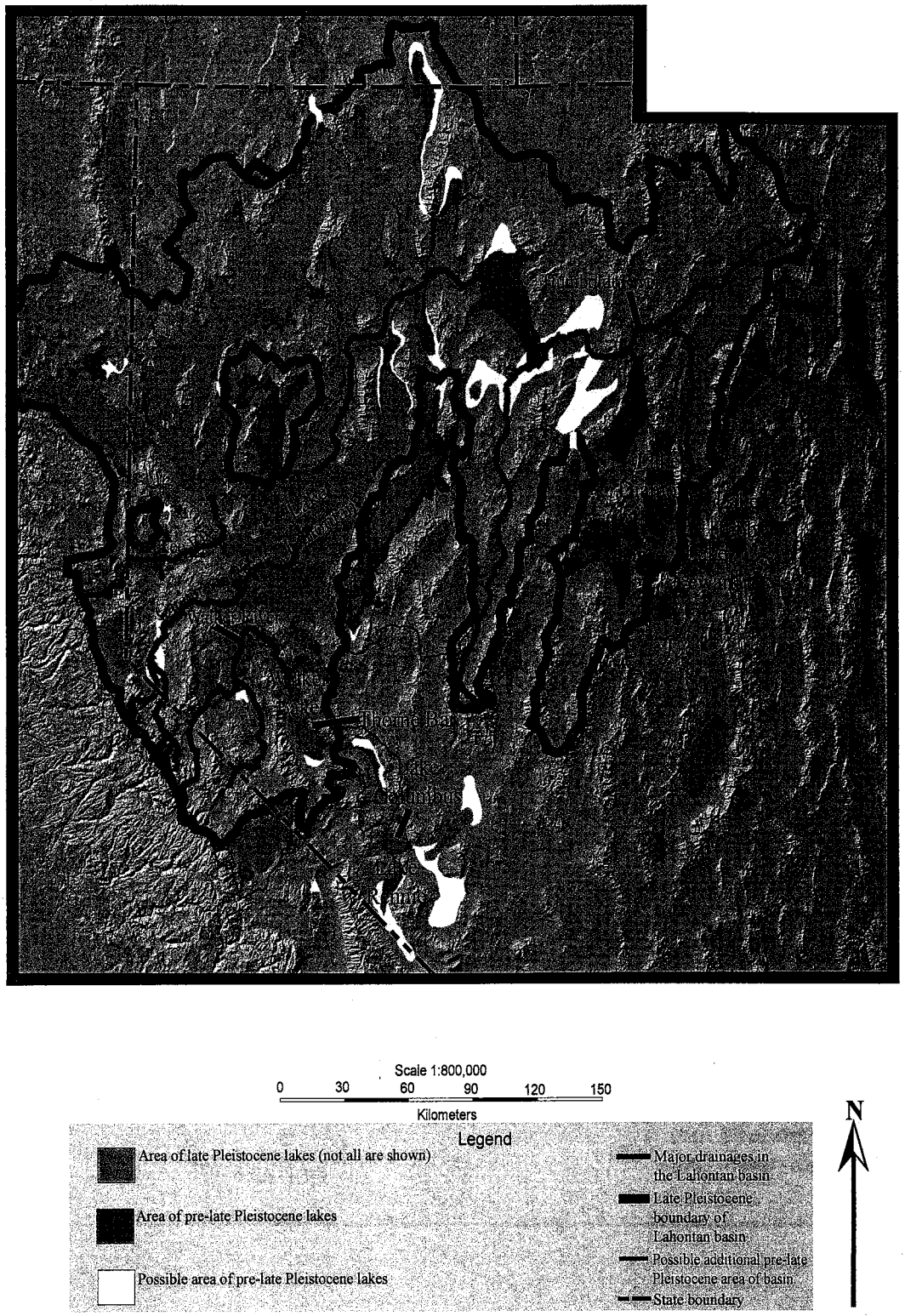

Figure 1.1. Locations of Pleistocene lakes in the western Great Basin with study sites indicated. Modified from Reheis, 1999b.

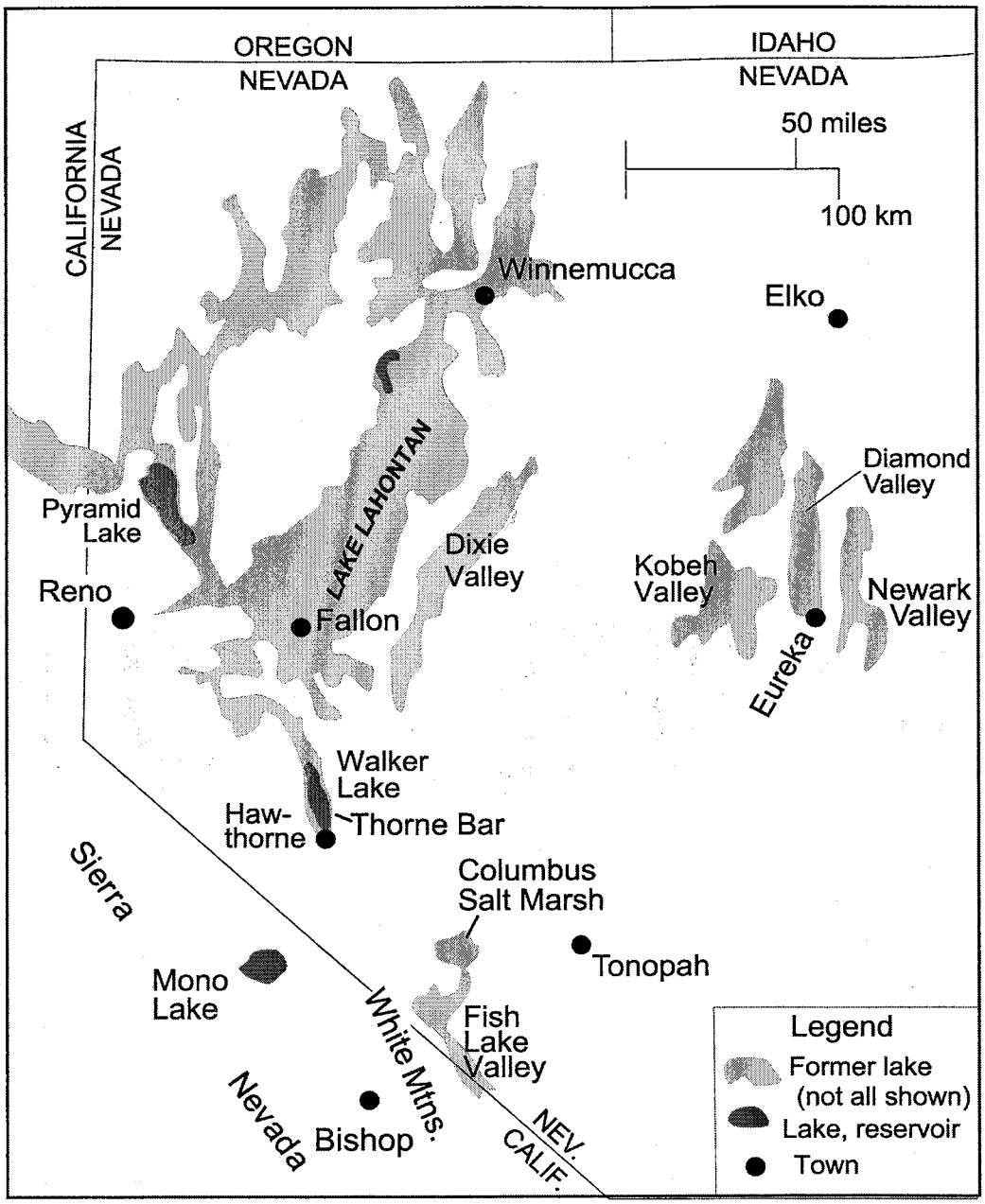

Figure 1.2. Location map of some pluvial lakes in the western Great Basin with the study sites indicated. Modified from Reheis et al. (*in press*).

to climate change. Under large amounts of precipitation, closed lakes may overflow, but Russell concluded that because most Great Basin lakes did not overflow, Pleistocene precipitation was probably not excessive. Russell also made what may be the first estimate of pluvial climate conditions. He stated that if temperature conditions were similar to today's conditions, the mean annual precipitation would have to increase by about 20 inches (~51 cm) to form lakes at the observed levels.

In addition to his observations about the types of lakes and probable pluvial climate conditions, Russell (1885) also studied the lacustrine sediments of the western Great Basin. He completed extensive mapping work of Lake Lahontan and identified several lacustrine deposits. He also determined that the lake did not have an outlet. In his monograph, he noted a "lower lacustral clay" and an "upper lacustral clay" separated by a "medial" gravel. This evidence he interpreted as representing two deep lake periods separated by long period of low water or complete desiccation. He also concluded that during the second inundation, the lake rose 30 ft higher than its first maximum and remained at this second highstand for a comparatively brief period of time.

Russell (1885) stated that prior to these two lake cycles, the Lahontan Basin was dry for a long period of time. He based this conclusion on the presence of large alluvial cones in many of the basins, onto which some of the lacustrine features were constructed. He believed that the large quantities of alluvial material would have had to be developed over a long period of time, which suggested that the basin had been principally arid before the two deep-lake cycles. There may have been fluctuations in relative amounts of precipitation and evaporation but, when lakes formed, they

remained at relatively low levels. He determined that the thick deposits of lacustrine marls, clays, and gravels suggested that lakes existed in the Lahontan Basin at least during intervals throughout the Quaternary but reached only low levels.

Hubbs and Miller (1948) related Great Basin Pleistocene fish distributions to the history of lakes in the region. They examined known physiographic evidence of pluvial lake connections and found additional, previously undocumented evidence as well. They also established ichthyologic evidence to support or refute pluvial connections. Their work included a map of the pluvial lakes known at that time in the western Great Basin.

In their work, Hubbs and Miller (1948) addressed the timing of lake cycles in Great Basin. They believed that lake connections probably developed a number of times during the last three millennia. The zoogeographical evidence does not suggest a specific time of the most recent pluvial. Some speciation occurred locally during the post-pluvial period but there was not enough data to suggest a rate of species evolution. Their evidence is in agreement with the most recent pluvial period ending in the late Pleistocene but does not refute a more recent pluvial time.

Broecker and Orr (1958) used radiocarbon measurements on lake-deposited carbonates to estimate ages of paleolake levels in the Lahontan basin. They determined that Lake Lahontan filled during the Wisconsin Glaciation and they established a chronology of lake fluctuations during Wisconsinan time. They found that there was a period of low water from 25 ka to at least 34 ka. This was followed by a period of high water from 25 ka to 14 ka and a water recession to low levels around 13 ka.

Morrison (1964) published an extensive report focusing on the palaeosols, lacustrine stratigraphy, and stratigraphic correlations of the Lahontan basin. In particular, he described the geology of the southern part of the Carson Desert, near Fallon, Nevada, concentrating on late Quaternary deposits, especially those related to Lake Lahontan. He identified and characterized stratigraphic units associated with the lake. Morrison's results are discussed in Section 2. In his work, he proposed that Lake Lahontan filled during the lat-middle Pleistocene and underwent a long period of aridity until the late Pleistocene, when two major lake cycles were recorded (Morrison, 1991).

Mifflin and Wheat (1979) studied pluvial lakes and pluvial climate conditions in Nevada. They recognized that most researchers agree that pluvial conditions had to have been "wetter" and "cooler" in order to form the substantial wave-cut terraces still visible today. In addition, they found that quantitative estimates of pluvial climatic conditions are possible in hydrographically closed basins in arid regions. To make these estimates, the authors defined a "Pluvial Hydrologic Index" (Z), which relates lake area to basin area and is a measure of hydrologic response to climate change. A hydrologic budget approach using Z assumes that a closed basin lake is in equilibrium, or that the amount of water entering the lake equals the amount leaving.

In their study, Mifflin and Wheat (1979) combined empirical climatic measurements, shoreline morphometric statistics, and Z to make estimates of pluvial climatic conditions. They concluded that effective precipitation during the last glacial maximum (LGM) was about ten times greater than present-day values with precipitation itself being about 68 percent greater than modern values. In order to

produce the observed climate changes, they determined that a drop in mean annual temperature of 5°F (~15°C) was needed. They also noted evidence against significantly lower pluvial temperatures: the absence of ice features at high shoreline elevations, the presence of tufa at high Lahontan levels, and the existence of indigenous fish in Pyramid Lake that are well adapted to present-day water temperatures. Based on these observations, they suggested that, in order to create observed hydrologic indices, there must have been significantly more moisture input during glacial periods.

In addition to their work on pluvial climates, Mifflin and Wheat (1979) also noted the presence of shorelines higher than those thought to be related to the LGM. They stated that Lake Lahontan might have overflowed to the south during one or more pre-LGM pluvials. Specifically, they recognized well-sorted and rounded lacustrine gravels to at least 1366 m (4480 ft) MSL in the Walker Lake basin (Figures 1.1 and 1.2). They attributed this evidence of very high lake levels to regional downwarping of the Lahontan Basin to the north and northeast during and since the LGM, which they believed to be sufficient to raise the gravels to this level.

In the late 1990's, Marith Reheis identified abundant geomorphic and stratigraphic evidence for lakes much older and higher than several sites of late Pleistocene lakes throughout the Lahontan Basin, including the Walker Lake basin (Reheis and Morrison, 1997; Reheis, 1999; Reheis et al., 2003). Evidence of highstands well above previously studied highstands includes: (1) lacustrine and deltaic deposits grading into beach gravel, (2) ancient V-bars and arcuate shoreline berms, and (3) rounded beach gravels on bedrock benches. Specific lakes where this

type of evidence was identified include: Lahontan, Columbus, Rennie (Fish Lake Valley), Jonathan (Kobeh Valley), Diamond, Newark, Hubbs (Long Valley), and Clover (Figure 1.1). Reheis correlated certain very high lake levels in these basins to Lake Lahontan's Rye Patch Alloformation (~700,000-600,000 ka), which Morrison (1991) assigned to oxygen isotope stage (OIS) (Shackleton and Opdyke, 1976) 16.

Although older, higher shorelines in the Lahontan Basin have been attributed to local tectonic movements (King, 1978) or to northward tilting of the basin (Mifflin and Wheat, 1979), the recently discovered shorelines cannot be explained in this manner. These shorelines are in unfaulted, undeformed localities (Reheis and Morrison, 1997). Furthermore, old, high shorelines have been found in numerous basins throughout the western Great Basin, which suggests that they are not simply rare occurrences of displaced shorelines (Reheis and Morrison, 1997).

Reheis (1997) concluded that these very high levels show that early to middle Pleistocene lakes filled to higher levels and were areally much larger than late Pleistocene events. She stated that the western Great Basin may have responded to more cooling periods than previously thought. The descending bathtub-ring nature of western Great Basin shorelines suggests that lakes filled to increasingly lower levels from the early middle to late Pleistocene, which may imply that pluvials became generally drier with time, the possible causes of which are discussed below.

1.3 Causes of progressively drier lake-filling cycles during the middle to late Pleistocene

According to the evidence presented in Reheis et al. (2003), the shoreline sequences of Lake Lahontan appear to decrease in elevation with decreasing age.

This apparent pattern may be the result of (1) random lake-level fluctuations or (2) pluvial periods becoming drier from the middle to late Pleistocene. If the shorelines are the result of random fluctuations, then there may have been lake cycles that obliterated some, but not all, of the previously constructed shorelines. The preserved shorelines may then decrease in age with decreasing elevation, but evidence of highstands that did not follow this pattern may have been erased by more recent lake cycles. If the apparent pattern is the result of western Great Basin pluvial periods becoming drier, then reasons for this apparent decrease in moisture are complex combinations of factors that include: climate, tectonics, and drainage changes. The relative importance of each of these factors is difficult to distinguish (Thompson et al., 1993), however, and has probably changed with time (Reheis et al., 2003).

One climate mechanism that could lead to a progressive drying of pluvial cycles in the western Great Basin is a change in the position of the jet stream caused by changes in the configuration of the Laurentide ice sheet (Benson and Thompson, 1987). Global circulation models suggest that this would strongly affect temperatures and precipitation amounts in the western United States. The ice sheet causes the jet stream to split and its two branches and their associated storm tracks can account for lake fluctuations in the Basin and Range during pluvial periods. The ice sheet position helps explain the precipitation changes during pluvial periods, but since configurations of older ice sheets are not well known, it is difficult to estimate the effects of this factor with confidence.

The second factor that may have affected moisture amounts in the western Great Basin is tectonic activity, specifically uplift of the Sierra Nevada and

Transverse and Cascade Ranges since the late Pliocene. These mountain ranges have produced an increasingly larger rain shadow over time. There are disagreements in the literature regarding the timing of Sierra Nevadan uplift (e.g., Winograd et al., 1985; Small and Anderson, 1995) but these can be resolved somewhat by Small and Anderson's (1995) model of geomorphic, rather than tectonic, uplift of the Sierra Nevada during the Pleistocene. This relative uplift does not explain the very high lake levels correlated to the middle Pleistocene (OIS 16), but it does help explain a progressive drying of the western Great Basin.

A third factor that probably influenced the progressive drying of pluvial periods in the western Great Basin is drainage changes between basins. Some lake basins that are presently part of the Lahontan basin were isolated at times during the Pleistocene. For example, the lake in Kobeh Valley (Lake Jonathan) was internally drained until after 670 ka. Lakes Jonathan and Diamond probably became integrated with each other and with the Humboldt River during a very high spillover of Lake Jonathan sometime after 670 ka (Reheis et al., 2003). Drainage changes such as these affect basin lake levels and help explain the changing lake levels of Lahontan from the middle to late Pleistocene.

Clearly, a complex interaction of factors related to climate, tectonics, and drainage changes controlled lake levels in the western Great Basin from the middle to late Pleistocene. It is difficult to distinguish the relative importance of these factors because their relative influences probably changed with time. The sequence of older and higher shorelines may suggest a progressive drying of pluvial cycles from the middle to late Pleistocene. This pattern may also result from random lake

fluctuations and it is not possible to determine whether the apparent drying trend is real or the result of lake cycle stochastics.

1.4 Pluvial record of Lake Lahontan vs. Lake Bonneville

If Lake Lahontan did fill to progressively lower levels with time from the middle to the late Pleistocene, as the shoreline record may suggest, then its longer-term history contrasts markedly with that of its contemporary large pluvial lake in the Great Basin, Lake Bonneville. Lake Bonneville covered about 51,640 km^2 at its highest level and was the largest pluvial lake in the Western Hemisphere. At its highest level, it covered much of northwestern Utah and extended into Nevada and Idaho. Today, Lake Bonneville's remnants exist as the Great Salt and Utah Lakes.

The history of Lake Bonneville is somewhat controversial for a number of reasons. The stratigraphic record is ambiguous and disjunctive and there are inconsistencies in the use of some stratigraphic names (Morrison, 1991). Also, there are relatively few good exposures of lake sediments and few dated tephra layers within them. Erosion due to strong wave action during lake transgressions and from valley-cutting streams has led to large unconformities at some important sites. Finally, good stratotypes with adequate type localities were not defined for many significant stratigraphic units. These factors have given rise to workers using stratigraphic names differently at different sites, leading to conflicting interpretations of Lake Bonneville's history (Morrison, 1991).

Most research on Lake Bonneville has focused on its LGM, or Bonneville, highstand. This was the last and largest highstand and also the only one known to have overflowed. The early and middle Pleistocene history of the basin has been

studied to some extent but in part due to the reasons mentioned above, relatively little is known about older lake cycles (Oviatt and Currey, 1987). Evidence from the 307-m long Burmester core from the South shore of the Great Salt Lake suggests that four large, freshwater lakes formed during the Brunhes Chron (the last 780 x 10^3 yr) (Oviatt et al., 1999). These deep lake cycles appear correlative with marine oxygen isotope stages 2, 6, 12, and 16 (Oviatt et al., 1999). If the Lahontan shorelines reflect a pattern of progressive drying, then this record would suggest that pluvial climates became drier with time in the western Great Basin. This would contrast sharply with the Bonneville record, which shows a number of recent deep-lake cycles as well as a very high magnitude LGM filling event. Due to the lack of dateable material from the Lahontan basin, it has been difficult to adequately compare the two records.

1.5 Purpose of research

There is abundant geomorphic evidence of the most recent lake cycle in the Lahontan Basin. This evidence exists in the forms of shoreline terraces and beach berms and has helped make it the focus of geological research for over 100 years (Russell, 1885). In comparison, relatively little is known about prior lake cycles in the basin. In recent years, older and higher shorelines than the most recent cycle have been discovered. Some of their ages can be chronologically constrained through correlation with ash beds, but age control in this manner is not possible for all of them.

Two hypotheses have been put forward to explain the response of the western Great Basin to Pleistocene global climate changes. The first is that Lake Lahontan filled to at least the level of the LGM in the middle Pleistocene Epoch (OIS 16); this

period was followed by a long episode of aridity until OIS 6 and 2 (Morrison, 1991). This hypothesis is often regarded as the classical interpretation of the evidence of lake cycles in the Lahontan Basin. Under this interpretation, the recently discovered shorelines may be recessional features from the OIS 16 highstand. The second hypothesis that may explain the cycles of Lake Lahontan states that the highstands also occurred during glacial stages between 16 and 2, possibly in connection with 100 kyr glacial cycles. This explanation is in agreement with the idea that the western Great Basin responded in a predictable manner to the forcing of global climatic cycles. If true, it would suggest an apparent pattern of Lake Lahontan decreasing in size with younger lakes. This could suggest a regional climatic trend of drier lake cycles over time. This thesis addresses these questions and the main goals are to:

(1) Date shorelines from three sites in the Lahontan Basin using cosmogenic nuclides.

(2) Use the shoreline ages to study the relationship between the timing of lake filling events and the Pleistocene global climate record.

(3) Answer the questions posed by the two competing hypotheses regarding the response of the western Great Basin to the forcing of global climate changes and address the paleoclimate implications of the shoreline ages.

2 Physiographic setting

2.1 Introduction

Three sites of older, higher shorelines in the western Great Basin are the focus of this thesis (Figures 1.1 and 1.2). Each site is in a different subbasin of the Lahontan basin but there is evidence that all were connected to the Lahontan system at some time during the Quaternary. Due to difficulties in age control, the question of when these connections were active is not resolved. The first site is the Thorne Bar, the second is Newark Valley, and the third is Columbus Salt Marsh. This section describes the physiography of these sites and the current knowledge of their pluvial histories.

2.2 Pluvial Lake Lahontan

Lake Lahontan was the second-largest pluvial lake in the Western Hemisphere several times during the Pleistocene Epoch (Figures 1.1 and 1.2). King (1878) published the first map of Lake Lahontan's late Pleistocene extent and named the lake for Baron LaHontan, an early explorer. The Lahontan basin is a closed system that has neither overflowed in the last 600,000 years, nor experienced any sudden diversions of inflow (Morrison, 1991). It is composed of seven subbasins separated by sills of different altitudes. Connections between these subbasins depended to some extent on the threshold levels between them. As a result, some of these

subbasins have independent lacustrine histories for times during the Quaternary when lake levels were below certain thresholds (Morrison, 1991). The Lahontan drainage basin is large and covers about 115,000 km^2 in the northwestern part of the Great Basin. At its highest level during the LGM (13,000 years ago), its area was about 22,300 km^2, its volume 2,020 km^3, and its maximum depth 276 m (Benson and Thompson, 1987).

In this thesis, the name Lake Lahontan refers to both the lake's areal extent and to the lacustrine deposits in a stratigraphic sense. The areal extent is the area encompassed by the lake's highest strandline, which encloses a number of intermontane basins. Under the stratigraphic definition, the name refers to all the Quaternary lake cycles that occurred within this strandline.

Four principal rivers fed into the Lahontan basin (Figure 1.1): Carson River, Walker River, Humboldt River, and the Truckee River. The Carson River followed the same course that it does today, flowing from the Sierra Nevada into the Carson Sink. The Walker River also begins in the Sierra Nevada and flowed via Adrian Valley into the Carson River during the middle and late Quaternary but today flows into Walker Lake (King, 1993). The Humboldt River heads in northeastern Nevada and terminates in the Carson sink, although it also terminated in the Black Rock Desert many times during the Quaternary (Morrison, 1991). The Truckee River drains Lake Tahoe and terminates in Pyramid Lake but flowed at least at one time into the Carson Desert.

Complicating studies of Lake Lahontan stratigraphy and history is Quaternary tectonic activity throughout the area. The region has been subject to local faulting

and warping as well as isostatic depression and rebound due to lake filling and draining (Adams et al., 1999). These factors can make stratigraphic correlations between some areas of the basin difficult because they can change the elevations of lacustrine deposits.

2.3 Lake Lahontan stratigraphic record

The stratigraphic record of Lake Lahontan has been used to make interpretations regarding the lacustrine history of the basin and pluvial climates. As a terminal-lake basin record, it is sensitive to climate changes and is complete enough to allow for relatively good age control of a number of lake cycles. The Lahontan record owes its completeness to the following: (1) it was a closed basin so no sediment was carried out of the basin by rivers, (2) it was fed by streamflow, not catastrophic overflows from other basins, and (3) the arid climate is favorable for preserving exposures in bluffs and badlands (Morrison, 1991).

Most of the work on the Lake Lahontan lacustrine chronology has relied on radiocarbon dates. The ages listed below have been converted to years before present using the program, CALIB, that is written and distributed by the Quaternary Isotope Lab, University of Washington (Stuiver and Reimer, 1993 (version 4.1)). Ages equal to or greater than about 21 ka were beyond the calibration of this program and were not converted.

Much research has been done on the stratigraphy of Lake Lahontan, beginning with Russell (1885). Russell (1885) identified the Upper and Lower Lacustral Clays, which he interpreted to represent two deep-lake episodes. This work was not greatly elaborated on until Morrison (1964) mapped and described the Quaternary deposits

near Fallon, Nevada. In this work, he assigned formal stratigraphic names to both the lacustrine and terrestrial deposits. Sections of the stratigraphic record that record one or more deep lake cycles (lacustrals) are known as alloformations (AFs) (Morrison, 1964). Separating these lacustrals are interlacustral formations that represent long periods of dryness or very low water levels.

Morrison (1965, 1991) concluded that exposures in the basin reveal five major deep-lake cycles, four of which occurred during the last one million years. The four lake cycles within the last 1 Ma are: the lowermost (unnamed) unit, the Rye Patch AF, the Eetza AF, and the Sehoo AF.

The lowermost (unnamed) deposits are possibly lacustrine or deltaic deposits found in the Humboldt River Valley below Rye Patch Dam (Morrison, 1964). They have received relatively little stratigraphic or sedimentologic study but radiocarbon dates on snail shells from this unit are suggestive of a middle Pleistocene age (Morrison and Frye, 1965).

The Rye Patch AF records a major middle Pleistocene lacustral period with two main lake cycles (Morrison and Frye, 1965). Morrison (1991) identified tephra layers within each cycle: the ~630 ka Rye Patch tephra in the lower member and the 620 ka Lava Creek B tephra in the upper member. Based on this tephrochronological evidence, he correlated the Rye Patch AF with OIS 16. The Rye Patch AF underlies the subaerial (interlacustral) Paiute Formation.

Overlying the Paiute Formation is the Eetza AF, which was deposited by the first of two major highstands of Lake Lahontan. This lacustral was Lahontan's longest in duration and the formation comprises the thickest of its deposits (Morrison,

1991). The Eetza AF is equivalent to Russell's Lower Lacustral Clay. Morrison (1964) interpreted the deposits to represent three major lake cycles and at least three minor ones. At the time of these early studies, absolute chronology of the Eetza AF was difficult to determine because the age is beyond the range of radiocarbon dating. Based on radiocarbon dates indicating that the lake cycle occurred more than 35,000 ^{14}C yr B. P., Morrison and Frye (1965) concluded that the lake cycle occurred between about 75,000 and 35,000 ^{14}C yr B. P. This age was subsequently revised, and in his 1991 paper, Morrison chronologically constrained the age of the Eetza AF based on the presence of the Wadsworth tephra layer (~150-200 ka) and uranium-thorium dates on snail shells of ages between ~300 and 100 ka. Therefore, the early conclusions of Morrison and Frye (1965) are consistent with a large lake during OIS 4, but it was later determined that this large lake occurred during OIS 6. An alternative possibility, that there were large lake cycles during OIS 2, 4 and 6, has not been proposed in the literature, most likely because the majority of workers agreed that there were only two major lake cycles during the late-middle to late Pleistocene.

After the lake cycle associated with the Eetza AF, the Wyemaha Formation was deposited, onto which the Churchill Soil developed. The Wyemaha Formation is made up of eolian sand, alluvial sand, gravel, and shallow lake sediments. The Churchill Soil developed on top of the Wyemaha Formation before the second deep-lake cycle of Lake Lahontan. Broecker and Kaufman (1965) published dates based on radiocarbon data from the Wyemaha Formation of about 27,500 and 33,500 ^{14}C yr B. P. Based on the stratigraphic relationships and the available radiocarbon dates of Broecker and others (Broecker and Orr, 1958; Broecker and Kaufman, 1965),

Morrison and Frye (1965) concluded that this period between the two major lake cycles occurred between about 25,000 and 30,000 ^{14}C yr B. P.

Davis (1978) used a suite of radiocarbon dates on noncarbonate material as well as the radiocarbon data of Broecker and others (Broecker and Orr, 1958; Broecker and Kaufman, 1965) to revise this interpretation and show that the second deep-lake cycle began about 35,000 ^{14}C yr B. P, and therefore that the interlacustral period of the Churchill Soil ended about 35,000 ^{14}C yr B. P. Davis (1978) also noted that some of the Wyemaha Formation, as mapped by Morrison (1964) might, in fact, be within clay of the second deep-lake cycle. Morrison (1991) is in general agreement with this chronology, as he stated that the Wyemaha Formation and the Churchill Soil were formed between about 130 and 35 ka. In addition, Morrison (1991) noted that the Saint Helens G tephra layer (35 ka) marks the boundary between deposition of the Wyemaha Formation and the second deep-lake cycle.

The Sehoo AF records the second deep-lake period of Lake Lahontan, the equivalent to Russell's Upper Lacustral Clay. The lake cycle associated with the Sehoo AF is thought to have been the last major lake cycle in the western Great Basin. Within the Sehoo AF, three members are recognized: the Lower Member, the Dendritic Member, and the Upper Member (Morrison, 1991). Between the lake cycles represented by these members, Lake Lahontan dried to all or near completion but these recessional periods are evidenced by minimal soil horizonation (Davis, 1978). The subaerial deposits of these recessional periods are called the Indian Lakes Formation (Morrison, 1964). The chronology of the highstands within the Sehoo AF has been subject to debate in the literature.

Broecker and Kaufman (1965), used radiocarbon data to determine that the maximum lake highstands within this period occurred at about 12,000 and 9,500 ^{14}C yr B. P. (~14 and 10 ka). Morrison and Frye (1965) refuted this work by stating that some of the stratigraphy was incorrect, and that the highest highstand occurred about 18,000 ^{14}C yr B. P. (~21 ka) Davis (1978) grouped the Lower Member and Dendritic Member of the Sehoo AF together and determined that they formed between 11,500 (~13.5 ka) and 35,000 ^{14}C yr B. P. He agreed with Morrison (1964) that the time of Sehoo AF deposition ended about 8,000 ^{14}C yr B. P. (~8.8 ka) (Davis, 1978). Davis (1983) also concluded that a major highstand occurred soon after deposition of the Trego Hot Springs Tephra about 23,400 years ago.

Thompson and others (1986) produced a revised chronology for this late Pleistocene cycle. They relied on tephrochronological information and radiocarbon dates on tufa, gastropods, non-tufa carbonates, and wood from deltaic sediments. They focused on the time period from ~24,000 to 8,000 ^{14}C yr B. P. and found that the highest lake highstand of the Sehoo lacustral occurred between 21,000 and 16,000 (~19 ka) ^{14}C yr B. P.

Morrison (1991) then presented a revised chronology based on his work and that of others (e.g., Morrison and Davis, 1984; Benson and Thompson, 1987) for the members of the Sehoo AF: the Lower Member from 35 to 18.5 ka, the Dendritic Member from 17 to 11.5 ka, and the Upper Member from 9 to 8 ka. He stated that the maximum lake level was reached around 15 ka (Morrison, 1991).

3 STUDY SITES

Three sites of older, higher shorelines were selected for cosmogenic nuclide dating. The sites were chosen based on the presence of well-preserved lacustrine features that had not been deformed by tectonic activity.

The first site is the Thorne Bar, a shoreline complex located southeast of Walker Lake in western Nevada near the town of Hawthorne (Figures 1.1 and 1.2). The Walker River feeds into Walker Lake from the north and the basin is bounded by the Wassuck Mountains to the west and the Gillis range to the east. Like other basins in the Basin and Range province, the Walker Lake basin trends primarily north-south and there are a number of active normal and strike-slip faults within the basin. At Lake Lahontan's highest levels (>1308 m), the Walker Lake basin was part of the Lahontan system and the basin contains evidence of pre-late Pleistocene lake highstands as well. The pluvial connection of the Walker Basin to Lake Lahontan was to the north by way of the now-dry Adrian Valley (King, 1993).

The Thorne Bar site was selected for this study because it contains a suite of old, high shorelines that are essentially undeformed (Demsey, 1987). There are a number of shorelines preserved at the Sehoo level (~1335 m) and above to about 1400 m.

The second site is Newark Valley, which is a north-south trending basin in east-central Nevada that contained Lake Newark during pluvial periods of the Quaternary (Figures 1.1 and 1.2). With an area of about 1000 km^2, Newark Valley is a relatively small basin and has not been studied in detail until recently. Previous studies have consisted primarily of topographic map interpretation (Russell, 1885; Hubbs and Miller, 1948; Mifflin and Wheat, 1979; Reheis, 1999; and Redwine *in progress*). Like the Thorne Bar features, the Newark Valley shorelines studied for this work show a relatively high degree of preservation and no signs of tectonic deformation.

The third site is of old, high shorelines Columbus Salt Marsh, located south of Walker Lake (Figures 1.1 and 1.2). The basin contained Lake Columbus during pluvial periods of the Quaternary. Lake Columbus was probably connected to lakes in nearby Soda Springs Valley, Rhodes Salt Marsh, and Fish Lake Valley; it was also possibly connected to the Walker Lake basin (Reheis and Morrison, 1997).

4 COSMOGENIC NUCLIDE DATING OF DEPOSITIONAL FEATURES

4.1 Introduction

Quaternary geologists in the western Great Basin have understood the value of studying paleolake shorelines to help unravel the lacustrine history of the region. Radiocarbon dating on noncarbonate and lacustrine carbonate materials has been used since the 1950s in the attempt to establish a chronology for the most recent lake cycle but these attempts have been hindered both by contamination problems and by the lack of suitable material (e.g., Broecker, 1958; Thompson et al., 1986). Surface exposure dating techniques have been established as a relatively new tool for understanding exposure ages of geomorphic surfaces. These methods are based on the buildup of terrestrial cosmogenic nuclides (TCN) within terrestrial material. Nuclear reactions between cosmic ray particles and geologic material produce TCN. TCN (e.g., ^{36}Cl, ^{10}Be, ^{26}Al, ^{3}He, and ^{14}C) then accumulate in geologic materials at and near the surface of the earth at a rate dictated by the composition of the material and the local cosmic-ray flux. They are commonly applied in Quaternary studies in order to determine how long a particular surface has been in place.

TCN have been studied for decades, but only in the last two decades (Phillips et al., 1986) has it become feasible to use them in a widespread manner. The advent

of accelerator mass spectrometry (AMS) in the 1980s (Elmore and Phillips, 1987) made it possible to detect low levels of a number of different radioisotopes, and thus the use of cosmogenic nuclide dating has become more widespread. Some of the first applications for TCN were the dating of lava flows and boulders on glacial moraines, two features usually assumed to not have been exposed to cosmic radiation before deposition as the feature of interest (e.g., Phillips et al., 1990). The use of these materials helped validate the technique because it was often possible to also date them with other, more established techniques.

The accumulation of TCN is proportional to the cosmic ray flux intensity, the abundance of target nuclides within the geologic material (Zreda, 1994). The intensity of the cosmic ray flux varies both spatially and temporally (Lal, 1991; Cerling and Craig, 1994). The flux is greatest directly overhead, where the thickness of the atmosphere that the rays must pass through is the minimum. The flux decreases toward the horizon, as the atmospheric depth increases. The flux varies temporally based on factors including: variations in primary cosmic radiation intensity, changes in the interplanetary magnetic field, and changes in the geomagnetic field.

Depositional features are often difficult to date because they are composed of materials that traveled from many different sources before being placed on the feature of interest. Traditional radiometric methods reveal the age of rock, not the landform it is part of, and therefore do not provide an age of the landforms. Measuring cosmogenic nuclide accumulation within a rock, however, allows one to determine how long it has been sitting at or near the surface. This assumes that the rock has no

prior exposure to cosmic rays before being placed on the surface of interest. If there is a TCN concentration from prior exposures, or inheritance, then the amount of inheritance must be determined and subtracted. This section addresses cosmogenic nuclide buildup in terrestrial material and the technique used to date shorelines for this work.

4.2 Cosmogenic ^{36}Cl production at and near the Earth's surface

The two main factors that control the intensity of cosmic radiation on the earth's surface are the earth's magnetic field and interactions with atmospheric nuclei. The result of these two factors combined is that the greatest cosmic-ray intensity is found at high geomagnetic latitudes and at high altitudes (Gosse and Phillips, 2001). While passing through the atmosphere, many cosmic rays interact with the nuclei of atmospheric gases and are attenuated before they hit the earth (Cerling and Craig, 1994). The cosmic rays that reach the surface of the earth interact with the nuclei of minerals at and near the surface. These interactions produce TCN within the rock material. Three main reactions between the cosmic ray and the target nuclide produce TCN: high-energy nucleon-induced spallation reactions, low energy neutron capture reactions, and muon-induced reactions (Gosse and Phillips, 2001).

Spallation reactions require high-energy (between 1 and 30 MeV) nucleons and produce daughter nuclides with smaller mass numbers (A, sum of neutrons (N) plus protons (Z)) than the target nuclide (Cerling and Craig, 1994). In these reactions, a neutron collides with a target nucleus and breaks particles from that nucleus, leaving it lighter than it was before the collision. The attenuation length controls the concentration of spallogenic cosmogenic nuclides with depth and the flux

is attenuated exponentially with mass depth (g cm^{-2}) (Cerling and Craig, 1994; Gosse and Phillips, 2001). The rate of interaction for the production of ^{36}Cl by spallation is therefore proportional to the density of the medium and the cosmogenic nuclide concentration decreases approximately exponentially with depth; most production occurs in the upper two meters of earth's surface. Spallation reactions within potassium and calcium are major contributors to the total production of ^{36}Cl (Cerling and Craig, 1994).

The production rate of cosmogenic ^{36}Cl by spallation is characterized by the cumulative mass traversed, or mass length, Z (g cm^{-2}) (Gosse and Phillips, 2001):

$$Z(z) = \int_0^z \rho(z)dz \tag{4.1}$$

where z is the linear distance (cm) and ρ is the bulk density of the material (g cm^{-3}). From a single direction, the rate of particle interception is then proportional to the flux of particles which pass through the medium, or:

$$\frac{dF}{dZ} = \frac{F}{\Lambda_{f,p}} \tag{4.2}$$

In equation (4.2), F is the cosmic ray intensity (particles cm^{-2} s^{-1}) and $\Lambda_{f,p}$ is the particle attenuation length (g cm^{-2}) (Gosse and Phillips, 2001). For the boundary condition of $F = F_{ref}$ at some reference point, the solution of equation (4.2) is:

$$F = F_{ref} \exp\left(-\frac{Z}{\Lambda_{f,p}}\right) \tag{4.3}$$

Finally, this equation for the cosmic ray flux is integrated over the entire sky, to obtain the total flux on a horizontal land surface:

$$\Phi(Z) = \Phi(0)\exp\left(-\frac{Z}{\Lambda_f}\right) \tag{4.4}$$

where Φ is the cosmic ray flux integrated over the entire sky (particles cm^{-2} yr^{-1}), $\Phi(0)$ is the flux at a depth of zero (the land surface), and Λ_f is the apparent attenuation length (g cm^{-2}). The apparent attenuation length is an empirically calculated parameter derived by fitting an exponential function to measured cosmogenic nuclide concentrations with depth (Gosse and Phillips, 2001).

Once the total cosmic ray flux is known, the cosmogenic ^{36}Cl production rate by spallation can be calculated. It is presented in terms of $\Psi(0)$, the product of the flux and the target element cross section, at the reference position (atoms (g target element)$^{-1}$ yr^{-1}):

$$P_s(Z) = \Psi(0)C\exp\left(-\frac{Z}{\Lambda_f}\right) \tag{4.5}$$

In this equation, P_s is the total production rate of ^{36}Cl by spallation (atoms ^{36}Cl g^{-1} yr^{-1}) and C is the concentration of the element of interest (g of element (g of material)$^{-1}$), which is K or Ca for ^{36}Cl.

The second type of reaction is thermal neutron capture, which is associated with lower energy (~0.1 MeV-0.5 eV for epithermal and ~0.025 eV for thermal) reactions than spallation reactions (Cerling and Craig, 1994). Thermal neutron capture reactions are important in the production of lithospheric ^{36}Cl occur when the energy becomes low enough that neutrons are absorbed by the nuclei of the atoms they encounter. For *in situ* geomorphic studies using ^{36}Cl, the most important thermal neutron capture reactions are: $^{35}Cl(n,\gamma)^{36}Cl$ and $^{39}K(n,\alpha)^{36}Cl$ (Cerling and Craig, 1994).

The epithermal and thermal neutron fluxes are modeled with diffusion equations because, at these low energies, there is very little net directional transfer of momentum. The equations that describe this diffusion for the two types of reactions differ in their parameter values and the source term. Epithermal neutrons are derived from the moderation of secondary higher energy neutrons (>0.1 MeV); epithermal neutrons that escape capture by nuclei in atmospheric gases are the source of thermal neutrons. The equations that describe the subsurface epithermal and thermal neutron fluxes are as follows (Gosse and Phillips, 2001):

$$\Phi_{epi} = \Phi'_{epi} \exp\left(-\frac{Z}{\Lambda_f}\right) + \left(F\Delta\Phi\right)'_{epi} \exp\left(-\frac{|Z|}{L_{epi}}\right) \tag{4.6}$$

$$\Phi_{th} = \Phi'_{th} \exp\left(-\frac{Z}{\Lambda_f}\right) + \left(\Im\Delta\Phi\right)'_{epi} \exp\left(-\frac{|Z|}{L_{epi}}\right) + \left(\Im\Delta\Phi\right)'_{th} \exp\left(-\frac{|Z|}{L_{th}}\right) \tag{4.7}$$

The parameters in equations (4.6) and (4.7) are as follows: Φ_{epi} and Φ_{th} are the subsurface fluxes of epithermal or thermal neutrons (neutrons cm^{-2} yr); Φ'_{epi} and Φ'_{th} represent the epithermal and thermal neutron fluxes that would be found at the position of the land surface if the atmosphere had the same epithermal neutron transport properties as the subsurface; $(F\Delta\Phi)'_{epi}$ is the difference between the flux that would be observed at Z = 0 in the absence of a land-atmosphere interface; L_{epi} and L_{th} are the epithermal and thermal neutron diffusion lengths (g cm^{-2}); and $(\Im\Delta\Phi)'_{epi}$ and $(\Im\Delta\Phi)'_{th}$ quantify the deviations of the thermal neutron profile at the land-atmosphere interface from one in the atmosphere only (Gosse and Phillips, 2001).

Like the production of ^{36}Cl by spallation, the production rates of ^{36}Cl by epithermal and thermal neutrons can be modeled mathematically. The equation that describes the production rate of ^{36}Cl from epithermal and thermal neutrons is:

$$P_{le} = \frac{f_{le}\Phi_{le}(Z)}{\Lambda_{le}} \tag{4.8}$$

In this equation, P_{le} is the production rate from low-energy neutrons ("le" refers to epithermal or thermal) and f_{le} is the fraction of low-energy (epithermal or thermal) neutrons absorbed by the target (Gosse and Phillips, 2001).

The thermal neutron flux is attenuated differently than most other cosmic ray-related nucleons, for which neutron production decreases with depth below the rock surface. Because the thermal neutron absorption cross-section is much greater in the atmosphere than in rock, some thermal neutrons escape from the lithosphere into the atmosphere, where they are absorbed by nitrogen atoms (Gosse and Phillips, 2001). The end result is a ^{36}Cl concentration profile that increases below the land surface to about 50 g cm^{-2}, and then decreases with depth.

The third type of reaction arises from secondary cosmic-ray muons. Production of terrestrial cosmogenic nuclides by muons is primarily caused by capture of slow negative muons by charged nuclei (Cerling and Craig, 1994). Muons are less reactive than the particles that cause the reactions discussed above and have lifetimes of about 10^{-6} s. Because of their relatively low reactivities, muons penetrate much deeper than neutrons and can become important in localities that are close to sea level or those characterized by high erosion rates (Cerling and Craig, 1994). In addition, these longer transport lengths mean that the muon flux is not in equilibrium with the local high-energy flux and separate scaling factors and attenuation lengths

must be considered (Gosse and Phillips, 2001). There are a number of different mechanisms by which muons can produce ^{36}Cl but the most important of these is slow negative muon capture (Gosse and Phillips, 2001). The equation describing the total ^{36}Cl production by muons is:

$$P_m = Y\psi_m(z) \tag{4.9}$$

In the above equation, P_m is the total nuclide production by muons (atoms g^{-1} yr^{-1}), Y is the total production constant for ^{36}Cl from slow negative muon absorption reactions, and ψ (z) is the muon stopping rate as a function of depth ((stopped negative muons) g^{-1} yr^{-1}).

The production rates must be scaled for the elevation and latitude of the sample according to Lal (1991). The equation (4.10) that describes the total production of ^{36}Cl in rocks (P_{36}) is then the sum of the three production components multiplied by scaling factors for elevation (S_{el}), topographic shielding (S_T), and shielding by snow or soil (S_S).

$$P_{36} = S_{el}S_T S_S\left(P_s + P_{le} + P_m\right) \tag{4.10}$$

Once the parameters in equation (4.10) are known, it is possible to date features using ^{36}Cl.

4.3 Dating depositional features using cosmogenic nuclides

Depositional features such as shorelines are inherently difficult to date using traditional Quaternary techniques such as radiocarbon or thermoluminescence dating. Some methods do not have the required age range while others can only be used with specific lithologies. TCN are a relatively new way to date depositional features if the

pre-depositional exposure history of the clasts can be accounted for. The technique involves measuring TCN concentrations with depth to construct a concentration-depth profile. The clasts within a deposit most likely have had an exposure history prior to being emplaced at the final site of deposition. As the shoreline gravels were carried to the shorelines, they were exposed to cosmic rays and, therefore, have an inheritance of TCN. There was TCN buildup in all of the clasts as they were exhumed from one site, transported to another, redeposited, and possibly transported again or many more times before coming to rest at the final depositional site. In order to date depositional features, this inherited component must be accounted for in a systematic manner.

In this work, inheritance is treated as first described by Anderson et al. (1996). In this technique, numerous individual clasts from a specified depth are amalgamated into one sample. Samples are taken from the surface and in 15-20 cm intervals in a vertical transect below the surface down to a depth of about 2 m. The concentrations of these samples should equal the sum of the mean inherited concentration plus the concentration gained since final deposition. If the assumption of a short period of deposition relative to the time of exposure in its final position is valid, then the mean inherited concentration should be equal for all the samples in the profile.

In this manner, the inherited component of the clasts in a profile can be quantified and subtracted out of the sample concentrations. The result is a depth profile related to nuclide production that occurred only within the final depositional surface. The resulting depth profile is controlled by the exposure time and the

erosion rate and therefore, if erosion rates can be adequately estimated, the age of the depositional feature can be calculated.

4.4 The effects of surficial erosion and accumulation on cosmogenic nuclide accumulation in depositional features

Because the natural environment is dynamic and constantly changing, exposure ages of landforms are almost never simply the exposure age found in the above equation. Rather, the calculated age must be corrected for landform modifications or other environmental changes that may affect the exposure ages. This section focuses on the factors most likely to affect cosmogenic nuclide buildup in shoreline features: post-depositional erosion and eolian inflation of the shoreline.

Erosion of lacustrine features is likely to have an influence on the determined age. In this work, the least eroded shorelines were selected for sampling but some erosion is unavoidable. Because the production rates of cosmogenic nuclides vary with depth below the surface, when erosion occurs the production rates will vary with time as well as depth. The result of erosion is to make surfaces apparently younger than the true age, making it difficult to estimate an exposure age.

The other post-depositional factor that may affect the shoreline ages in this work is eolian inflation. Because of their location in the western Great Basin, all the shorelines are subject to some dust flux that increases the rate of soil development (Chadwick and Davis, 1990). A gravel pavement overlying a layer of silt commonly covers the shorelines. Desert pavement clasts rise upward on a vertically accreting eolian mantle, suggesting that the shorelines have undergone accretion rather than erosion (Wells, 1995; Anderson, 2002). It has also been shown that the dust flux is

more active during interpluvial periods (Chadwick and Davis, 1990). This suggests that shorelines that have undergone multiple pluvial and interpluvial periods may have undergone a combination of erosion and inflation, making their morphologic histories more complex.

5 THE USE OF SOIL DEVELOPMENT AS A RELATIVE AGE INDICATOR

5.1 Background

The degree of soil development in semiarid regions was used in this study as an indicator of the relative ages of the shorelines to corroborate the ^{36}Cl ages. Examination of variations among certain soil properties at a particular site can support the ^{36}Cl data because, given relatively low erosion rates, older shorelines show higher degrees of soil development. With the exception of one hand-dug pit sampled during the summer of 2002, the soils in all of the trenches sampled for cosmogenic nuclide dating were described and sampled for soil analyses. The soil data is useful in comparing shoreline ages from the same site, especially where the ^{36}Cl data is ambiguous, because it provides an indication of the relative ages of shorelines. A soil comparison between the three sites, however, is less helpful because different local factors and soil parent materials influence the apparent degree of development and lead to variations in soil properties between sites.

Soil development indicators specifically addressed in this work are profile masses of carbonate, silt, and clay. These masses are cumulative properties, and therefore greater masses are suggestive of older soils. Pedogenic carbonate generally develops in soils where the mean annual precipitation (MAP) is less than 50 cm

(Birkeland, 1999). The sources of carbonate material are the Ca^{2+} in precipitation and also eolian deposition (Birkeland, 1999). The masses of silt and clay are used to compare soil development because fine particles are primarily the result of eolian deposition. Therefore, older shorelines have been exposed to more eolian deposition and may be expected to contain more fine material than younger shorelines. The goal of examining these indicators is to use the degree of soil development in shorelines from each of the three sites to help interpret and support the ^{36}Cl ages.

In addition to the profile masses, profile development indices (PDIs) were also calculated for each described soil. The PDI is based on soil properties that are suggestive of the degree of development, such as texture or structure. Higher PDIs indicate greater pedogenic development (Birkeland, 1999).

5.2 Soil development in the western Great Basin shorelines

Chadwick and Davis (1990) found that soil development on lacustrine features in the western Great Basin is most rapid in the lee of exposed playa surfaces. They determined that this factor could cause confusion between soils <12 ka and <130 ka. They also found that the most soil development occurs in sediment pulses during interpluvials when there is more eolian dust available. Therefore, comparison of soil development between shorelines must take dominant wind directions into account. Also, younger features may appear older if they are located in the lee of playas.

Adams and Wesnousky (1999) studied the soil characteristics of the OIS 2 highstand at several sites (including the Thorne Bar site) in the Lahontan basin and compared this data between sites and with some higher shorelines. Similar morphologies and soil characteristics led them to conclude that the widespread and

almost continuous high shoreline in the basin is related to the most recent lake cycle (OIS 2) in the basin. They found that spatial variability among OIS 2 profiles is most often the result of (1) local variations in water infiltration and (2) bioturbation redistributing the fine material in the profiles.

These works suggest that the degree of soil development may be used to further support the ^{36}Cl ages of the shorelines. Soil development does not provide definitive shoreline ages and local factors (e.g., excessive eolian deposition) can lead to confusion among shoreline ages. The relative degrees of soil development at a particular site, however, can be used to determine whether the ^{36}Cl ages are realistic.

In addition to corroborating the ^{36}Cl dates, soil development is used to investigate the amounts of erosion on the shorelines. Shorelines at a particular site should display increasing degrees of soil development with increasing ages. If a progressive increase in development is not found, then the older shorelines may be more eroded relative to the younger shorelines. Older soils can show apparently young degrees of development if they have been eroded because the soil is eroded at a faster rate than the rate of soil profile development. In these cases, the shoreline preservation and morphology can be used as a basis for determining whether the surface is young or apparently young. If the surface exhibits evidence of erosion (e.g., stream dissection), it may be an older surface in which the soil development is apparently young.

In arid regions, the formation of desert pavement on top of a surface can protect it from erosion (Wells, 1995). In many arid regions, desert pavements form as stones that have been exposed on the surface since their time of deposition. Over

time, stone pavements remain at the land surface but are inflated vertically due to the accumulation of windblown dust (McFadden et al., 1987). The mechanisms that control the initiation of accumulation are not well understood, but it is likely that they are influenced by adhesion and surface tension of water and sediment acting to form laminar crusts adhering to clast undersides (Anderson et. al, 2002). Over time, eolian material is trapped by gravel clasts at the land surface and develops pedogenically into a vesicular horizon. Fine-textured eolian material accumulates beneath gravel pavements despite the occurrence of processes such as rain splash or surface wash, resulting in cumulic soil development beneath the pavements (Anderson et. al, 2002).

The presence of a gravel-free layer beneath a stone pavement is a criterion used to distinguish between pavements that have always been at the surface and pavements that are derived from wind and water erosion (Wells, 1995). Stone pavements are ubiquitous on alluvial fan surfaces of Pleistocene age throughout the Southwest (McFadden et al., 1987). Like alluvial fans, the lacustrine features studied in this work are primarily composed of coarse gravels, which suggests that pavements develop in a similar manner in both features. The implication for this work is that surfaces with a stone pavement underlain by a gravel-free layer may have undergone little to no erosion and instead, inflation.

6 METHODS

6.1 Background

Establishing the ages of shorelines in the western Great Basin is valuable because it reveals information on both the timing and the magnitudes of lake cycles. The coarse gravel composition of the shorelines is not conducive to preserving sufficient material for radiocarbon ages and the higher shorelines may be beyond the age range of this method. Other possible Quaternary dating techniques include uranium/thorium or thermoluminescence dating. Uranium/thorium dating can sometimes help determine ages of lacustrine carbonates but problems such as detrital contamination of carbonates, recrystallization, and unknown initial thorium ratios often arise. The coarse grain size of the shorelines makes the possibility of thermoluminescence dating doubtful at best. Because these often-used Quaternary dating techniques are not likely to be useful in dating the shorelines, the recently developed cosmogenic surface exposure methods were selected to date these shorelines.

6.2 Sampling methodology

Shoreline sampling sites were selected based on mapping and field observations by Marith Reheis. Three localities of older, higher shorelines in the

western Great Basin were selected for their high degrees of shoreline preservation, where erosional effects would be minimized.

Shoreline sampling for cosmogenic nuclide dating was based on the depth profile method, following a procedure established by Anderson (1996). The specific technique for ^{36}Cl dating was based on the procedure of Ayarbe et al. (2001). To collect a sufficient number of samples to construct a depth profile, backhoe pits ~2 m deep were dug into a flat, apparently stable part of each shoreline. In each pit, soil profiles were studied, logged, photographed, and sampled; samples for cosmogenic nuclides were taken at 15-20 cm intervals in a vertical line down the depth of the trench. An effort was made to avoid sampling areas of the pit that showed signs of bioturbation.

Sieves were used in the field to collect the clast size fraction of ~1.5-2.5 cm diameters with a minimum total sample weight of about 500 g. This clast size was previously determined to give a useful estimation of average inheritance while keeping the sample weight down to a feasible size (Ayarbe et al., 2001). The sieving process was also performed to ensure that eolian material was not incorporated into the samples; the samples consisted only of *in situ* beach gravel. In addition, the location and elevation of each pit was determined by a Global Positioning System and recorded.

6.3 Analytical methodology

After sample collection, the samples were processed in a laboratory in preparation for analysis by accelerator mass spectrometry. The beach gravels were crushed, leached, and digested in acids (hydrofluoric and nitric). A stable ^{35}Cl carrier

was added to help produce a stronger AMS beam as well as to recover greater sample masses at the end of the laboratory procedure. Chlorine was then extracted from the dissolved rock in the form of silver chloride (AgCl) and purified. The purification steps required precipitating sulfur (an isobar of ^{36}Cl) out of the samples in the form of barium sulfate ($BaSO_4$) and removing it. The laboratory procedure for preparing samples for ^{36}Cl analysis are described in Appendices 1-4. Finally, the AgCl samples were analyzed for $^{36}Cl/^{35}Cl$ and for $^{35}Cl/^{37}Cl$ ratios by AMS at Purdue Rare Isotope Mass Spectrometry Laboratory (Purdue, Indiana) and at the Center for Accelerator Mass Spectrometry (Livermore, California). Table A1 contains the chemical data of the samples obtained for this work. Table A2 contains the AMS results and calculated cosmogenic ^{36}Cl concentrations of the samples.

6.4 Exposure age modeling

After AMS results were obtained, exposure ages and erosion rates were modeled to fit the ^{36}Cl data using the computer program, CHLOE (Phillips and Plummer, 1996). CHLOE is an analytical model used to interpret *in situ* cosmogenic nuclide analyses for surface exposure dating studies. The model takes into account a number of factors that influence ^{36}Cl accumulation in rocks, including: bulk chemistry of the samples, shielding, geographic coordinates, and elevation of the geomorphic surface. Determination of the bulk chemistry is necessary to obtain the concentrations of 1) the target elements in the rock, and 2) the various elements with different nuclear cross-sections. Shielding measurements are used to determine the degree of exposure of a sampling locality to cosmic rays. Geographic coordinates and elevations dictate the intensity of cosmic rays at different locations on Earth.

Using the factors above, CHLOE can then calculate the cosmogenic ^{36}Cl concentrations in the rock. The ^{36}Cl concentration with depth was plotted for each shoreline and this profile was used to calculate the average inheritance of the clasts and the exposure age of the shoreline. The ^{36}Cl concentrations of each profile were normalized to the sample within the profile that represented the average production rate of the profile. The purpose of this normalization was to account for small chemical variations among the samples in the profile.

To perform the normalization, the average inheritance was first calculated by minimizing the χ^2 (see below) and subtracted out. Then the thickness-averaged surface production rates were summed for each sample, and the average total surface production of each profile was calculated. The sample within the profile nearest to the profile average was selected to be the sample used for profile normalization and is referred to as the curve sample (CS). Then, based on the CS, the production rate at each sample depth was determined. Next, the production rate at each sample depth based on each particular sample was found. The ^{36}Cl concentrations were then normalized by Equation (6.1):

$$C_{Norm} = \frac{C_{spl}}{A_{spl}} C_0 \tag{6.1}$$

In Equation (6.1), C_{Norm} is the normalized ^{36}Cl concentration, C_{spl} is the production rate of the sample based on the CS, A_{spl} is the actual production rate of the sample, and C_0 is the original sample ^{36}Cl concentration. More detailed instructions on the normalization procedure are given in Appendix 5.

The shoreline ages and erosion rates were determined by minimizing the chi-squared (χ^2)-error between the observed (O) ^{36}Cl concentrations and the modeled (M) concentrations using Equation (6.2):

$$\chi^2 = \sum_{i=1}^{n} \frac{(O_i - M_i)^2}{S_i^2} \qquad (6.2)$$

In this equation, S_i is the standard deviation of the I^{th} sample, specified as 15% of the observed concentration. The 15% standard deviation was selected based on adding 2% to a mean-corrected standard deviation of Phillips et al. (2001). Phillips et al. (2001) calculated a mean deviation of about 5% between ^{36}Cl ages and independently determined ages with a standard deviation of 18%. When corrected to zero, the standard deviation is 13%. To make a conservative estimate for this work, 2% was added to the corrected standard deviation, following the procedure of Ayarbe (2000). This standard deviation of ^{36}Cl ages was also used to estimate the uncertainty of each shoreline age, also following the procedure of Phillips et al. (2001) and Ayarbe (2000). The 15% standard deviation used includes uncertainties associated with ^{36}Cl production rates, sample depths, and analytical protocols (Ayarbe, 2000). Following the procedure of Ayarbe (2000), the uncertainties associated with the shoreline ages are also based on this 15% deviation of ^{36}Cl ages.

After calculating the χ^2, the reduced χ^2 was found to interpret the agreement between the samples and the modeled ages. The reduced χ^2 is the χ^2 divided by the number of degrees of freedom where the number of degrees of freedom is equal to the number of samples minus the number of parameters. In this work, the parameters are the age and the erosion rate.

Once the shoreline ages and erosion rates were determined by minimizing the reduced χ^2, the model was used to investigate the potential effects of silt cap emplacement on the calculated age of the shoreline. The shorelines in this study have been subjected to a dust flux, as indicated by a silt layer underlain by a stone pavement at the surfaces. The possibility that these surfaces have undergone eolian inflation rather than erosion was explored for each shoreline. In order to quantify the possible effects of silt cap deposition on the shoreline ages, three cases were addressed for each shoreline: (1) the initial age estimate assuming that the silt caps were emplaced instantly after shoreline construction, (2) a constant accumulation rate that would produce the silt cap thickness measured today, and (2) a recent deposition of the silt cap, or recent relative to when the shoreline was deposited. These two cases were selected because they were deemed most appropriate for understanding the maximum possible change in shoreline age.

In the western Great Basin, most silt accumulation occurs during interpluvial periods (Chadwick and Davis, 1990), so the constant silt accumulation case is a simplistic model but still allows for a better understanding of the extent to which the calculated shoreline age would be affected by a similar condition. If the silt cap were emplaced recently relative to when the shoreline was deposited, then the measured sample depths would overestimate the mean depth since deposition and cause the average production rate for each sample to be underestimated. The samples would have a ^{36}Cl concentration based on production rates at shallower depths than the depths at which they were sampled.

It is also possible that the older shorelines undergo a variable erosion rate. After they are first deposited, the coarse gravels are very permeable, leading to less runoff and therefore less erosion. Over time, eolian dust and carbonate development would be expected to fill in the pore spaces, making the shorelines less permeable. This would increase runoff and result in more erosion. If this variable erosion rate is true for these shorelines, then its effects would be more pronounced in the older shorelines because they have undergone more carbonate and dust accumulation.

The calculated ^{36}Cl ages are more sensitive to erosion in the older features than the younger ones. Figures 6.1 and 6.2 illustrate this effect. Figure 6.1 presents the modeled fit to ^{36}Cl data from a relatively young feature, ~13 ka. Figure 6.2 presents the modeled fit to ^{36}Cl data from a relatively older feature, ~288 ka. Both plots show three modeled fits to the data using a constant age but three different erosion rates: 0, 5, and 10 mm/kyr. On the younger feature, all three modeled curves result in similar curves while on the older feature, the different erosion rates produce distinctly different curves. This is because the effect of erosion on cosmogenic nuclide accumulation is dependent on the total depth of material that has been eroded, not on the erosion rate (Gosse and Phillips, 2002). Therefore, relatively high erosion rates do not produce pronounced effects in the data until enough time has passed for significant amount of erosion to have been removed. The older feature has had a long enough exposure time that a high erosion rate leads to large amounts of total erosion, whereas the younger feature has had a short enough exposure time that even relatively high erosion rates do not result in distinctly different accumulations.

In order to test the hypothesis that the shorelines were constructed during glacial intervals, the reduced χ^2 values for shoreline ages constructed during other oxygen isotope periods (Shakleton and Opdyke, 1976) were calculated. Previous

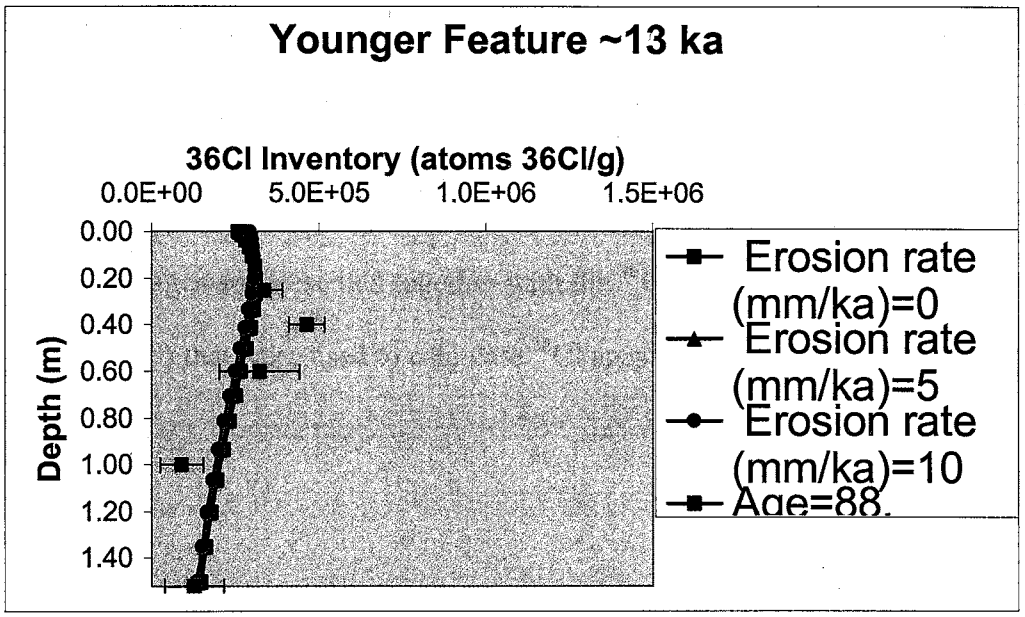

Figure 6.1. Modeled 36Cl ages of a feature using three different erosion rates. The feature is about 13 ka.

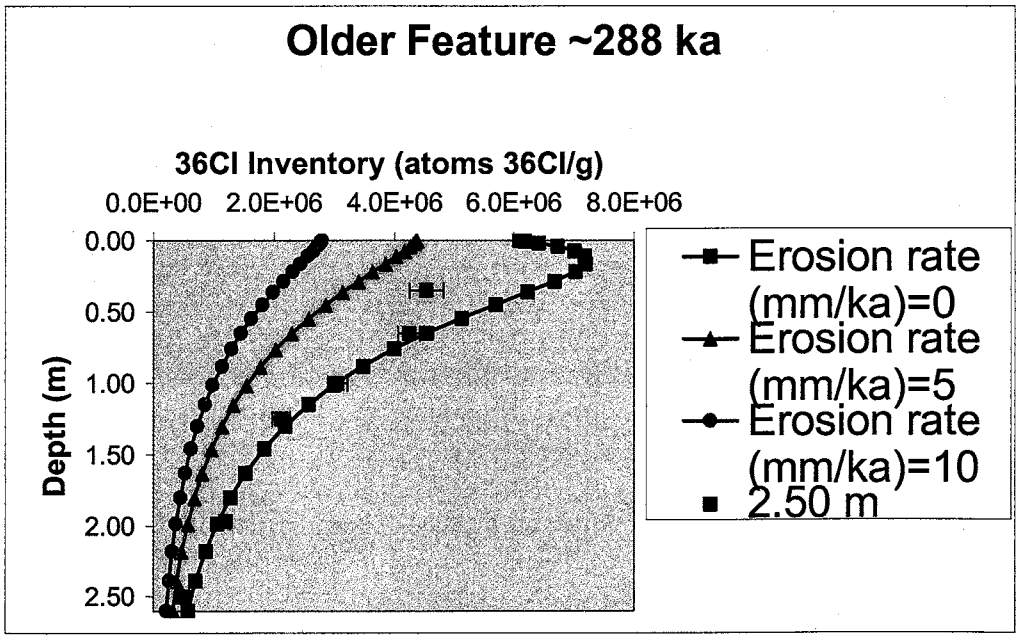

Figure 6. 6.2. Modeled ^{36}Cl ages of a feature using three different erosion rates. The feature is about 288 ka.

work has generally suggested that western Great Basin lake cycles occurred during glacial intervals (e.g., Russell, 1885; Broecker and Orr, 1958; Morrison, 1991). To test this relationship, the reduced χ^2 was calculated for each shoreline assuming ages at the midpoints of each oxygen isotope period.

Finally, for purposes of comparison, the shoreline ages were also calculated using the ^{36}Cl production rates determined by Stone et al. (1996). These production rates vary from those used in this work in their calibration and certain parameters used. The ages are presented together with the ^{36}Cl production rates of Phillips (1996, 2000) that were used to calculate ^{36}Cl ages in this work.

7 THORNE BAR RESULTS AND DISCUSSION

7.1 Geological Background

The Thorne Bar shoreline complex (Figures 1.1 and 1.2), near Walker Lake, is a V-bar composed of shoreline gravel formed at the mouth of a large canyon out of the Gillis Range. A geologic map of the Thorne Bar with topographic contours and trench locations is presented in Figure 7.1. Figure 7.2 is a photo of the Thorne Bar from the north in which the V-shape of the barrier is visible. Gilbert (1890) described V-bars as triangular in shape with one side resting against land and the opposite angle pointing towards the water. It grows outward through the addition of sediment to both sides. Gilbert wrote that when Pleistocene lakes increased in the size, the V-bar outer terraces grew higher, enclosing a triangular lagoon, which now is evidenced by flat, triangular basins. The Thorne Bar is a well-preserved V-bar with shorelines at the Sehoo level (~1335 m) and above to about 1400 m.

Despite the active tectonics of the region, the Thorne Bar is tectonically quiescent with essentially undeformed shorelines (Demsey, 1987). Previous workers identified shoreline features at elevations above the Sehoo shoreline level but attributed them to Gillis Range faulting during pre-Sehoo times (King, 1978) or to northward tilting of the Lahontan Basin (Mifflin and Wheat, 1979). Since then,

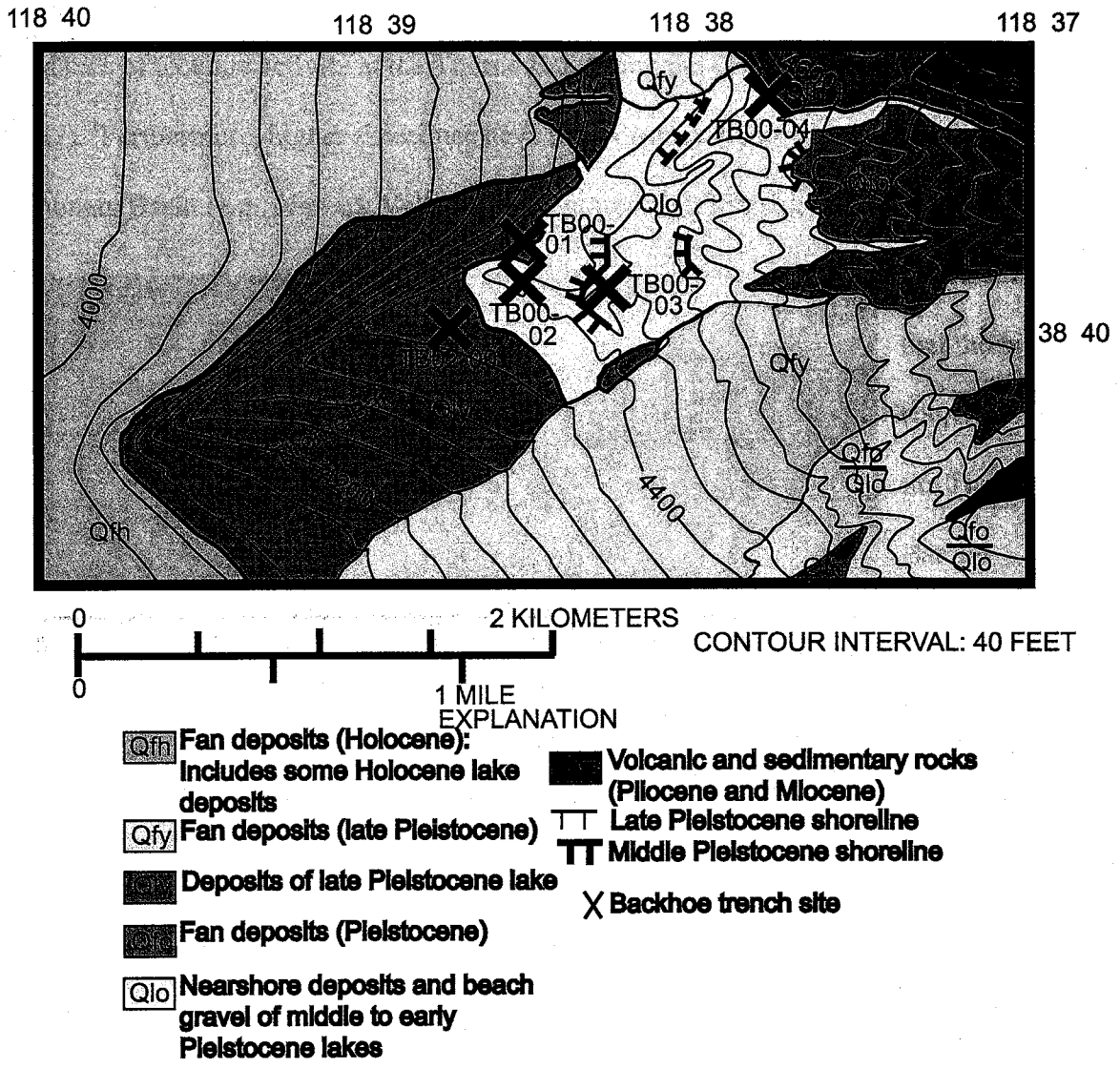

Figure 7.1. Geologic map of the Thorne Bar shoreline complex with the trench locations marked.

detailed leveling studies and air photo interpretation have failed to reveal any evidence of tectonic activity at the Thorne Bar during the Quaternary (Demsey, 1987). Furthermore, higher shorelines have been discovered in other areas of the Lahontan Basin (e.g., Newark Valley and Columbus Salt Marsh), which supports the hypothesis that the high shorelines at the Thorne Bar are evidence of Lahontan highstands older and larger than the LGM.

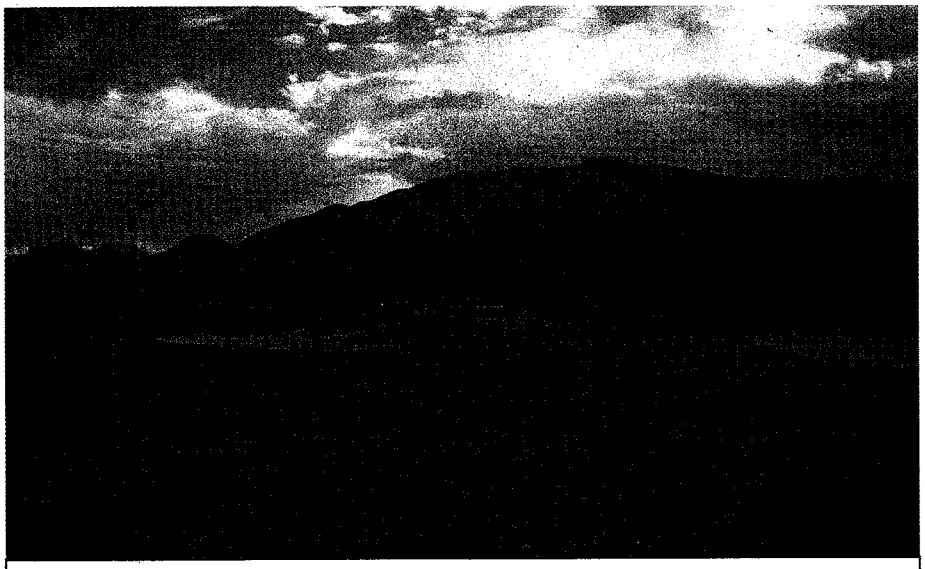

Figure 7.2. View of Thorne Bar from the north. The V-bar shape as well as the outlines of individual shorelines are visible.

The lithology of the bar is primarily pebble- and cobble-sized gravel with some tufa cementation. Bedding within shorelines ranges from horizontal to about 25° (Reheis et al., in press). The beach gravels are reworked during successive lake highstands, resulting in well sorted, well rounded gravels within the bars. At the base of the complex, there is a group of historic shorelines below 1250 m that were deposited within the last 100 years. Above these shorelines are the Pleistocene shorelines, which reach up to about 1402 m in elevation.

Figure 7.3. Photo of the inside of pit TB02-00, with sample points indicated by green circles.

The Sehoo-aged bar was sampled from a hand-dug pit in May of 2002 after it was determined that the bar thought to be related to OIS 2 is instead related to OIS 4. The exact elevation of the pit was not determined with a GPS, but based on the topographic map, the elevation was estimated to be about 1325 m. This shoreline was selected because it is a distinct shoreline close to the level of the OIS 4 shoreline. The maximum elevation of the Sehoo-age barrier onto which the pit was dug is approximately 1337 m. To ensure that a feature of OIS 2 age was dated, a constructional part of the barrier at a lower elevation (about 1325 m) was selected for ^{36}Cl dating (TB02-00 on the geologic map). Figure 7.3 is a photo of the inside of this pit with the ^{36}Cl sampling points indicated by green circles. The depth of the pit was 1.52 m and the material excavated consisted of loosely consolidated beach gravels.

The flat morphology of the bar suggests that it has undergone little, if any, erosion. There was a large, flat surface to dig into, which suggests that little of the bar has been cut and rounded by erosional processes. Also, Figure 7.3 shows the presence of a gravel-free silt layer underlying the gravel pavement and below about 50 cm, there is little silt present within the gravel matrix. This silt accumulation, together with the flat morphology or the bar, suggests that the TB02-00 surface has undergone surficial inflation rather than erosion.

The soil profile in this pit was studied but not described or sampled for soil analyses. The relative degree of soil development is visible in Figure 7.3. Field observations suggest that soil development is weak, resulting in the interpretation that the soil is younger than the other soils described at the Thorne Bar (Reheis, M., U.S. Geological Survey, personal communication, 2002).

A well-preserved shoreline, originally thought to be of Sehoo age, is found at an elevation of about 1330 m. It is in the form of a distinct, small barrier bar across the mouth of a small drainage cut into the north side of the main Thorne Bar barrier. It was sampled for ^{36}Cl dating at the point labeled TB00-01 on the geologic map (Figure 7.1).

Figure 7.4 is a photo of the inside of the pit trench dug into this shoreline. Backsets dominate the bedding in this trench. Like the other shorelines at the Thorne Bar, the clasts found in TB00-01 are primarily subrounded pebbles to cobbles but are more strongly cemented than the clasts in TB02-00. The silt at and near the surface suggests that eolian accumulation rather than erosion has modified the surface of the

bar. The presence of the gravel-free silt layer just below the surface pavement is an indicator of eolian accumulation, and on Figure 7.4, this silt layer is visible. The

Figure 7.4. The inside of pit TB00-01, with green circles indicating ^{36}Cl sampling points.

presence of the silt layer below the gravel pavement, together with the distinct morphology of the bar, suggest that the shoreline has undergone eolian inflation rather than erosion.

Table A3 gives the soil horizons and soil laboratory data for the Thorne Bar shorelines. Soil profile masses of carbonate, silt, and clay from this shoreline and the three older shorelines above it are given in Figures 7.5, 7.6, and 7.7. In a sequence of shorelines, the youngest shorelines are expected to contain the lowest amounts of these materials because they have been exposed to eolian deposition for the shortest length of time. The figures show that TB00-01 has the lower amounts of these materials than the other Thorne Bar shorelines, in support of a younger age of this shoreline. Field observations suggest that this soil is older than that of TB02-00

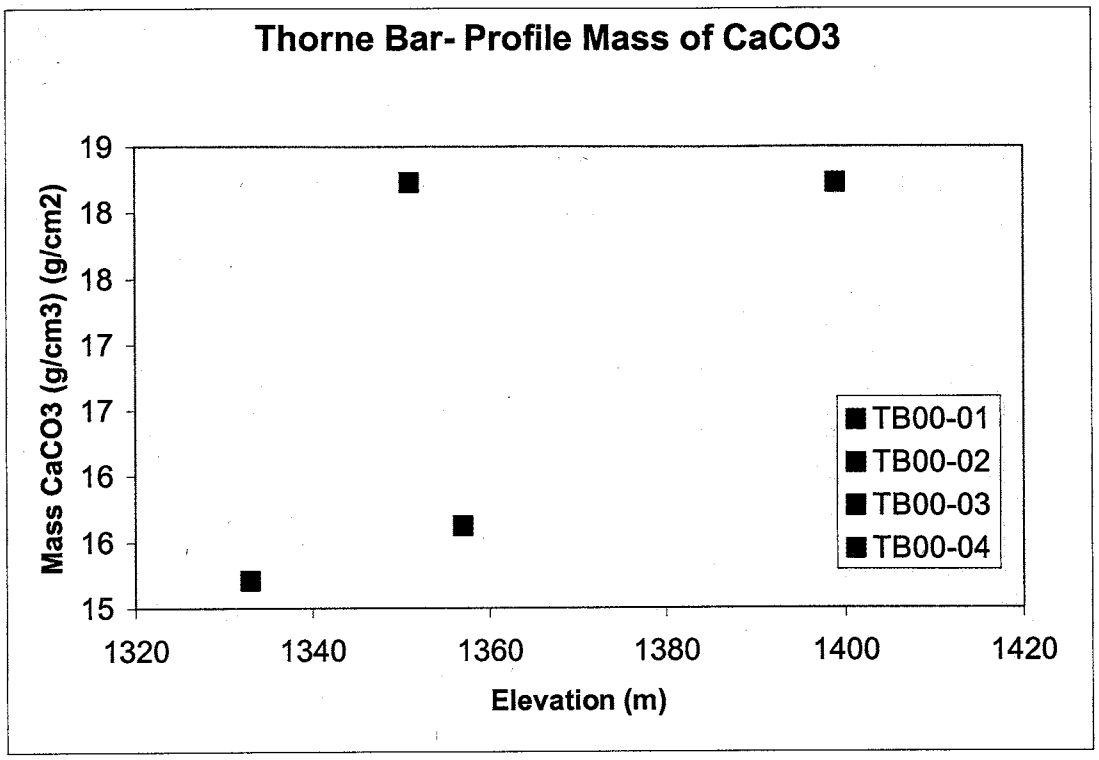

Figure 7.5. Profile masses of CaCO3 for the four higher shorelines studied at Thorne Bar.

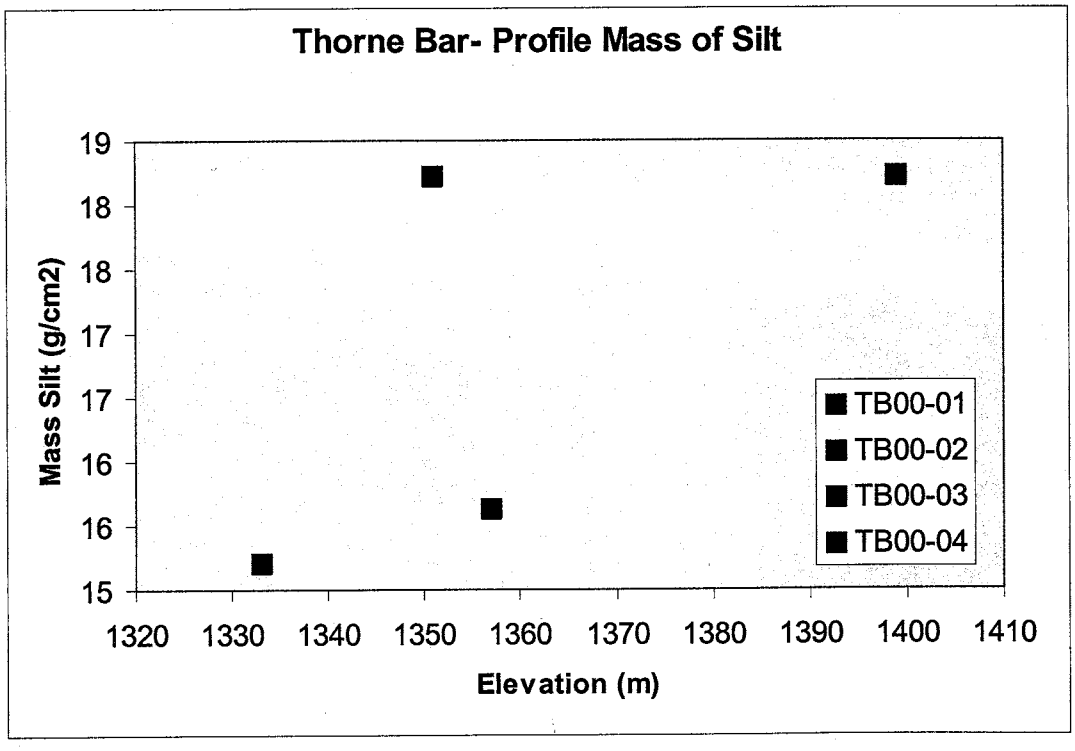

Figure 7.6. Profile masses of silt for the four higher shorelines studied at Thorne Bar.

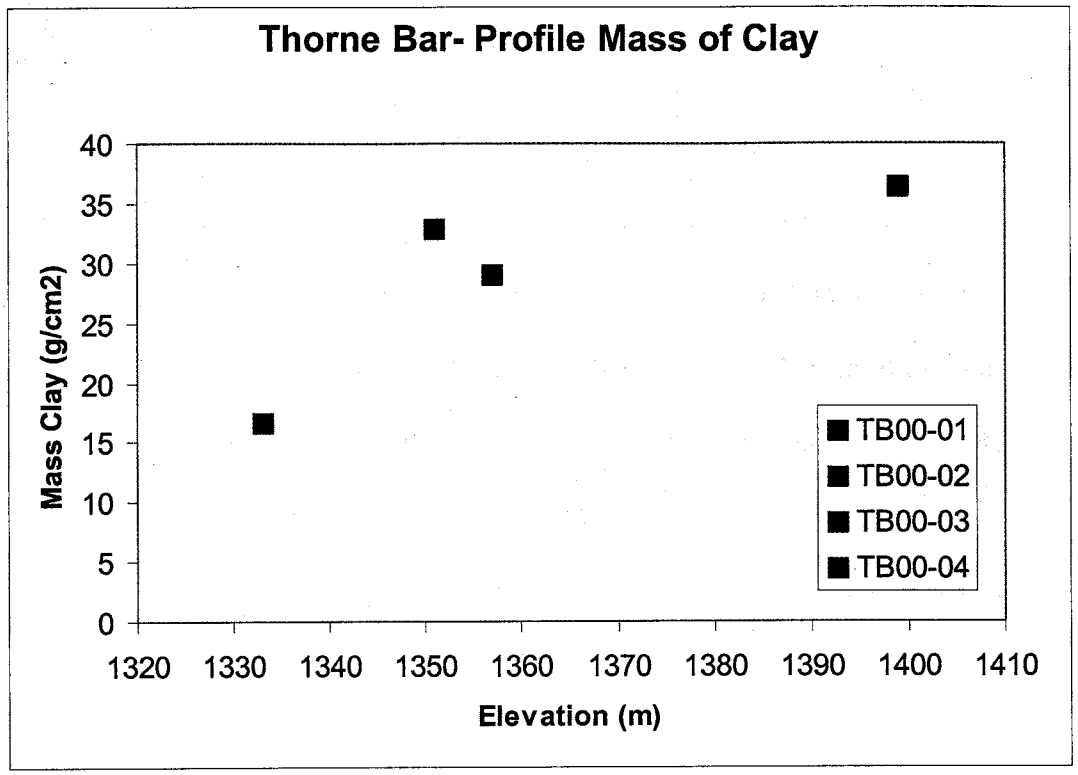

Figure 7.7. Profile masses of clay for the four higher shorelines studied at Thorne Bar.

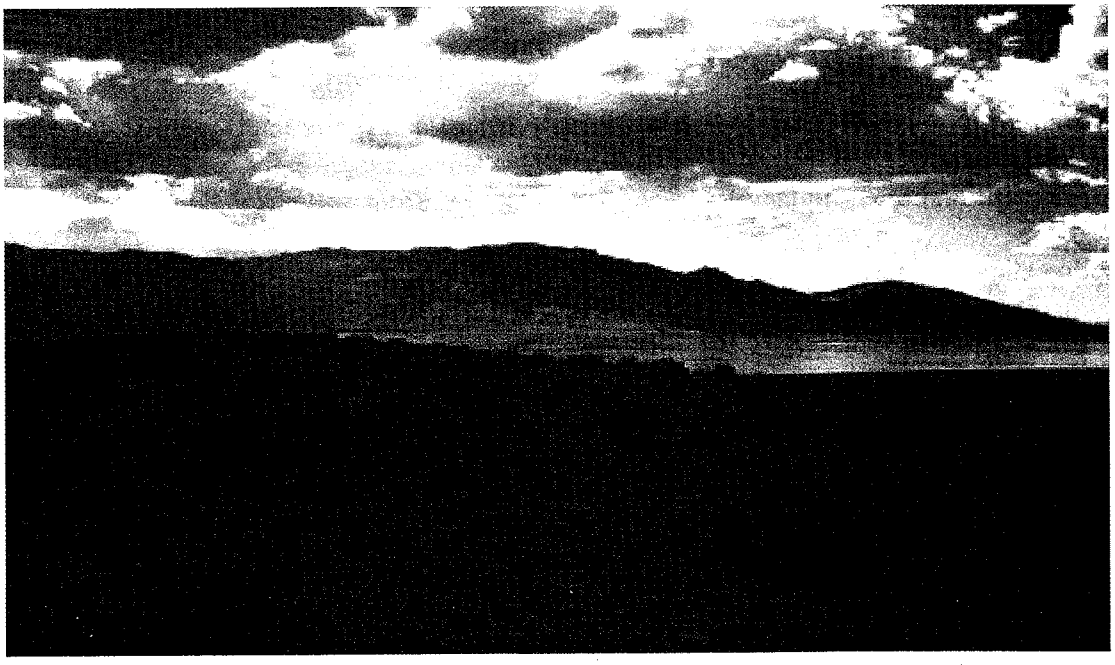

Figure 7.8. View of the top of TB00-02 looking east towards Walker Lake.

because it has a higher degree of soil development (Reheis, M., U.S. Geological Survey, 2002, personal communication).

Above the loop bar, there are two nested barriers that form part of the main Thorne Bar barrier and mark highstands between about 1335 and 1370 m. The lower bar is better preserved than the upper and was sampled at the point labeled TB00-02 on the geologic map. There is some independent age control on this bar from a tufa sample taken from the same elevation as the bar. U-series data from the tufa sample indicates that the bar is about 128 +/- 6 ka (Paces, J., U. S. Geological Survey, 2001, personal communication), which suggests that the bar is related to OIS 6.

The soil development suggests that the bar is older than TB00-01 but younger than TB00-03, and the amounts of carbonate, silt, and clay are expected to reflect this intermediate value. These profile masses are shown in Figures 7.5, 7.6, and 7.7. TB00-02 contains higher masses of carbonate, silt, and clay than the shorelines below it as well as the shoreline above it, TB00-03. One reason for the relatively high masses of these materials is that this shoreline juts out of the V-bar more prominently than the other Thorne Bar shorelines. TB00-01 is somewhat protected on the north side of the main barrier and so, unlike the other bars, it may receive most of its eolian material from one direction. The top two shorelines are higher and set further back from the lake basin; this longer distance from the lake bed (a major silt source) would cause them to accumulate less eolian material. This position may make it more susceptible to eolian deposition of these materials. A second reason is that there may have been primary deposition of these materials when the shoreline was constructed. This possibility is difficult to support with evidence, but there are clay films on

pebbles at about 1.50 to 2.00 m depth in the pit that are probably from primary deposition from the lake (Reheis, M., U.S.G.S., 2002, *personal communication*).

Another indicator of soil development is profile development index (PDI). For this soil, the PDI is 17.6, whereas for the TB00-01 soil, the PDI is 13.1 (Reheis et al., *in press*). Higher PDI values suggest greater degrees of soil development, and therefore the soil data suggests that TB00-02 is an older soil than TB00-01.

Figure 7.8 shows a view of the top of the bar, in which the flat surface is visible. Figure 7.9 is a photo of the inside of the trench, and shows the presence of a gravel-free silt layer below the gravel pavement. This evidence suggests that the bar is well-preserved and may have undergone inflation rather than erosion.

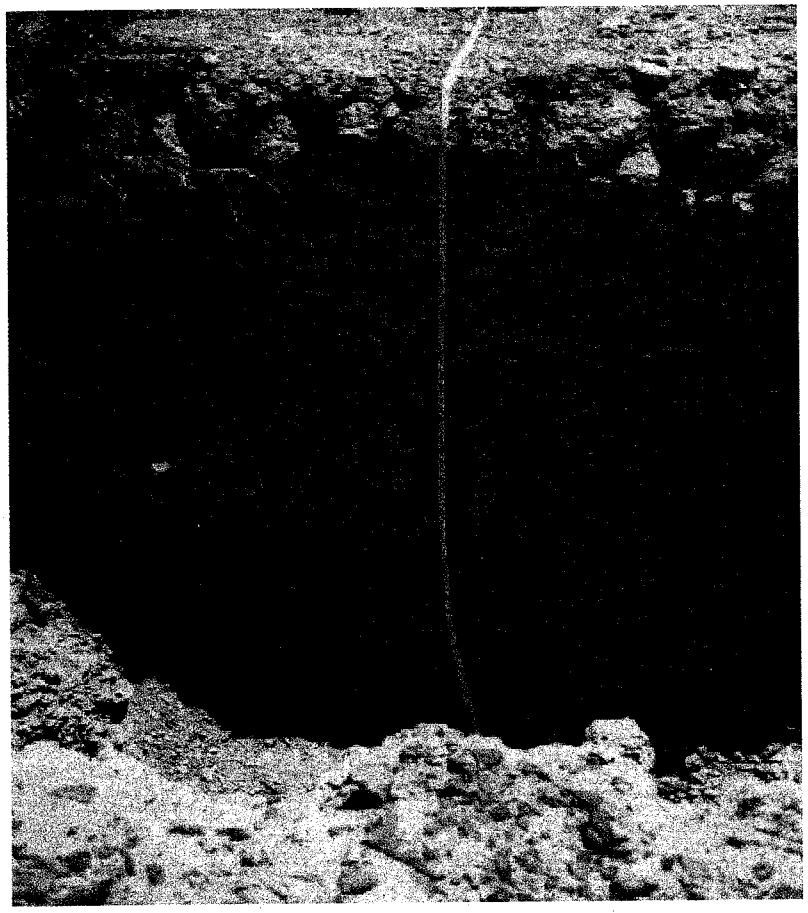

Figure 7.9. Photo of the inside of TB00-02, with sample points indicated by green circles.

The upper bar of the nested bars is at an elevation of 1357 m and was sampled at the point labeled TB00-03 on the geologic map (Figure 7.1). Figure 7.10 is a photo of the inside of the

trench with ^{36}Cl sampling points indicated by green circles. The presence of a gravel-free silt layer underlying the gravel pavement is evident in the photo, and suggestive of eolian inflation of the surface, not erosion. Both the silt layer and the well-preserved appearance of the shoreline suggest that surface inflation has been an important surficial process on this shoreline.

The degree of soil development suggests that this bar is older than those below it but younger than the highest Thorne Bar shoreline. As Figures 7.5, 7.6, and 7.7 show, the profile masses of carbonate, silt, and clay are higher in this shoreline than TB00-01 but lower than those in TB00-04. TB00-02, however, deviates from this trend and the possible reasons for this are given above.

The PDI calculated for this soil is 15.8, lower than TB00-02 but higher than TB00-01. This could suggest that this soil is younger than TB00-02, but this may not necessarily be the case. TB00-02 also has higher profile masses of carbonate, silt, and clay, due to its prominent position on the main barrier and its proximity to the exposed part of the lake bed. These higher masses may also influence the PDI, and

Figure 7.10. The inside of pit TB00-03, with sample points indicated by green circles.

cause TB00-02 to have a higher PDI than TB00-03. Therefore, TB00-02 is apparently older (based on profile masses and the PDI) because of its position on the Thorne Bar but may not necessarily be older.

U-series dates from tufa samples taken at the elevation of this bar yield dates of 167 +/- 17 and 210 +/- 37 (Paces, J., U. S. Geological Survey, personal communication, 2001). These dates suggest that the bar is older than TB00-02 and may be related to OIS 6 or 8.

Finally, there is at least one older barrier at an elevation of about 1402 m (Reheis et al., in press). This bar was sampled at the point labeled TB00-04 on the geologic map (Figure 7.1). This is the highest shoreline at the Thorne Bar site

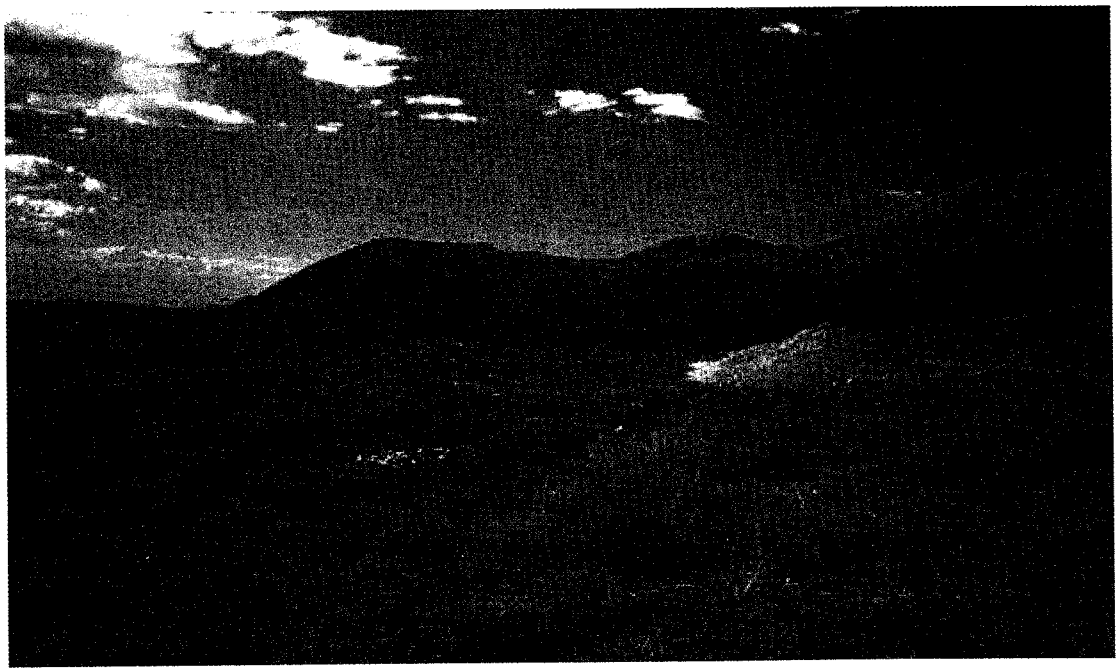

Figure 7.11. View of the top of TB00-04.

investigated for this work. Figure 7.11 is a photograph of the top of the shoreline, and the relative degree of preservation is visible. It is more rounded and less distinct than the shorelines below it, suggesting that more erosion has occurred on this shoreline than on the other Thorne Bar shorelines. In addition, it is less flat than the

others and there is evidence of stream dissection through it. The inside of trench indicates that the shoreline is composed of coarse beach gravels like the other Thorne Bar shorelines (Figure 7.12).

The soil profile development suggests that this bar is the oldest of the bars studied at the Thorne Bar. The profile masses are presented in Figures 7.5, 7.6, and 7.7. The soil in this bar has the highest profile masses in all three categories, suggesting that it is the oldest soil. In addition, the PDI is 23.3 (Reheis et al., *in press*), which is the highest PDI value calculated at the Thorne Bar and also supports an older age for this soil. Therefore, the lesser degree of preservation and the higher degree of soil development suggest that this is the oldest of the bars studied at the Thorne Bar.

Figure 7.12. Photo of the inside of TB00-04, with sample points indicated by green circles.

Some tephrochronological control exists in the Walker Lake Basin that helps to constrain the ages of this highstand (Reheis et al., 2003). About 4 km north of the Thorne Bar, there is an exposure showing four sequences of lacustrine gravel and sand, separated by palaeosols and alluvium. These deposits overlie bedrock that is well above the Sehoo highstand level. A tephra layer contained in the second-youngest lacustrine unit correlates chemically to the Bishop-Glass Mountain family of tephras from Long Valley, California. Because paleomagnetic data from silty layers indicate a normal polarity, this tephra may be the 760-ka Bishop ash bed. The youngest unit in this outcrop is about 38 m thick and is made up of tufa-cemented pebble and cobble shore gravel. The top of this unit is at an altitude of about 1393 m but a lag of beach pebbles is found up to about 1395 m. Because these deposits are similar in character and elevation to the oldest shoreline at the Thorne Bar, it is likely that they are equivalent (Reheis et al., 2003). Therefore, based on this tephrochronological evidence, the oldest bar at Thorne Bar may be correlative with OIS 16.

7.2 Thorne Bar ^{36}Cl results

During June of 2000, four backhoe trenches were dug into each of the four shorelines higher Thorne Bar shorelines (Figure 7.1). The lowest, thought to be the Sehoo shoreline (associated with OIS 2), was sampled as a control shoreline. This shoreline yielded interesting and somewhat unexpected ^{36}Cl results, so the Thorne Bar was revisited in May of 2002 to sample a fifth shoreline close to the same elevation. The geographic coordinates, elevations, and determined ages before the silt deposition analysis of each shoreline are given in Table 7.1. In this section, ^{36}Cl

results from the five shorelines are presented and the implications of these shoreline ages are discussed.

Shoreline	Elevation (m)	Latitude	Longitude	Characteristic Features	Age (ka)	Estimated erosion Rate (mm/kyr)	Average Inheritance (atoms ^{36}Cl/g)
TB02-00	~1325	38.66°	-118.65°	Weak soil development	16	0	2.57×10^{6}
TB00-01	1333	38.670497 57°	-118.6418 794°		70	0	1.31×10^{6}
TB00-02	1351	38.668870 88°	-118.6415 271°	U-series date of 128 +/- 6 ka	139	0	7.59×10^{5}
TB00-03	1357	38.668241 99°	-118.6386 6033°	U-series date of 167 +/- 17, 210 +/- 37 ka	258	0	1.13×10^{6}
TB00-04	1399	38.676142 34°	-118.6294 708°	Tephra correlation to OIS 16	400-600	2-4 depending on age	2.95×10^{5}

Table 7.1. Geographic coordinates and elevations of the five trenches dug at the Thorne Bar complex. The table also includes characteristic features of the shoreline as well as its modeled age and erosion rate before silt deposition analysis.

7.3 TB02-00, Elevation 1325 m

The modeled ages and erosion rates of TB02-00 are shown in Figure 7.13. In the figure, the horizontal axis represents ^{36}Cl concentration, the vertical axis represents depth, the small symbols represent sample points, and the curves show the modeled ages and erosion rates. The colors and shapes of the symbols correspond to the colors and symbol shapes of the modeled curves. Solid symbols represent samples that were used for the reduced χ^2 minimization to estimate the age and erosion rate of the shoreline and hollow symbols are outlying samples that were not used in the minimization. Each modeled result is normalized by dividing the samples and the curve by the average surface production rate of each profile.

Figure 7.14 shows different modeled ages plotted with their corresponding reduced χ^2 values. Several ages for each shoreline are plotted and the age of TB00-02 appears constrained to a small time interval.

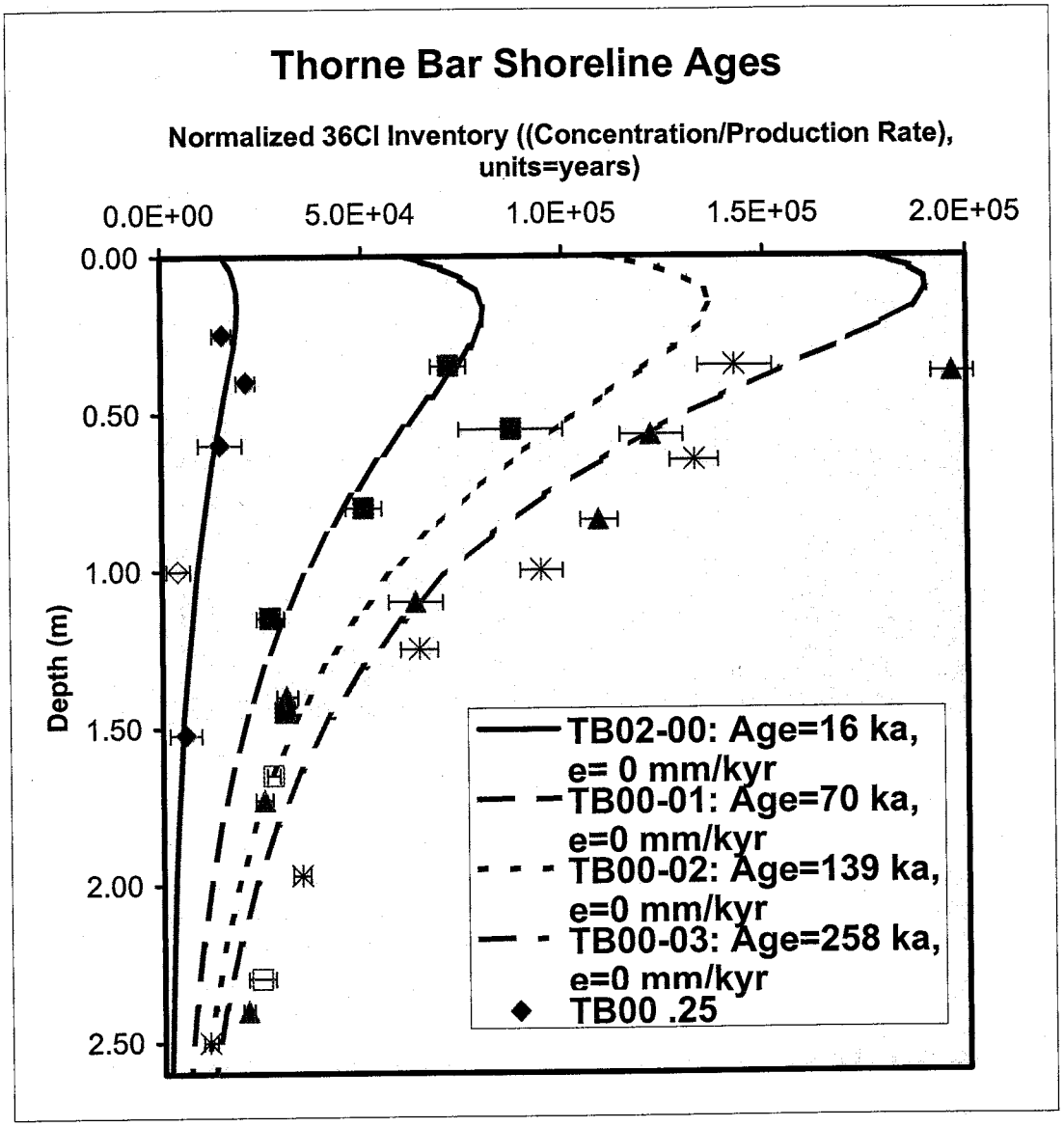

Figure 7.13. Normalized ^{36}Cl data with modeled ages and erosion rates for the Thorne Bar shorelines. Inheritance has been subtracted out and the samples and curves have been normalized by the average production rate of each profile. Symbols correspond to modeled curves by color and hollow symbols indicate outlying samples that were not included in the reduced χ^2 minimization.

In the analysis of TB02-00, the point at 1.00 m was found to be an outlier and not used in the reduced χ^2 minimization. As Figure 7.13 shows, the modeled curve

captures all the sample points except for the sample point at 1.00 m. It is not possible to fit a curve to all the samples but it is possible to fit all the samples to one curve without the sample at 1.00 m. The most likely explanation for why this sample is an outlier is a subtle stratigraphic change that was not apparent during sampling. As Figure 6.2 shows, the sample point at 1.00 m corresponds to a thin layer of well-

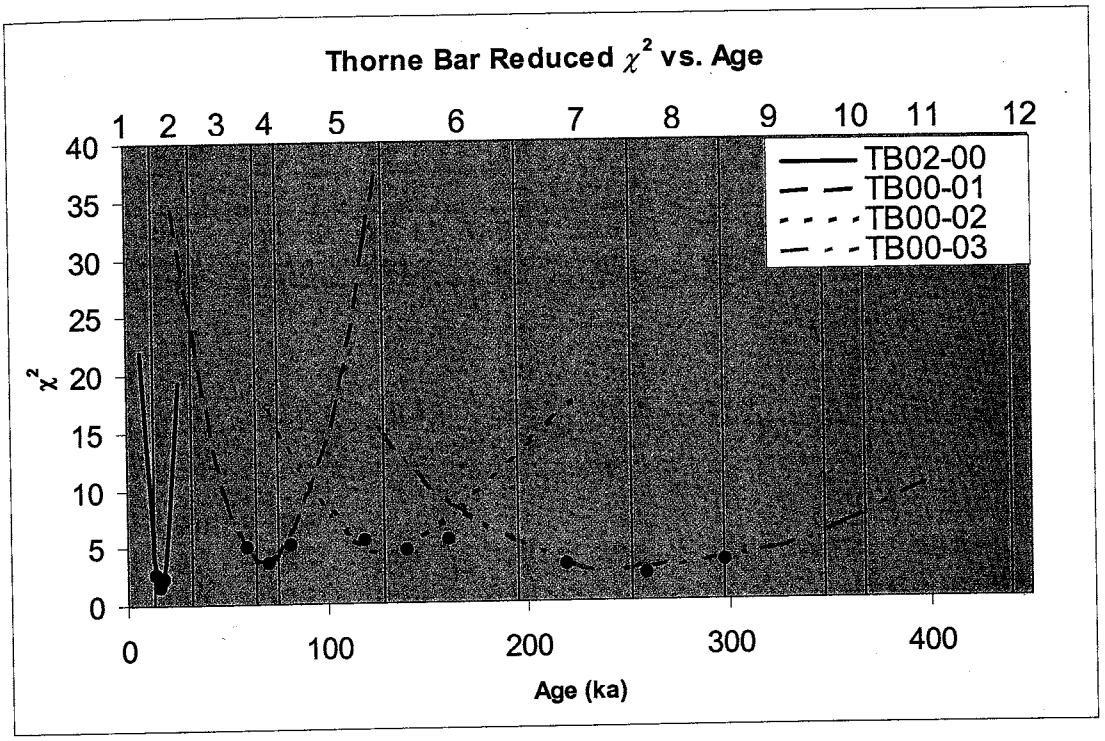

Figure 7.14. Reduced χ2 versus age for the Thorne Bar shorelines. Black dots correspond to the shoreline age and to fifteen percent uncertainties. The black lines represent marine oxygen isotope stage boundaries and the stages are numbered along the top.

sorted, small pebbles. Although this did not seem unusual during sampling, this layer may be related to a specific depositional event that favored a particular source area. This would result in the sample at 1.00 m not containing the same average inheritance as the other samples in the profile. Therefore, in order to use the samples most effectively to estimate the age of the feature, the point at 1.00 m was not used in the minimization.

	OIS 1 6.5	OIS 2 22.5	OIS 3 48	OIS 4 69.5	OIS 5 101.5	OIS 6 161.5	OIS 7 223	OIS 8 274
TB02-00	22.0	1.6	177.4					
TB00-01	60.7	34.2	9.7	3.7	15.4	88.7		
TB00-02	56.1	42.9	26.5	16.7	7.9	4.6	17.4	34.0
TB00-03	62.5	53.0	40.2	31.3	20.9	8.6	3.2	2.5
P1	27.2	0.7	14.5	56.3	152.6			
P2	52.8	38.9	22.2	12.6	4.1	1.2	12.0	25.0
P3	79.9	60.8	37.6	23.7	10.3	1.9	2.3	7.8
N1	59.7	45.1	28.4	19.0	10.8	6.7	10.1	15.0
CM01-1	35.0	6.5	78.4	223.1				
CM01-2	73.2	41.7	11.0	0.9	4.3	42.9	103.1	
CM01-3	59.7	42.8	22.7	11.4	2.8	1.6	5.0	9.7

	OIS 9 322	OIS 10 357	OIS 11 403.5	OIS 12 456	OIS 13 487	OIS 14 522	OIS 15 567	OIS 16 609.5
TB02-00								
TB00-01								
TB00-02	53.1							
TB00-03	4.3	6.5	10.4	15.5	18.8	22.6	27.7	32.4
P1								
P2	39.0	49.8						
P3	14.2	19.1	25.5	32.1	35.6	39.3	43.4	46.8
N1	19.8	23.2	27.3	31.4				
CM01-1								
CM01-2								
CM01-3	14.3	17.5	21.3	25.0	26.8	28.6	30.6	32.1

Table 7.2. Reduced χ^2 values of the shoreline ages using different oxygen isotope periods. The midpoint of each period is used.

As shown in Table 7.2,the reduced χ^2 minimization suggests that the shoreline is about 16 ka and the erosion rate is 0 mm/kyr, an age corresponding to OIS 2. The uncertainty was calculated using a 15% uncertainty of the age of the feature, following the procedure of Ayarbe (2001). Other reduced χ^2 minimizations were performed to explore how well the model could fit data using other oxygen isotope periods and the results of this work are given in Table 7.2. These reduced χ^2 values

are greater than the OIS 2 age and support the interpretation that the shoreline was constructed during OIS 2.

Inflation of the surface was also examined to quantify its effects on the shoreline age. There is a stone pavement underlain by a gravel-free layer on the surface of this shoreline (Figure 7.3), suggesting that surface has inflated rather than eroded. The modeled results under the two eolian inflation conditions are presented in Table 7.3. The result of a lower reduced χ^2 under a constant accumulation is in agreement with the hypothesis that the shoreline has undergone inflation.

	Age (ka)	Erosion rate (mm/kyr)	Reduced χ^2
^{36}Cl age	16 +/- 2.4	0	2.6
Eolian inflation	16	-6.3	2.0
Recent silt cap deposition (10 cm)	15	0	1.4
Stone production rate	16	0	2.4

Table 7.3. Modeled ages, erosion rates, and reduced χ^2 values of theTB02-00 samples, under different conditions.

The result of a recent emplacement of the silt cap on the surface of the shoreline is also presented in Table 7.3. Applying a correction to the samples by changing the depths to 10 cm higher (the thickness of the silt cap) results in an 6% change in the age estimate. This suggests that under a scenario in which the silt cap was deposited recently relative to when the shoreline was constructed has a minimal impact on the shoreline age.

7.4 TB00-01, Elevation 1333 m

Figure 7.13 shows the modeled age and erosion rate for the ^{36}Cl data from this shoreline. Figure 7.14 shows the reduced χ^2 values for different ages of this shoreline. The modeled curve suggests that the shoreline is not related to OIS 2, as initially assumed. Instead, the ^{36}Cl age that yields a minimum reduced χ^2 is 70 ka with an erosion rate of 0 mm/kyr, suggesting that this shoreline is related to an OIS 4 lake cycle.

In performing the reduced χ^2 the lowest two samples (2.30 m and 1.65 m) were removed as outliers. One reason for this was that a reduced χ^2 minimization using one (2.30 m) or both of these samples resulted in large modeled erosion rates and large reduced χ^2 values. In both cases, the minimization suggested erosion rates of 3 mm/kyr or higher. If these erosion rates were correct, then the shoreline today

	Age (ka)	Erosion rate (mm/kyr)	Reduced χ^2
^{36}Cl age	70 +/- 11	0	3.7
Eolian inflation	73	-1.4	4.1
Recent silt cap deposition (10 cm)	65	0	2.3
Stone production rate	86	0	3.6

Table 7.4. Modeled ages, erosion rates, and reduced χ^2 values of theTB00-01 samples, under different conditions.

would have had about 30 cm eroded off of it. From our knowledge of the shoreline morphology, we know that the shoreline is one of the best preserved in the suite of shorelines. The level of preservation suggests that either the surface has not been eroded or it has undergone inflation. When the samples at 2.30 m and 1.65 m are

removed from the minimization, the modeled erosion rate is 0 mm/kyr and the reduced χ^2 is 3.7.

It is difficult to tell from Figure 7.4 whether the lowest two samples are related to an unconformity or stratigraphic change. There is no buried soil present between the samples at 1.65 m and 1.45 m, suggesting that there is not an unconformity at this level unless the soil was stripped away before deposition of the upper part of the shoreline during OIS 4. This explanation is not well supported by the stratigraphy, which does not show major changes at this depth. However, the bedding is steeper at the base of the trench, suggesting that a subtle stratigraphic change is possible. One explanation is that the lowest samples may be from a different source area than the other samples in the profile, resulting in variations in the average inheritance within the profile. Alternatively, they are statistical outliers for another reason that is not clear from field observations. The high erosion rates that are required when the lowest samples are used in the minimization, suggests that they are statistical outliers, although the specific factor(s) causing them to be outliers is not clear.

The relationship between shoreline construction and a Pleistocene cooling periods was also investigated, and the results of this work are given in Table 7.2. For both OIS 3 and OIS 5 ages, the reduced χ^2 values are higher than the reduced χ^2 obtained in the OIS 4 minimization. Therefore, the data is in agreement with the lake cycle occurring during a glacial period.

The effect of the silt cap on the age of the shoreline was also investigated and the results are given in Table 7.4. The modeled fits were first studied under a

constant accumulation scenario. The silt cap on this shoreline is approximately 10 cm thick. The reduced χ^2 suggests that the surface has undergone inflation at a rate of 1.4 mm/kyr, which results in a silt layer that is about 10 cm thick. The reduced χ^2 for constant inflation is close to the original reduced χ^2. This suggests that the surface has not undergone constant inflation but, because the values are similar and a silt layer is present below the gravel pavement, inflation of the surface cannot be discounted.

A recent deposition of the silt cap was investigated by estimating the age if the samples were at depths 10 cm higher (the thickness of the silt cap) and it was found that this resulted in a lower reduced χ^2 than the original minimization. This result and the result of constant accumulation suggest that the shoreline is related to OIS 4 and that surface has undergone eolian inflation.

7.5 TB00-02, Elevation 1351 m

This bar is the next shoreline in the sequence studied at the Thorne Bar. Figure 7.13 gives the ^{36}Cl data and modeled age and erosion rate for this shoreline. Figure 7.14 shows a plot of the reduced χ^2 for different ages of this shoreline. Table 7.5 presents the results of the reduced χ^2 minimizations under different conditions. Based on the reduced χ^2, the shoreline is 139 ka and has undergone an erosion rate of 0 mm/kyr. The data thus suggests that the shoreline is related to isotope stage 6.

In order to understand how this shoreline relates to OIS 6 versus other oxygen isotope periods the data was modeled as ages of other oxygen isotope periods and the results are given in Table 7.2. The OIS 5 and OIS 7 ages result in reduced χ^2 values that are higher than that of the OIS 6 age and therefore the results are in agreement

with the shoreline being related to a glacial period. In addition, the minimization suggests that for the shoreline to be related to OIS 7, it would have undergone an erosion rate of 3.1 mm/kyr, which would require a total of 43 cm of sediment to have been eroded off the shoreline. The level of preservation and lack of erosion, as previously described, suggests that this age and erosion rate is not a correct solution.

	Age (ka)	Erosion rate (mm/kyr)	Reduced χ^2
^{36}Cl age	139 +/- 21	0	4.6
Eolian inflation	113	-0.7	5.3
Recent silt cap deposition (10 cm)	121	0	4.3
Stone production rate	210	4.3	6.1

Table 7.5. Modeled ages, erosion rates, and χ2 values of theTB00-02 samples, under varying conditions.

The potential effects of silt cap deposition on the shoreline age were also explored and the results are given in Table 7.5. First, a silt accumulation rate of about 0.7 mm/kyr would be required to create a silt cap about 10 cm thick. In this case, the shoreline age would become 113 ka and the reduced χ^2 would be higher than the original minimization. This is about a 19% difference in age, suggesting that a constant silt accumulation could have a greater effect on the age of this shoreline than the shorelines below. The higher reduced χ^2 under this condition supports the original age of 139 ka more than this age.

The second possibility of recent silt cap emplacement required a depth correction of 10 cm to be applied to the sample depths. This condition results in an age of 121 ka and an erosion rate of 0 mm/kyr. This is a 13% difference in the

shoreline age and, because the reduced χ^2 is higher in this case, this condition does not negate the interpretation of an OIS 6 shoreline.

7.6 TB00-03, Elevation 1357 m

This shoreline is the next highest shoreline studied in the Thorne Bar shoreline sequence. The ^{36}Cl data for this shoreline and the modeled age and erosion rate are presented in Figure 7.13 and Figure 7.14 shows a plot of the reduced χ^2 for different shoreline ages. The results of the reduced χ^2 minimization work are given in Table 7.6. The ^{36}Cl data suggests that the shoreline is 258 ka, and related to OIS 8. Table 7.2 gives the reduced χ^2 for shoreline ages of different oxygen isotope stages, and the lowest value corresponds to OIS 8.

The effects of the silt cap on the shoreline age were also investigated and the results are given in Table 7.6. In order to accumulate a silt cap of about 0.15 m thickness over this time span, an accumulation rate of 0.6 mm/kyr is necessary. In this condition, the reduced χ^2 is greater than the original value, which supports the original shoreline age. The result of constant eolian accumulation implies that this condition could result in a maximum difference in the shoreline age of 16%.

The second scenario of recent silt cap emplacement suggests that this condition could affect the shoreline age by as much as 20%. This case could change the age of this shoreline more than the previously discussed shorelines because the feature is older and therefore more sensitive to surficial processes. As indicated by the silt layer below the gravel pavement, the surface has undergone eolian inflation but may also have undergone erosion at some earlier time. A shoreline constructed

during OIS 8 would have undergone several pluvial and interpluvial periods; during these periods the surface would have been susceptible to erosion and eolian

	Age (ka)	Erosion rate (mm/kyr)	Reduced χ^2
^{36}Cl age	258 +/- 38.7	0	2.5
Eolian inflation	218	-0.6	2.8
Recent silt cap deposition (15 cm)	203	0	1.8
Stone production rate	192	0	3.7

Table 7.6. Modeled ages, erosion rates, and reduced χ^2 values of theTB00-03 samples, under different conditions.

deposition, respectively. Therefore, the surface may have a complex history, which may explain why the silt cap emplacement possibilities have greater effects on the age of this shoreline than on the shorelines below it.

7.7 TB00-04, Elevation 1399 m

The highest barrier studied at the Thorne Bar is TB00-04. The ^{36}Cl data and two modeled ages and erosion rates are shown in Figure 7.15. The large range of ages results from the greater amount of total erosion on the shoreline. Depending on the erosion rate selected, the shoreline could be as young as 94 ka or as old as 600 ka. These two end members are not realistic estimates; an age of 94 ka requires no erosion and an age of 600 ka requires a total 6.8 m to be eroded off of the shoreline. This bar may have undergone the effects of a variable erosion rate, as discussed in Section 5. If so, the surface would have experienced little erosion after it was first deposited but, as the pore spaces filled over time, runoff would have increased and therefore erosion rates would have increased as well. The effects of this variable

erosion rate are more distinct for this shoreline than the others because it is older and has been exposed to more eolian deposition and also had more time for erosion to occur. The model age calculations assume a constant erosion rate. An estimate using two different erosion rates over two time periods was attempted and these time periods combined suggest an age of about 400 ka. Based on these observations, the age of the shoreline is probably 400 ka or older. Because the four lower shorelines were found to be related to Pleistocene glacial intervals, it may follow that this

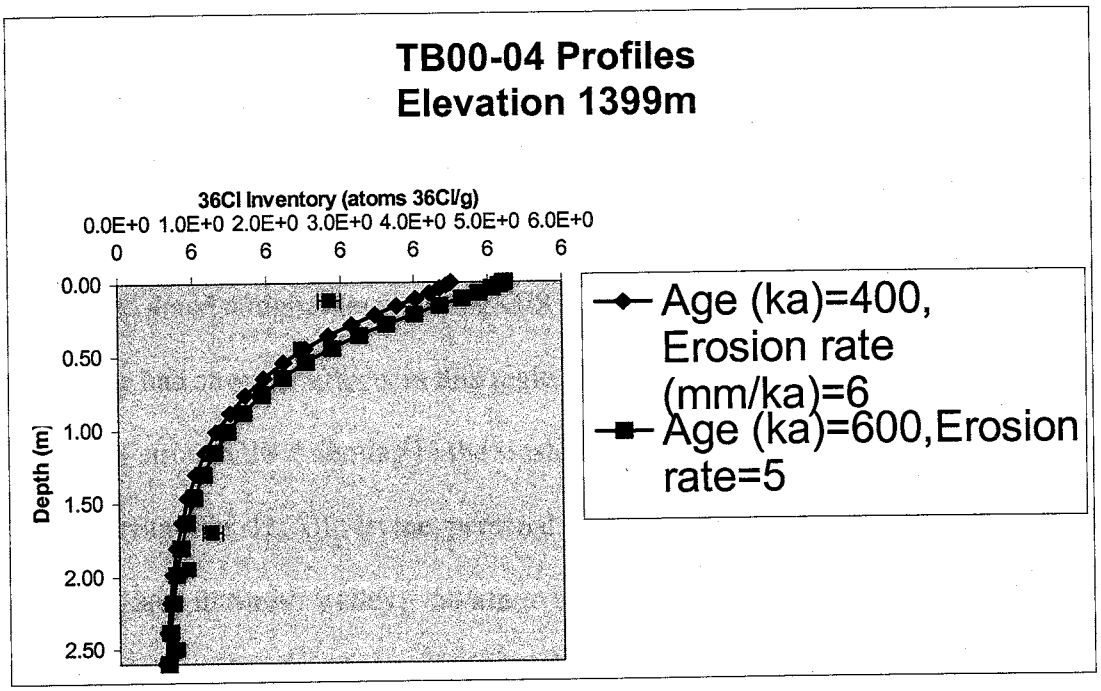

Figure 7.15. ^{36}Cl data and two different modeled ages and erosion rates for TB00-04.

shoreline is also associated with a glacial period. Under this assumption, the ^{36}Cl data is interpreted to suggest that this shoreline is related to OIS 12 or 16. It is hoped that secondary nuclide data from ^{10}Be will help to better constrain the age of this shoreline.

7.8 Implications of the Thorne Bar shoreline ages

The results obtained at the Thorne Bar shoreline complex are significant because they show that Lake Lahontan filled during more pluvial periods and to higher levels than previously thought. The ^{36}Cl data suggests that Lake Lahontan filled during oxygen isotope stages 2, 4, 6, 8, and 12 or 16. Clearly, Lake Lahontan responded to a number of glacial periods during the middle-to-late Pleistocene. The soil data and the independent age confirmations are in agreement with these age interpretations.

The existence of the OIS 4 highstand is notable. This glacial period has been thought to be relatively weak compared to OIS 2 or 6 (Shackleton & Opdyke, 1976). The ^{36}Cl results suggest that Lake Lahontan filled to close to the same level during OIS 2 and 4 and a higher level during OIS 6. This suggests that the OIS 4 cooling may have had stronger effects in this region than previously thought. Evidence for relatively strong OIS 4 cooling in the western Great Basin is not entirely new. Stauffer (Stauffer, H., UC-Irvine, personal communication, 2001) found evidence for an OIS 4 lake in Smith Valley, ~50 km to the west of the Thorne Bar. She found a tephra layer within lacustrine sediments believed to be associated with the most prominent shoreline in the valley. This tephra layer is correlated to a Mono Basin tephra that erupted between 60 and 80 ka. This evidence supports the existence of a large response of the western Great Basin to the OIS 4 cooling period.

The discovery of the existence of an OIS 4 highstand was an unexpected result because TB00-01 was dug into the shoreline thought to be part of the Sehoo Formation. The earlier studies that have hypothesized that the OIS 4 bar was an OIS

2 bar have relied on the elevation of the bar and the soil development. It may be that it is difficult (or impossible at times) to differentiate between OIS 2 and OIS 4 highstands based on soil development alone. The two highstands rose to nearly the same level, indicating that elevation may not always be used to distinguish between bars of these ages.

The maximum elevation of the Sehoo bar means that the Sehoo highstand rose to a maximum level about 4 m higher than the previously-constructed bar at 1330 m (TB00-01); this raises questions as to why there is a high degree of preservation of the OIS 4 shoreline. Several factors probably influenced the Sehoo highstand rise not eroding away the OIS 4 barrier: (1) the Sehoo highstand elevation well above the OIS 4 level and (2) the position of the OIS 4 barrier. If the highstand rose relatively quickly over the OIS 4 barrier to a level about 4 m above it, then the wave action of the OIS 2 lake would not result in significant erosion of the OIS 4 barrier. The OIS 4 barrier is also protected by the main Thorne Bar barrier, which also would favor preservation of it during a later lake rise. The position and elevation of the TB00-01 barrier led to its preservation despite the OIS 2 lake rise.

Finally, these results suggest that, because the dated Thorne Bar shorelines are older with increasing elevation, pluvial cycles in the Lahontan Basin were apparently drier with time. This record contrasts markedly with the Lake Bonneville record discussed in the Introduction. The increasing dryness in the western Great Basin would not have been caused by one distinct factor and would be the result of a combination of factors. Alternatively, the apparent drying trend may be the result of lake level stochastics, and signify random lake level fluctuations. Because these

results suggest that the existence of a drying trend is possible, further investigation into this subject is warranted.

8 NEWARK VALLLEY RESULTS AND DISCUSSION

8.1 Geologic background

Newark Valley, in south-central Nevada (Figures 1.1 and 1.2), is the second site that was investigated for this work. A map of Newark Valley is presented in Figure 8.1. The Diamond Mountains and Fish Creek Range bound the valley to the west, the Ruby Mountains and Alligator Ridge are to the east, and the Pancake Range and Moody Mountains are to the south. The average elevations of the crests of these ranges are between 2,500 and 2,900 m. The lowest elevation within the basin is 1,778 m (Redwine, 2003, *in progress*).

Russell (1885) thought that Newark Valley was never connected to the Lake Lahontan drainage basin. Hubbs and Miller (1948) believed that Lake Newark, at a high level before OIS 2, was connected to Lake Lahontan, based on shoreline and ichthyologic evidence. Mifflin and Wheat (1979) noted OIS 6 shorelines higher than the late Pleistocene level near the south end of the basin but suggested that, because of regional basin tilting, the OIS 6 lake was not necessarily larger than the OIS 2 lake. They attributed the higher OIS 6 shorelines preserved on the southern end of the basin to regional northward tilting of the Lahontan Basin. They believed that the largest pluvial lake in Newark Valley occurred during OIS 2.

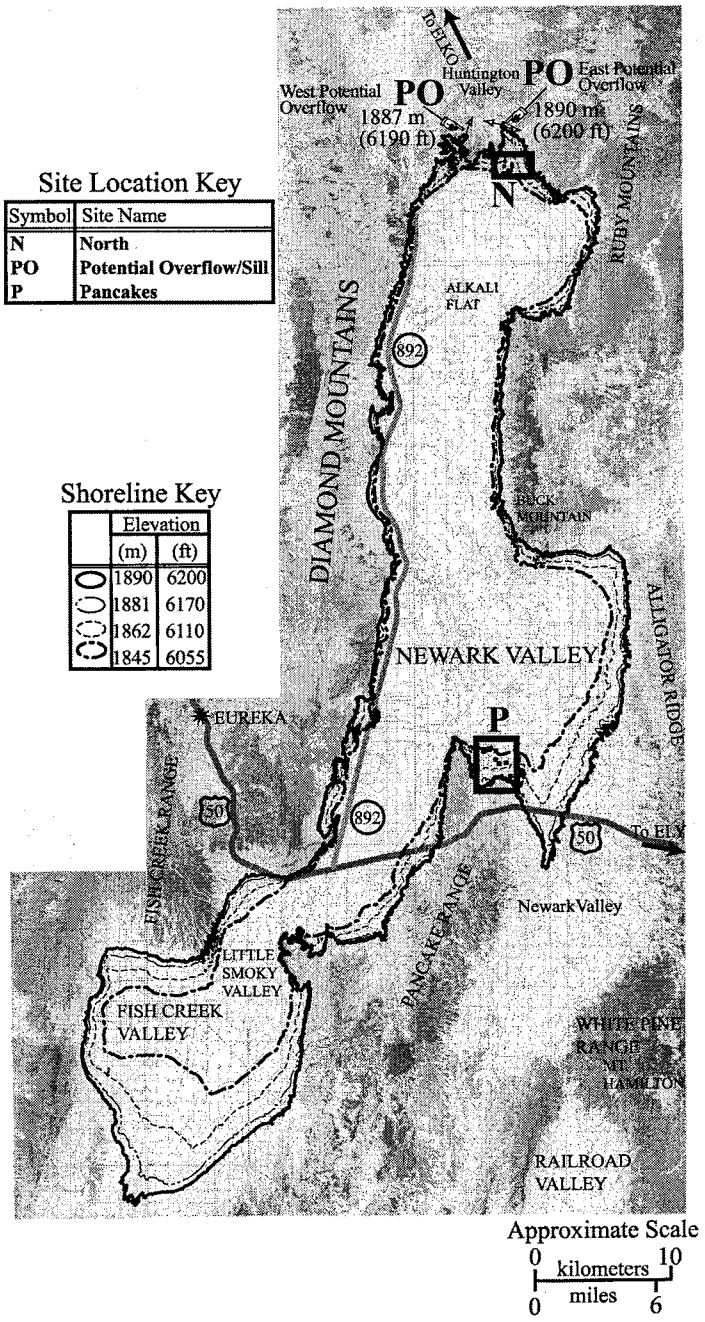

Figure 8.1. Location map of Newark Valley showing the Pancake (P) and North (N) sites, as well as the locations of possible overflow into the Lahontan system. Modified from Reheis et al. (*in press*).

Since then, other high shorelines (possibly OIS 6) have been observed at similar altitudes on the north and east sides of the basin, suggesting little basin tilting has occurred in this region (Redwine, 2003, *in progress*). Reheis (1999) noted higher shorelines in Newark Valley and tentatively correlated them to OIS 16, 6, and 2, with elevations decreasing with younger age. Redwine (2003, *in progress*) performed an extensive study correlating shorelines in the basin on the basis of similar elevations and soil development. She concluded that the highest suite of lacustrine deposits correlate with OIS 16, the suite of high well preserved shorelines correlate with OIS 6 and the lowest suite of preserved shorelines correlate to OIS 2.

Evidence for a pluvial connection between Lake Newark and Lake Lahontan is limited. There are two possible overflow localities in the northern part of the basin (Figure 8.1); both would mean overflow through Huntington Valley and into the Southern Humboldt River. The possible overflow channels are shallow with gentle slopes, suggesting that, if overflow occurred in either, it was intermittent and not continuous or catastrophic. The gentle slopes also suggest that, during overflow, the lake level would have been close to the overflow level because of the absence of strong downcutting. It is also possible that overflow occurred in both channels at the same time, especially because they are so similar in appearance.

Hubbs and Miller (1948) found ichthyologic evidence of a connection between Lakes Lahontan and Newark at Newark's highest recorded level. The fish data support this conclusion because springs within the remnants of pluvial Lake Newark are inhabited by a chub species, *Gila bicolor newarkensis*, which is similar to a common Lahontan fish now found in the Humboldt River, *Gila bicolor obesa.*

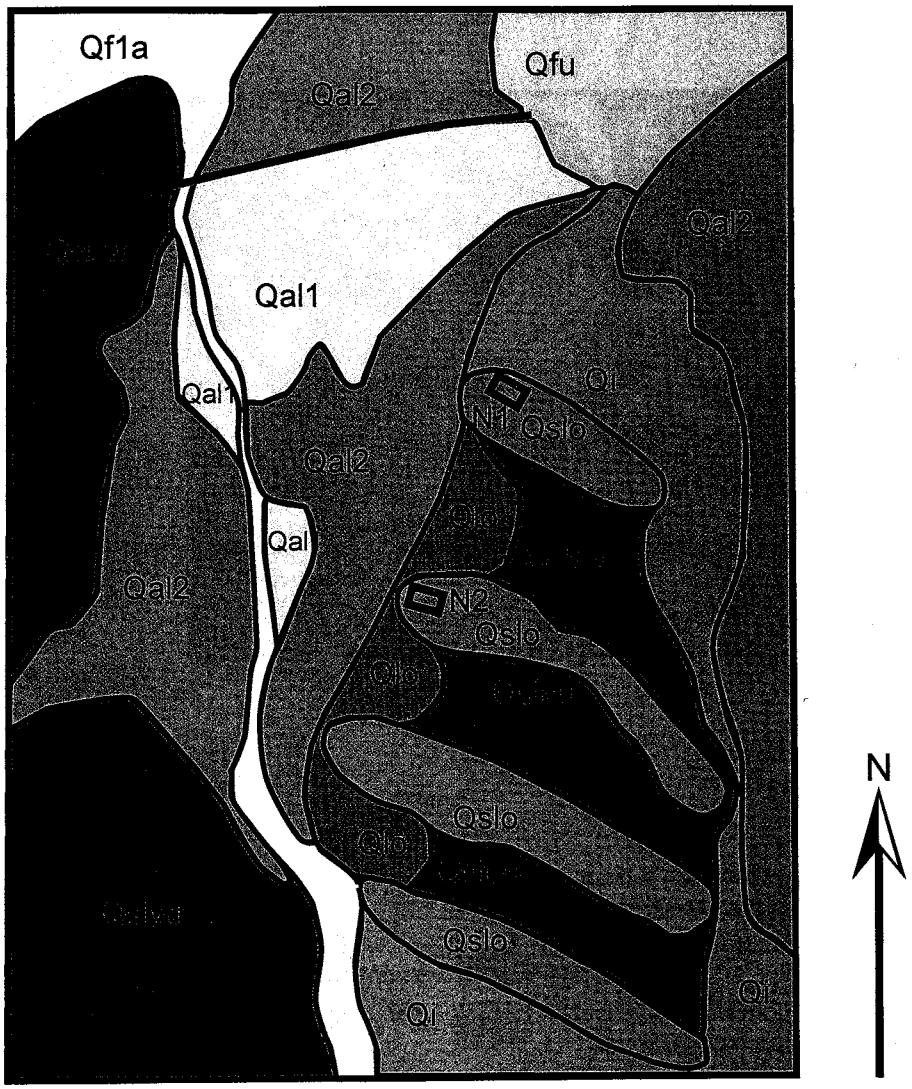

Scale 1:12,000

Legend

- Qal1 — Quaternary modern alluvium.
- Qf1a — Quaternary alluvial fan, youngest, but too high to interact with shorelines.
- Qal2 — Quaternary alluvium, commonly arroyo deposits.
- Qi — Quaternary indistinguishable.
- Quaternary shorelines, young and undifferentiated.
- Qslo — Quaternary shorelines, old, with distinct beach barriers.
- Quaternary shorelines, old and undifferentiated.
- Qlo — Quaternary lake deposits
- Qfu — Quaternary alluvial fans, undifferentiated by age.
- Fault

Figure 8.2. Geologic map of the north end of Newark Valley, where two shorelines were sampled for cosmogenic nuclide dating. Modified from Redwine, 2003, in progress.

Scale 1:40,000

Legend

- Qf1b — Quaternary alluvium and fan deposits, younger than Qf1a.
- Qf1a — Quaternary alluvium and fan deposits, younger than latest Pleistocene shorelines.
- Quaternary shoreline features, associated with Qsly.
- Quaternary shoreline deposits, latest Pleistocene.
- Quaternary alluvial fan deposits.
- Quaternary shoreline deposits correlative with marine oxygen isotope stage 6.
- Qf3 — Quaternary alluvial fan deposits older than Qslo.
- Mississippian Diamond Peak Formation, conglomerate and sandstone facies.
- Fault (approximate location)

Figure 8.3. Geologic map of the Pancakes locality of Newark Valley, where three shorelines were sampled for cosmogenic nuclide dating. Modified from Redwine, 2003, in progress.

There are three levels of beach gravels in Newark Valley (Redwine, 2003, *in progress*). Each level is less distinct with increasing elevation, suggesting that higher shoreline remnants are older. In general, the shoreline gravels in Newark Valley are less mature than those at the Thorne Bar. Within all the shorelines studied in Newark Valley, the gravels are more angular than the Thorne Bar gravels and sorting is weaker. Two specific localities of old, high shorelines in Newark Valley were selected for this study; geologic maps of these areas are presented in Figures 8.2 and 8.3. Figure 8.2 is a geologic map of the "North" site, labeled N on Figure 8.1. Figure 8.3 is a geologic map of the "Pancakes" site (P on Figure 8.1), so named because of its proximity to the Pancakes Range. Specific shorelines from this study that are located in the southeastern area of the valley are labeled P1, P2, and P3, and shorelines in the northern part of the valley are identified as N1 and N2.

Remnants of the highest lake levels consist of rounded beach gravel lags on bedrock slopes. There is little shoreline morphology preserved at these levels and highstands are commonly identified as erosional benches that resemble wavecut platforms. This evidence of very high lake levels is found at elevations of up to about 1890 m, the

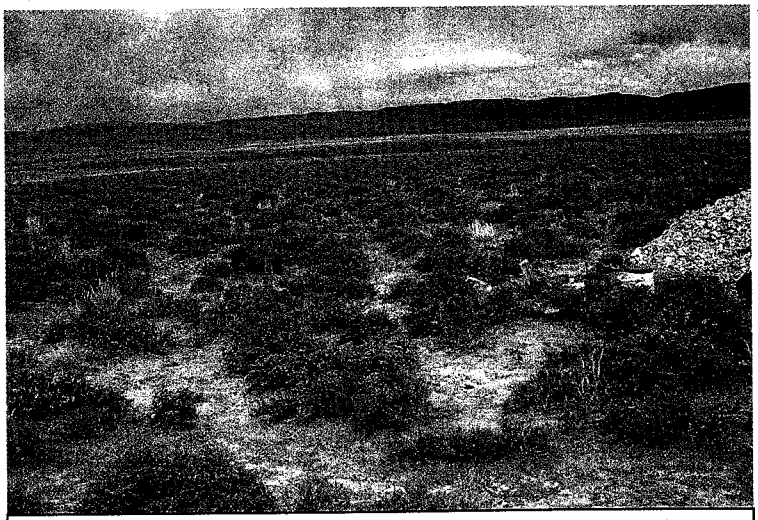

Figure 8.4. View of the P1 shoreline surface with debris from the trench visible on the right side.

level of the modern overflow threshold and possibly the overflow level of Lake Newark.

The second group of beach deposits in Newark Valley is the older, preserved shorelines. These shorelines are generally thought to (1) correlate to OIS 6 (Redwine, 2003, *in progress*) and (2) be the Eetza equivalent deposits (Morrison, 1964). The shorelines sampled for ^{36}Cl dating from this group are P3, P2, P1, and N1 but, as discussed below, the ^{36}Cl data suggests that P1 is actually associated with the youngest group of shorelines. The top of P1 is shown in Figure 8.4. Photos of the insides of these trenches are shown in Figures 8.5, 8.6, 8.7. Redwine (2003, *in progress*) believed that the soil development and associated index calculations support this conclusion. In addition, she found that amino acid racemization (AAR) analyses on freshwater snails suggest an OIS 6 age for this suite

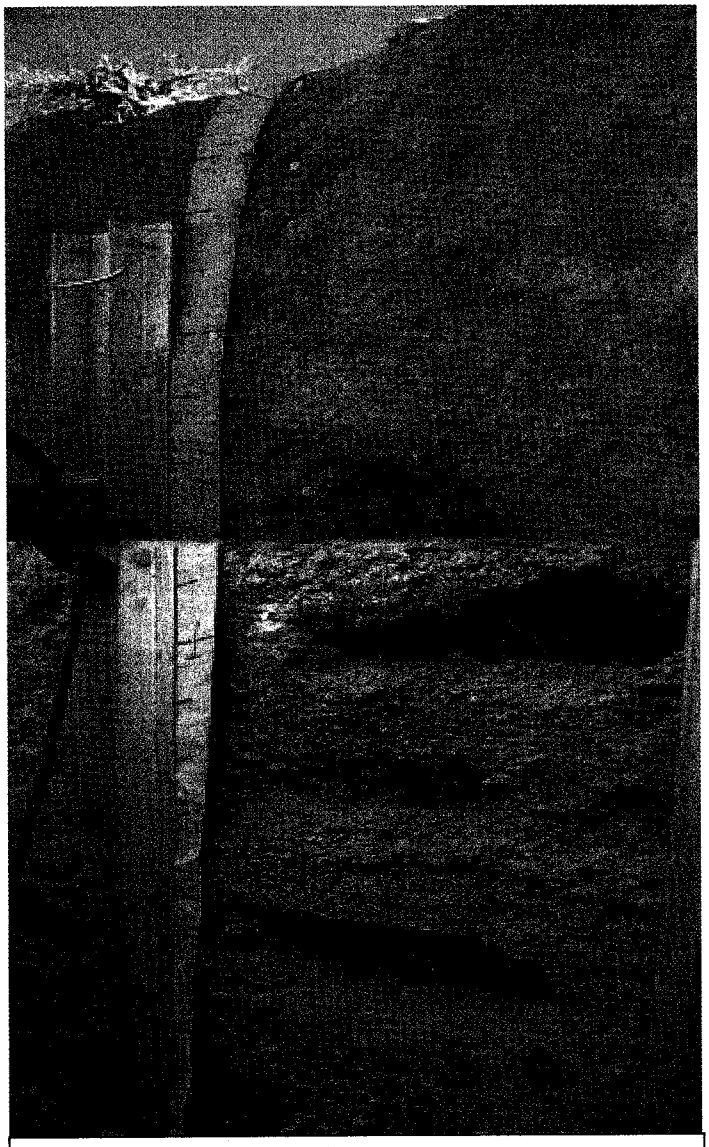

Figure 8.5. Photo of the inside of pit P3 with sample locations indicated by green circles.

of shorelines. These shorelines are found within an elevation range of 1848 and 1866 m; she stated that the 1866 shoreline represents the highest OIS 6 highstand.

The shorelines higher than 1860 m in the northern part of the basin and are likely affected by faulting. The degree of deformation on these shorelines is not well defined so she described them as potential OIS 6 highstands, without correlative shoreline elevations elsewhere in the basin.

Table A3 gives the soil horizons and soil laboratory data for the Newark Valley shorelines. The profile masses of carbonate, silt, and clay are presented in Figures 8.8, 8.9, and 8.10. The profile masses of carbonate may not be a good indicator of soil development at these sites because there is a large source of Mississipian limestone on the north side of the valley. This results in higher accumulation rates of carbonate material, and Stage III carbonate development is often interpreted to mean the soil is OIS 6 in age (Redwine, 2003, *in progress*). For example, Redwine (2003, *in progress*) reported that based on the carbonate development, the similarity in soil profile indices to the other OIS 6 shorelines, and an elevation correlation to other OIS 6 shorelines that P1 is an OIS 6 shoreline. Her evidence may contradict the ^{36}Cl age, but it is also possible that P1 is an OIS 2 shoreline, for reasons discussed below.

First, the carbonate development may be apparently greater than expected for OIS 2 shorelines at the Pancakes site due to a large eolian input of carbonate material. If the dominant wind direction during interpluvials were north to south, then one would expect to find more carbonate at the south end of the basin because of the limestone source at the north end of the valley. Winds would carry carbonate material both off the exposed limestone bedrock and off the playa and relatively large amounts of carbonate could have been caught by the shoreline. Field observations indicate that soils in the Pancake site have thicker silt caps than in the North, supporting the hypothesis that the dominant winds come from the north.

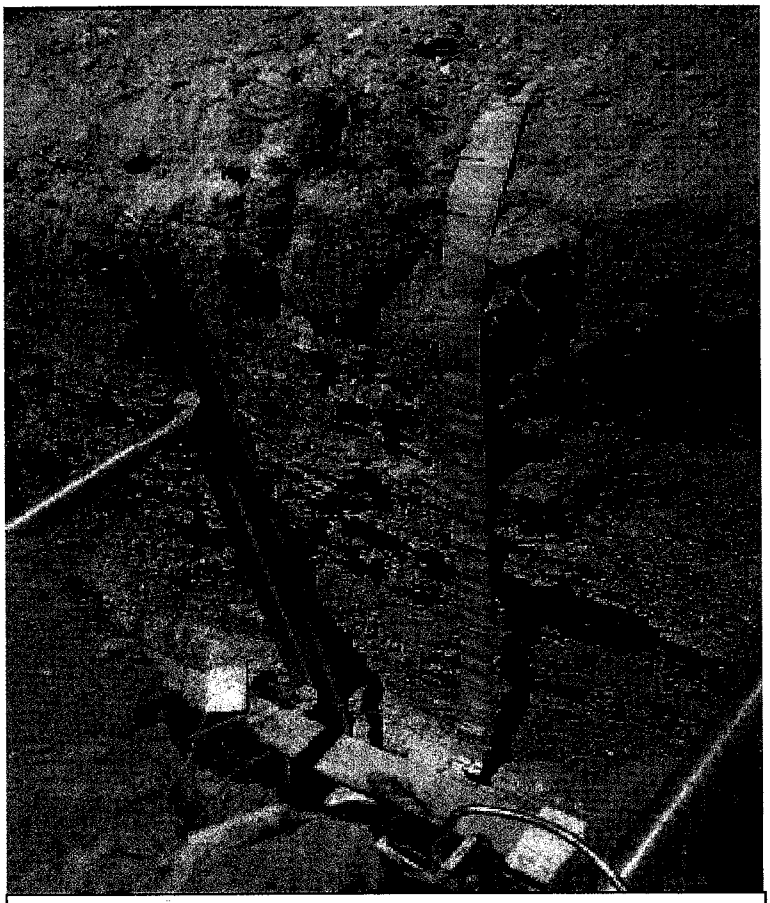

Figure 8.6. Photo of the inside of pit P2 (sample locations not available).

A second source for the relatively large amounts of carbonate material in P1 is primary carbonate deposition from the lake itself. If the OIS 2 lake were relatively enriched in carbonate due to carbonate-rich inflows or the erosion of limestone

bedrock, it is possible that relatively large amounts of carbonate were deposited along with the shoreline gravel during the lake event.

In addition, the elevation of the shoreline may correlate to other OIS 6 shorelines, but P1 is one of the lowest shorelines that Redwine (*in progress*) specifies as within the OIS 6 elevation range. At 1849 m, P1 is the lowest shoreline studied at the Pancakes site. According to Redwine (2003, *in progress*), the OIS 6 shorelines range between 1848 and 1866 m while the OIS 2 shorelines at an elevation of 1845 m or below. If there were problems constraining some shoreline elevations, then the intermediate status of P1 may support the possibility that this shoreline is related to OIS 2, not OIS 6. Therefore, the soil development and elevation of P1 may not be unequivocal evidence of an OIS 6 shoreline.

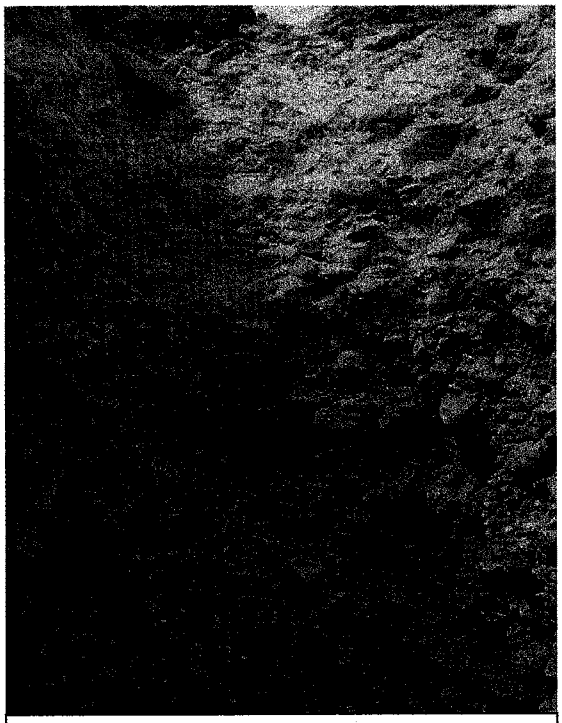

Figure 8.7. Photo of the inside of pit P1 (sample locations not available).

The profile masses suggest that N1 and P3 are the oldest shorelines because they contain the greatest amounts of carbonate, silt, and clay. This may support the hypothesis that they are related to OIS 6. N1 is a higher shoreline in the north end of the valley studied for this work. Soil development and the shoreline elevation support an OIS 6 age for this shoreline. When the N1 profile mass is compared with N2

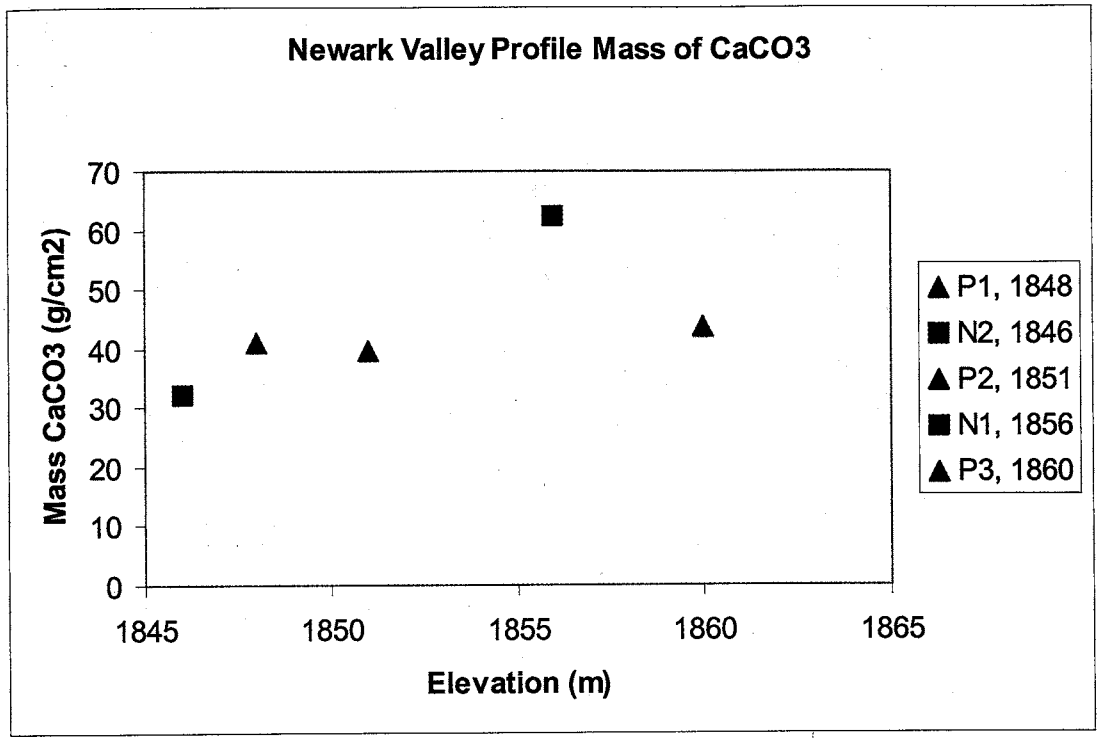

Figure 8.8. Profile masses of carbonate for the Newark Valley shorelines.

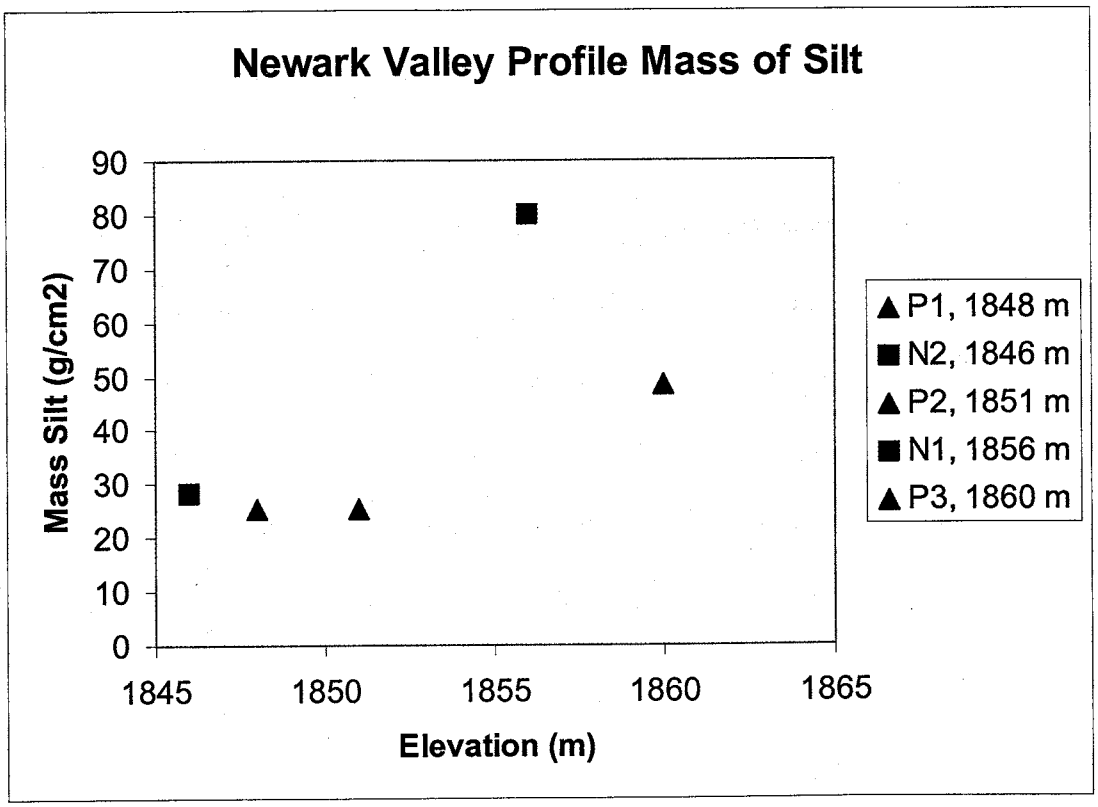

Figure 8.9. Profile masses of silt for the Newark Valley shorelines.

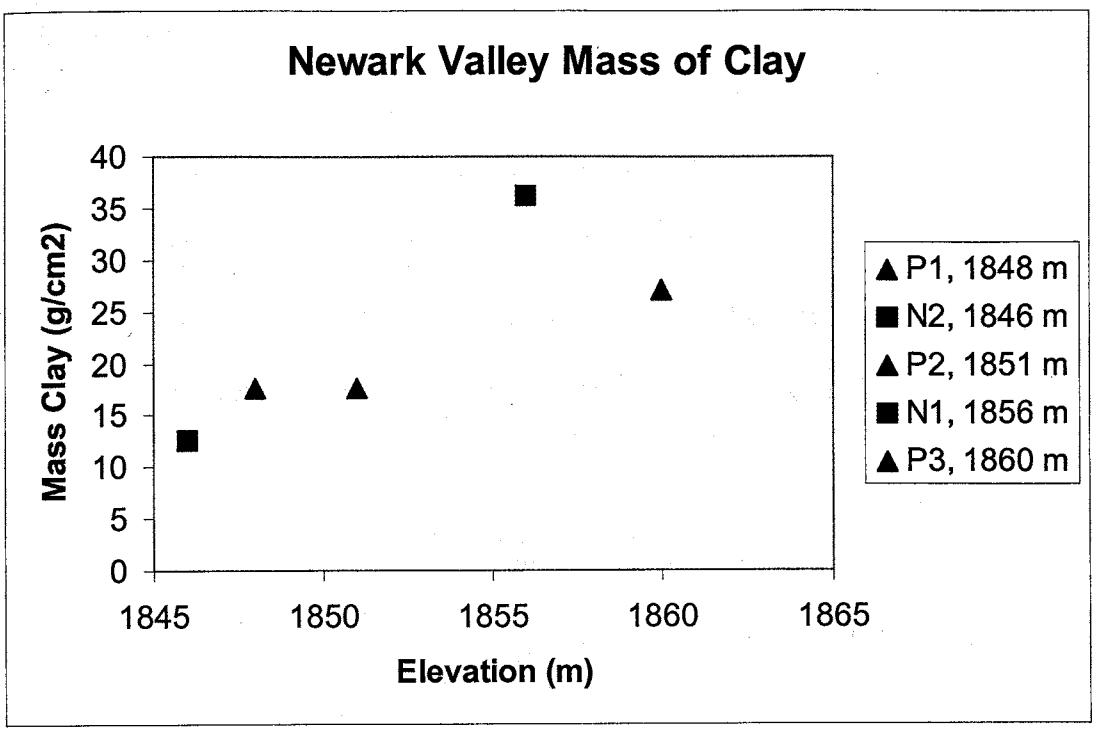

Figure 8.10. Profile masses of clay for the Newark Valley shorelines.

the data suggest that N1 is an older soil than N2 because its profile masses of carbonate, silt and clay are greater than N2. It also corresponds in elevation to other OIS 6 shorelines in Newark Valley.

The elevation of P3 also corresponds to other OIS 6 shorelines in the valley (Redwine, 2003, *in progress*). It has higher profile masses of silt and clay than the lower two shorelines, suggesting that it is older than the other shorelines studied at the Pancakes site.

P2 contains lower profile masses of carbonate, silt, and clay, but it falls within the OIS 6 group of shorelines (Redwine, 2003, *in progress*). The elevation corresponds to other OIS 6 shorelines in the valley. P2 has less carbonate and similar masses of silt and clay as P1. As discussed above, P1 may appear relatively old because of its high carbonate content but carbonate content may be misleading in Newark Valley. The data suggest that P2 is younger than P3 because P3 has greater

masses of these materials. Therefore, P2 corresponds to OIS 6 based on its elevation, but the soils data could suggest an OIS 6 or younger age.

The shorelines in this grouping contain gravel-free silt layers underlying a gravel pavement, but their morphologies are less distinct than the Thorne Bar shorelines. This suggests that erosion has probably modified the surfaces more than surface inflation has, but since the shorelines are still readily identified, erosion rates have been low.

Particle size distributions on the older suite of Newark Valley shorelines of Redwine (*in progress*) indicate one main grain size within the eolian caps. A bimodal grain size distribution could have suggested a minimum of two different eolian pulses, possibly from different interpluvial periods. The grain size distribution suggests that the silt caps were stripped off of the shorelines, probably during later pluvial periods. Stripping of the eolian caps means that some erosion

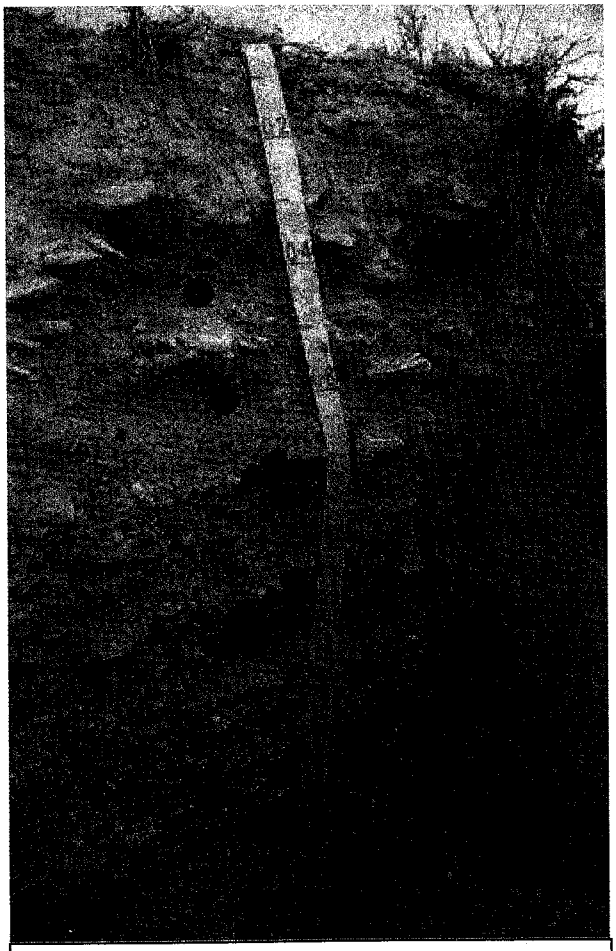

Figure 8.11. Photo of the inside of pit N2, with sample locations indicated by green circles.

of the gravel part of the shorelines may also have occurred. The possibility of erosion is supported by the gentle slopes of these shorelines; the morphology is less distinct than the Thorne Bar shorelines.

The third group of beach deposits is the younger suite of preserved shorelines, thought to be correlative with OIS 2 (Hubbs and Miller, 1948; Mifflin and Wheat, 1979; Reheis, 1999; and Redwine, 2003, *in progress*), and the Sehoo equivalent (Morrison, 1964). These shorelines are easily identified in Newark Valley because of their youthful shoreline morphology and the large number of rounded shoreline gravel found on their surfaces. A ^{14}C AMS age from lacustrine deposits associated with this shoreline level yielded an age of 13,780 $^{+}$/- 50 year, confirming the previous interpretations (Redwine, 2003, *in progress*). The highest of the OIS 2 shorelines is found at 1845 m and shorelines below this level are tentatively interpreted to be recessional features of this level. The shoreline at 1845 m is found at multiple localities throughout the basin and the soil development as well as shoreline morphology is consistent among them.

Of the shorelines sampled for this work, P1 may be related to the OIS 2 shorelines and N2 (Figure 8.11) is most likely related to OIS 2. The profile masses of carbonate, silt, and clay suggest that N2 is younger than N1. Furthermore, ^{14}C obtained from nearby lacustrine deposits at this elevation that yield OIS 2 ages (Redwine, *in progress*).

Like the OIS 6 shorelines, these features also show evidence of erosion. They both contain gravel-free silt layers underlying a gravel pavement, but the morphologies are less distinct and characterized by gentle slopes. This suggests that

erosion rates have been low, but that erosion has probably modified the surfaces more than surface inflation.

8.2 Newark Valley results

During June of 2000, three trenches were dug into three shorelines at the south end of the valley with a backhoe. Two other trenches in the north end of the valley, dug during the summer of 1999, were also sampled for this work. The geographic

Shoreline	Elevation (m)	Latitude	Longitude	Characteristic Features	Age (ka)	Estimated erosion Rate (mm/kyr)	Average Inheritance (atoms ^{36}Cl/g)
P1	1849	39.452011 48°	-115.6725 138°	Stage III carbonate	30	3	2.16×10^6
P2	1854	39.455982 15°	-115.6748 28°	Multiple stratigraphic changes	138	0.9	2.76×10^6
P3	1863	39.452717 54°	-115.6662 751°	Large amounts of gypsum	179	2	1.53×10^6
N1	1856	39.461941 61°	-115.6869 881°		155	2.6	1.19×10^6
N2	1846	39.461556 62°	-115.6846 083°	^{14}C data suggest OIS 2	~15 or 75	~1	1.3×10^6 or 1.9×10^6

Table 8.1. Geographic locations, elevations, as well as modeled ages and erosion rates before silt deposition analysis for the Newark Valley shorelines.

coordinates of the trenches, shoreline elevations, and determined ages before silt deposition analysis of each shoreline are given in Table 8.1. This section presents the ^{36}Cl ages of the shorelines and a discussion of these ages.

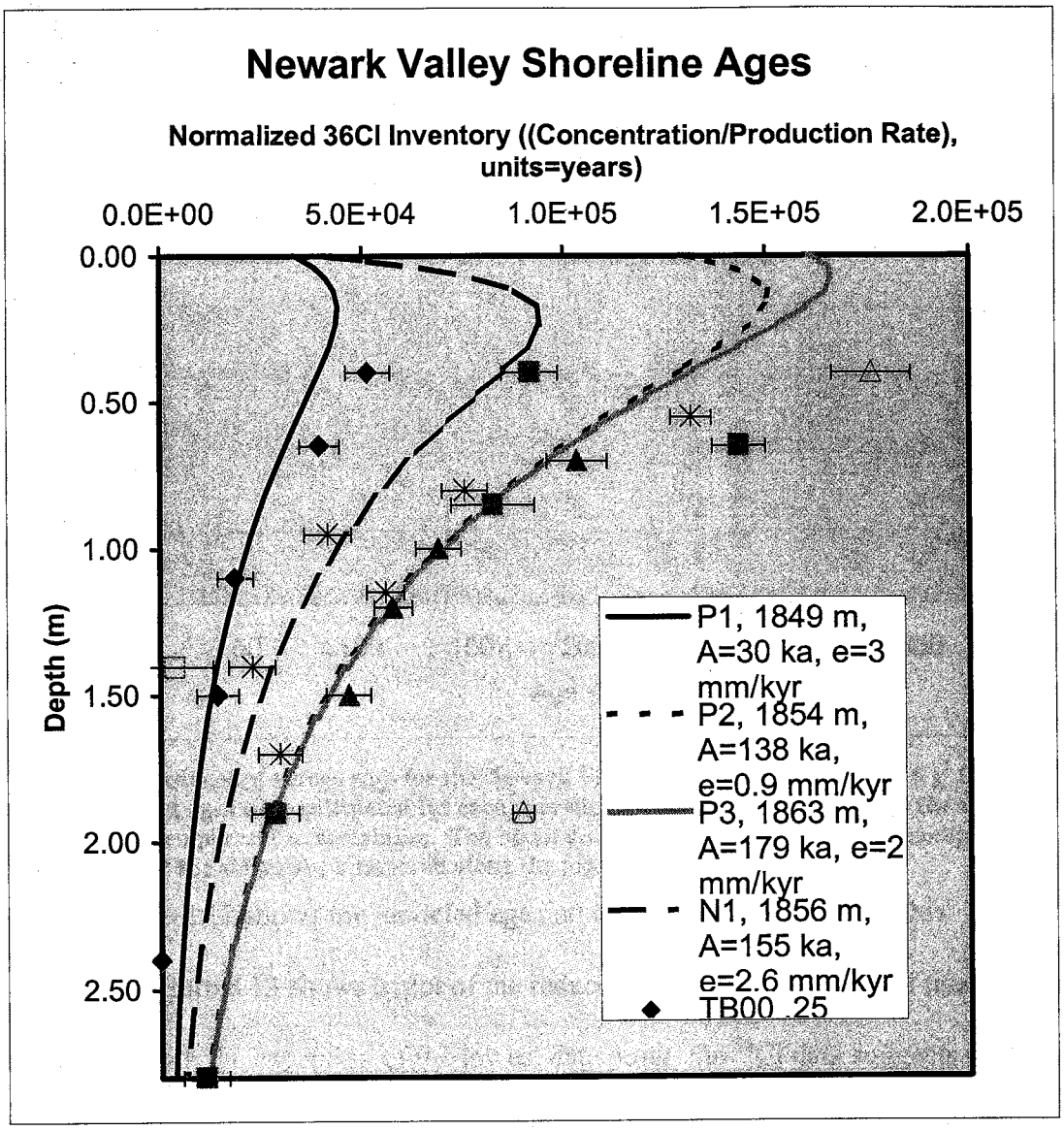

Figure 8.12. Normalized ^{36}Cl data with modeled ages and erosion rates for the Newark Valley shorelines. Inheritance has been subtracted out and the samples and curves have been normalized by the average production rate of each profile. Hollow symbols indicate outlying samples that were not included in the reduced χ^2 minimization.

8.3 P1: Elevation 1849 m

The shoreline P1 is the lowest shoreline sampled for cosmogenic nuclides on the southeastern end of the valley near the Pancakes Range. The location of this trench is shown on the geologic map of the Pancakes site (Figure 8.3).

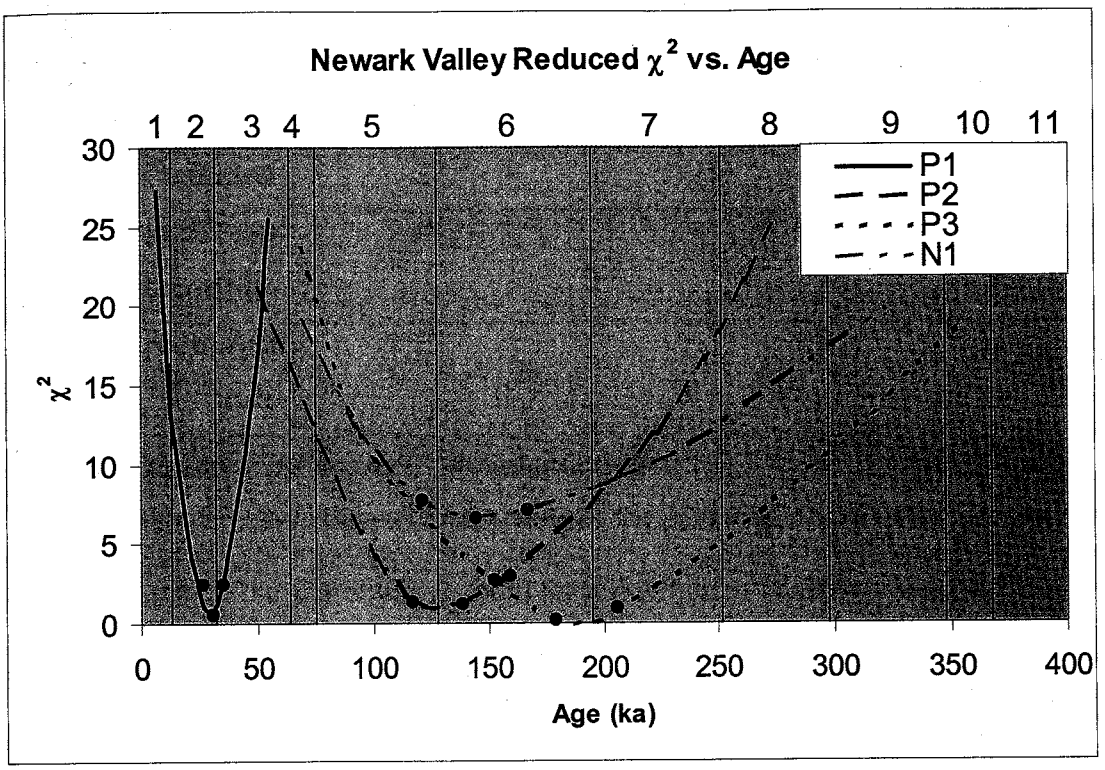

Figure 8.13. Reduced χ^2 versus ages for the Newark Valley shorelines. The reduced χ^2 for several different ages were calculated for each shoreline. Black dots correspond to the shoreline age and to fifteen percent uncertainties. The black lines represent marine oxygen isotope stage boundaries and the stages are numbered along the top.

Figure 8.12 shows the modeled age and erosion rate scenario for this shoreline. Figure 8.13 shows a plot of the reduced χ^2 for different ages of this shoreline. With the exception of the lowest data point, the ^{36}Cl data suggests that this shoreline is related to OIS 2. Table 8.2 gives the age and erosion rate for this shoreline using the reduced χ^2 minimization under different conditions.

Table 7.2 gives the modeled results if the shoreline were related to an oxygen isotope period other than OIS 2. The reduced χ^2 values are higher for these time periods than for the OIS 2 age, which supports the hypothesis that lake cycles occurred during glacial periods. The higher reduced χ^2 for an OIS 6 age also supports the OIS 2 age instead of an OIS 6 age, as suggested by the soil development (Redwine, *in progress*).

	Age (ka)	Erosion rate (mm/kyr)	Reduced χ^2
^{36}Cl age	30 +/- 4.5	3	0.7
Eolian inflation	23	-10	1.6
Recent silt cap deposition	21	3	2.1
Stone production rate	17	3	1.3

Table 8.2. Results of the reduced χ^2 minimization for P1.

Table 8.2 gives the modeled results of the potential effects of the silt cap emplacement on the shoreline age, both for a situation of constant eolian inflation and for a situation of recent silt cap emplacement. Both reduced χ^2 values for these scenarios are somewhat higher than without the silt cap corrections, suggesting that the original ^{36}Cl age is most correct. Under these two silt cap scenarios, the shoreline ages could change as much as 30%, but because these scenarios test the maximum possible effects on the shoreline age, the 30% age change is also a maximum. In addition, the shoreline ages in these two cases are within the boundaries OIS 2, supporting the initial calculated age.

8.4 P2: Elevation 1854 m

P2 is the second highest shoreline at the Pancakes site sampled for this work. The location of the trench is shown in Figure 8.3. Figure 8.12 shows the ^{36}Cl data for this shoreline and the modeled age and erosion rate. Figure 8.13 shows a plot of the reduced χ^2 for different ages of this shoreline. This ^{36}Cl profile shows more scatter among the sample ^{36}Cl concentrations than the others presented thus far. The data point at 1.40 m is an outlier based on a stratigraphic variation within the profile.

Field notes indicate that there are stratigraphic breaks at depths of about 1.30 m and about 1.50 m, with finely bedded pebbles and sand lenses in between. This break suggests the presence of a stratigraphic variation that may have favored a specific source area enough to skew the sample towards an inherited component less than the average inheritance of the profile. The five remaining points suggest that this is an OIS 6 shoreline.

	Age (ka)	Erosion rate (mm/kyr)	Reduced χ^2
^{36}Cl age	138 +/- 21	0.9	1.2
Eolian inflation	138	-0.7	2
Recent silt cap deposition	126	1.6	1.4
Stone production rate	143	0.5	1.2

Table 8.3. Results of the chi-squared minimization of the ^{36}Cl data for P2.

8.5 P3: Elevation 1863 m

P3 is the highest shoreline on the south end of the valley studied for this work. The location of the trench dug into this shoreline is indicated on Figure 8.3. Figure 8.12 shows the ^{36}Cl data for this shoreline and the modeled age and erosion rate. Figure 8.13 shows a plot of the reduced χ^2 for different ages of this shoreline. The ^{36}Cl data suggest that the shoreline is about 179 ka, suggesting the shoreline was constructed during OIS 6. The lowest point (1.90 m) and the highest point (0.40 m) in the data do not correspond to the rest of the samples and were regarded as outliers during the minimization. The outlier at 1.90 m can be explained by differences in the bulk chemistry. Figure 8.14 shows the abundances of certain elements in the profile

for each sample. The lowest sample shows differences in these abundances from the other samples, suggesting a difference in source material for this sample. The differences in abundances also result in a higher production rate for this sample than the other samples in the profile, due to elevated amounts of calcium and potassium (two major ^{36}Cl producers). If the source material is different for one particular sample in the profile, then the assumption of an equal average inherited component for all samples is invalid. Therefore, the lowest sample is an outlier that cannot be used to constrain the age of this shoreline.

The sample point at 0.40 m cannot be explained by chemical differences but can be explained by stratigraphic variations within the profile. According to field notes, there is one stratigraphic break at about 0.50 m depth. This suggests that the material above that point may have been deposited at a later time than the material below it, or that the material above that point is from a source area with an inherited component different from the average inheritance of the profile.

	Age (ka)	**Erosion rate (mm/kyr)**	χ^2
^{36}Cl age	179 +/- 27	0.9	1.9
Eolian inflation	138	-0.7	3
Recent silt cap deposition	126	1.6	2.1
Stone production rate	114	4.5	0.2

Table 8.4. Results of the reduced χ^2 minimization of the ^{36}Cl data for P3.

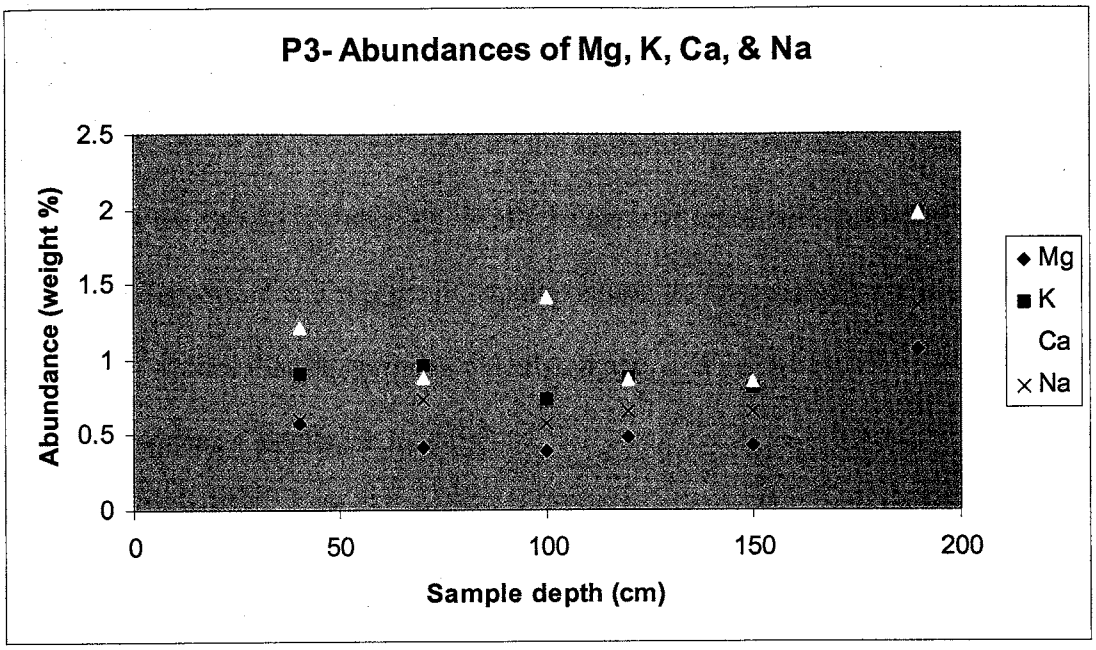

Figure 8.14. Abundances of selected elements in the P3 samples.

Table 7.2 presents the results of the reduced χ^2 minimizations during different oxygen isotope stages. The differences in the reduced χ^2 if the shoreline were constructed during an interglacial period (vs. a glacial period) were calculated and the reduced χ^2 for an interglacial age is slightly larger than for the glacial age, supporting the correlation between lake cycles and glacial intervals. Table 8.4 gives the potential effects of eolian inflation on the shoreline age. Both scenarios produce higher reduced χ^2 values.

8.6 N1: Elevation 1856 m

Figure 8.12 shows the ^{36}Cl data from N1 with the modeled age and erosion rate of the shoreline. Figure 8.13 shows a plot of the reduced χ^2 for different ages of this shoreline. The ^{36}Cl data suggests that the shoreline is about 144 ka, or related to OIS 6. Table 8.5 gives the results of the reduced χ^2 minimizations under different conditions for N1. The reduced χ^2 for this shoreline is relatively large. The

minimizations for the shoreline to be constructed during an interglacial period (OIS 5 or OIS 7) are also relatively large (Table 7.2).

The effect of eolian inflation on the shoreline age was also investigated and the results are shown in Table 8.5. Both the simulation of constant inflation since shoreline deposition and recent silt cap deposition do not produce significantly larger reduced χ^2 values than the original calculated age, and the recent silt cap deposition results produces a smaller reduced χ^2.

	Age (ka)	Erosion rate (mm/kyr)	Reduced χ^2
^{36}Cl age	155 +/- 23	2.6	6.7
OIS 5	126	0.5	6.7
OIS 7	191	3	7.3
Eolian inflation	106	-1.9	6.8
Recent silt cap deposition (30 cm)	103	2.9	5.5
Stone production rate	160	2.8	6.7

Table 8.5. Results of the reduced χ^2 minimization for the ^{36}Cl data of N1 for different conditions.

8.7 N2: Elevation 1846 m

The lower shoreline studied in the north end is N2. Like N1, the clast composition is heterogeneous and the clast size range is variable. Figure 8.10 is a photograph of the inside of N1 and shows some of the variability in clast size.

The ^{36}Cl results for this profile are less definitive than the others in this work. Figure 8.15 shows these results along with the modeled ages and erosion rates. Depending on which data points are selected, the shoreline could be OIS 2, 4 or

possibly 6 in age. In this case, field notes do not suggest that certain points may be stratigraphic outliers. Therefore, the ^{36}Cl data is equivocal for this shoreline.

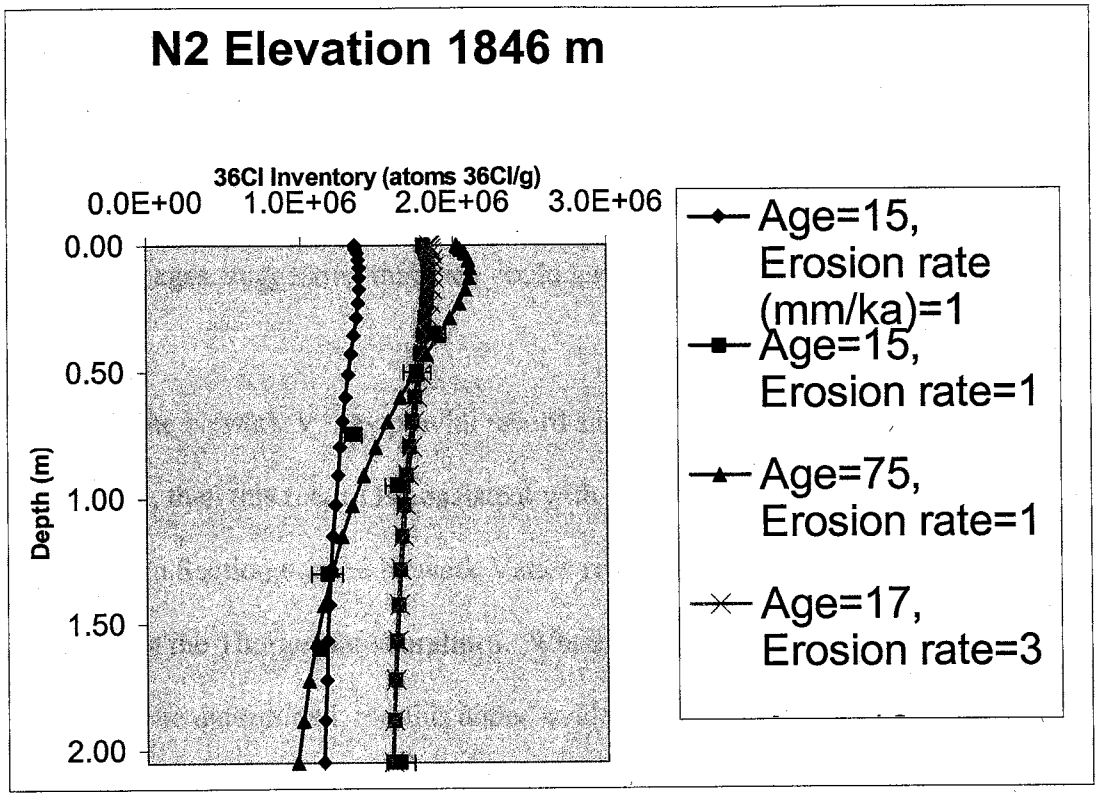

Figure 8.15. ^{36}Cl data and modeled ages for N2.

8.8 Implications of the Newark Valley shoreline ages

The Newark Valley shoreline record suggests that there were pluvial lakes in Newark Valley during OIS 2 and OIS 6. The OIS 6 highstand was greater in magnitude than the OIS 2 highstand. With the exception of results from P1, this interpretation of the ^{36}Cl data is supported by the degrees of soil development. In addition, they are supported by the available ^{14}C and AAR dates. The ^{36}Cl data suggests three different ages for the OIS 6 shorelines: (1) an elevation of 1863 m (P3) at 179 ka, (2) an elevation of 1856 m (N1) at 144 ka, and (3) an elevation of 1854 m (P2) at 138 ka. The OIS 6 ages apparently decrease with decreasing elevation. This

may suggests that the OIS 6 lake in Newark Valley rose to first to 1863 m and stayed at this elevation long enough to construct a shoreline. Then the shoreline may have dropped steadily or fluctuated in level before staying at an elevation of 1856 m long enough to construct another shoreline. Finally, the lake level may have dropped steadily or fluctuated in level once again until about 138 ka, when it recorded a shoreline at 1854 m. Alternatively, all three highstands are within the error margins of the ^{36}Cl ages, suggesting that they could have all three formed at about the same time.

If the Newark Valley pluvial record suggests a larger highstand during OIS 6 than OIS 2, then this record is consistent with the Thorne Bar shoreline record presented in Section 6. The Newark Valley record supports the apparent drying trend observed in the Thorne Bar shorelines. Whether the trend is actual or apparent remains to be determined, but this added evidence of a trend suggests that its existence warrants future investigations.

Another notable aspect of the Newark Valley record is the absence of a preserved OIS 4 shoreline. This contrasts to the Thorne Bar shorelines of Lake Lahontan, which does have an OIS 4 shoreline preserved. There may still have been a lake cycle during OIS 4 in Newark Valley. It is possible that an OIS 4 shoreline preserved in Newark Valley that was not incorporated into this study. Alternatively, if there was a lake during OIS 4, it may have reached a level close to but below the OIS 2 shoreline, and under this scenario the evidence of this highstand could have been erased during the OIS 2 lake cycle. Pluvial Lake Newark was only connected to

Lake Lahontan at its very highest levels, so it is not unreasonable to expect different records in the two basins.

9 COLUMBUS SALT MARSH RESULTS AND DISCUSSION

9.1 Geologic Background

Columbus Salt Marsh, south of the Thorne Bar (Figures 1.1 and 1.2), is the third site investigated for this work. A topographic map of the Columbus Salt Marsh area is presented in Figure 9.1, with stars indicating trench locations.

Hubbs and Miller (1948) determined that Lake Columbus contained fish during the Pliocene but found no evidence of Pleistocene fish, possibly because modern waters in Columbus Salt Marsh are not sufficient to support fish. A low saddle, with a maximum altitude of 1430 m, probably connected it to pluvial Lake Rennie in Fish Lake Valley the south, making some correlation between the fish in Fish Lake Valley and Lake Lahontan possible. Fish Creek contains an indigenous chub, *Gila bicolor euchila*, and so it is likely that Lake Columbus did as well. The Fish Creek chub is similar to some Lake Lahontan fish, suggesting that Lake Columbus did have a pluvial connection to Lake Lahontan (Hubbs and Miller, 1948).

Recent discoveries by Reheis et al. (1997) provide evidence of at least four lake cycles higher than the late Pleistocene level (1400 m) in the Columbus Salt Marsh area. These lacustrine features have not been affected by Quaternary faulting.

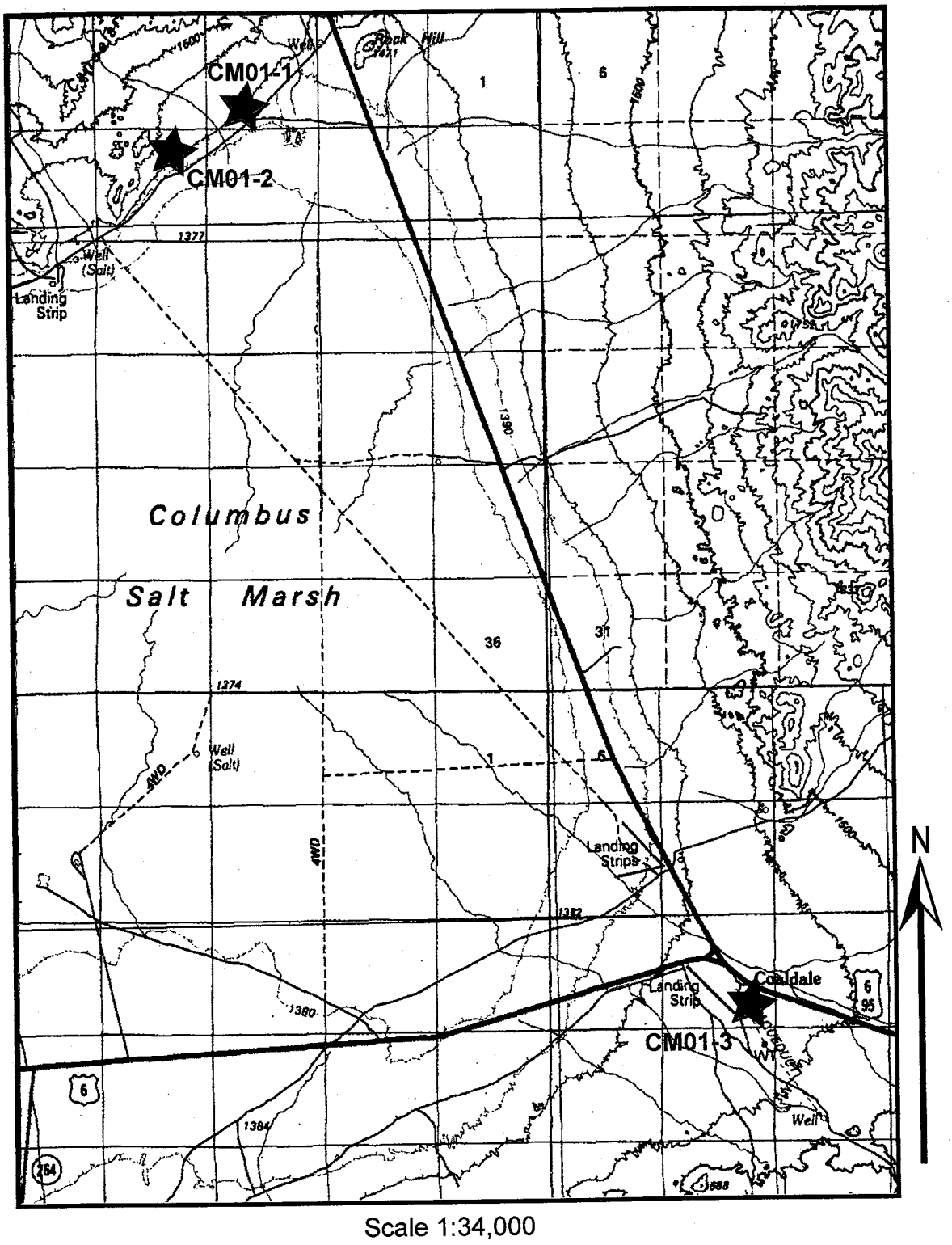

Figure 9.1. Topographic map of the Columbus Salt Marsh site. Purple stars indicate trench locations.

Lake Rennie was in Fish Lake Valley at about 760 ka and probably also at about 1 Ma with a highstand of 1460 m (Reheis et al., 1993). The elevation of this highstand thus suggests that Lakes Columbus and Rennie were connected during the early and early-middle Pleistocene.

The ages of some of the lacustrine deposits can be constrained by the presence of tephra layers. Lacustrine sand and gravel deposits are exposed in a large pit on the north end of the Columbus basin. In this pit, the Bishop ash is stratigraphically contained below late Pleistocene beach deposits (Reheis et al., 2003). A small hill on the south end of the basin shows outcrops of three units of beach gravel and lacustrine sand, which are separated by palaeosols. These deposits are not dated, but it is likely that one unit correlates to the Bishop-ash-containing unit on the north side of the basin. A prominent berm at an elevation of about 1435 m overlies the top unit in this exposure, which corresponds altitudinally to a similar bar on the

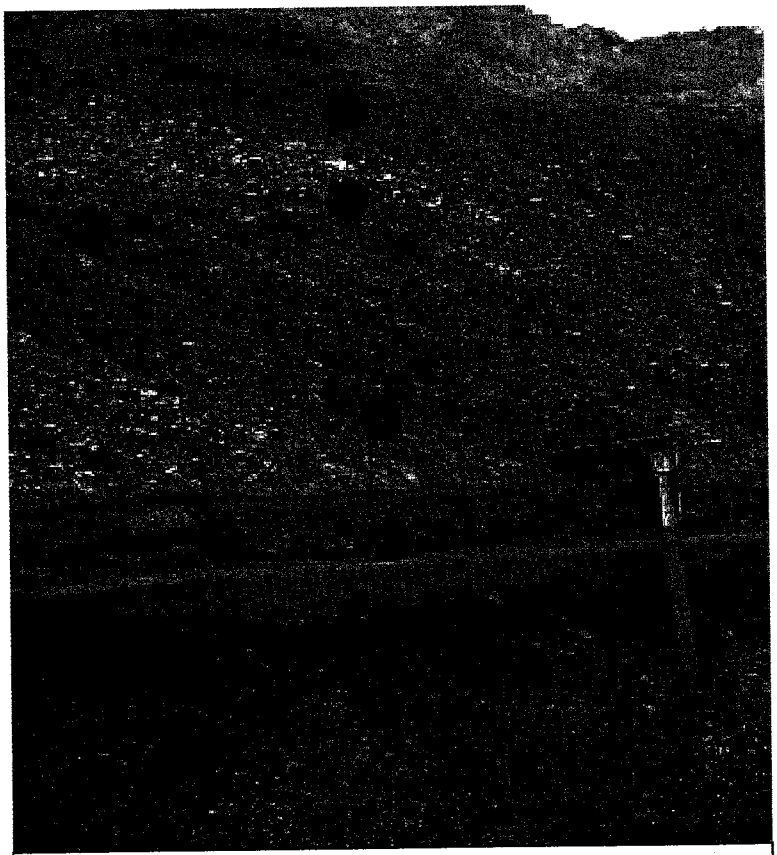

Figure 9.2. Photo of the inside of CM01-1, with sample locations indicated by green circles.

southeast side of basin, near Coaldale Junction. The youngest unit exposed in the small hill corresponds in elevation (~1417 m) to small beach bars on the north side of the basin. In summary, the evidence suggests that there were at least four lake cycles above the late Pleistocene highstand, one of which most likely occurred around 760 ka (Reheis et al., 2003).

The lowest shoreline sampled for this work is CM01-1, on the northern end of the Columbus basin (Figure 9.1) and thought to be the Sehoo-equivalent shoreline. Figure 9.2 is a photo of the inside of the pit. In this photo, the rounded, well-sorted nature of the beach gravels is visible. The gravels in this bar are loosely consolidated. Table A3 gives the soil horizons and soil laboratory data for the Columbus Salt Marsh shorelines.

Carbonate mass at Columbus Salt Marsh is highest for this shoreline (Figure 9.3). This relatively high amount of carbonate material may be primary carbonate from the lake itself, similar to the explanation given for P1 in Newark Valley. Alternatively, this shoreline may be trapping more carbonate material blown off the playa than the two higher shorelines. Its lower elevation and longer length may make it a more effective eolian trap than the two higher shorelines. It is closer to the playa than the other two shorelines and the second-highest shoreline is also tucked behind a bedrock obstruction. If eolian deposition of carbonate material were the explanation, then the shoreline would show elevated amounts of silt and possibly clay. Figures 9.4 and 9.5 present the profile masses of silt and clay, and CM01-1 shows a higher mass of silt than the other shorelines and a lower mass of clay than the two higher

shorelines. These profile masses suggest that the high carbonate content in this shoreline cannot be explained only by higher rates of eolian input.

A second possible explanation for the high carbonate content in the lowest shoreline is the soil parent material. The lower two shorelines were dug down to the soil parent material. The lowest soil horizons of CM01-01 have little in the way of pedogenic carbonate coatings but the total carbonate contents of are much higher than the carbonate contents of the two higher shorelines (7-9% vs. ~1.5%). This suggests that elevated carbonate mass in the CM01-1 soil profile may be due an elevated carbonate content in the parent material.

A third explanation for the high carbonate contents of the lowest Columbus Salt Marsh shoreline is variations in the amount of soluble salt. The two higher shorelines contain more soluble salt (mostly gypsum) than the lowest shoreline. Once salts such as gypsum start to accumulate in a soil profile, they lower the solubility of calcium carbonate. This decreases the amount of carbonate that can infiltrate into the profile. Therefore, even if eolian carbonate material is deposited on the shoreline, a large amount of it remains in the Av horizon or is blown away. This may explain why CM01-1 has a higher carbonate mass than CM01-2 or CM01-3 but may not necessarily be older.

The stratigraphy of the pit is irregular and four stratigraphic breaks were noted in the field. These breaks may suggest discontinuities in shoreline deposition. For example, the shoreline my have risen and fallen slightly during the highstand, resulting in erosion and deposition during the highstand. The discontinuities may also suggest that some of the gravel may be related to isolated depositional events,

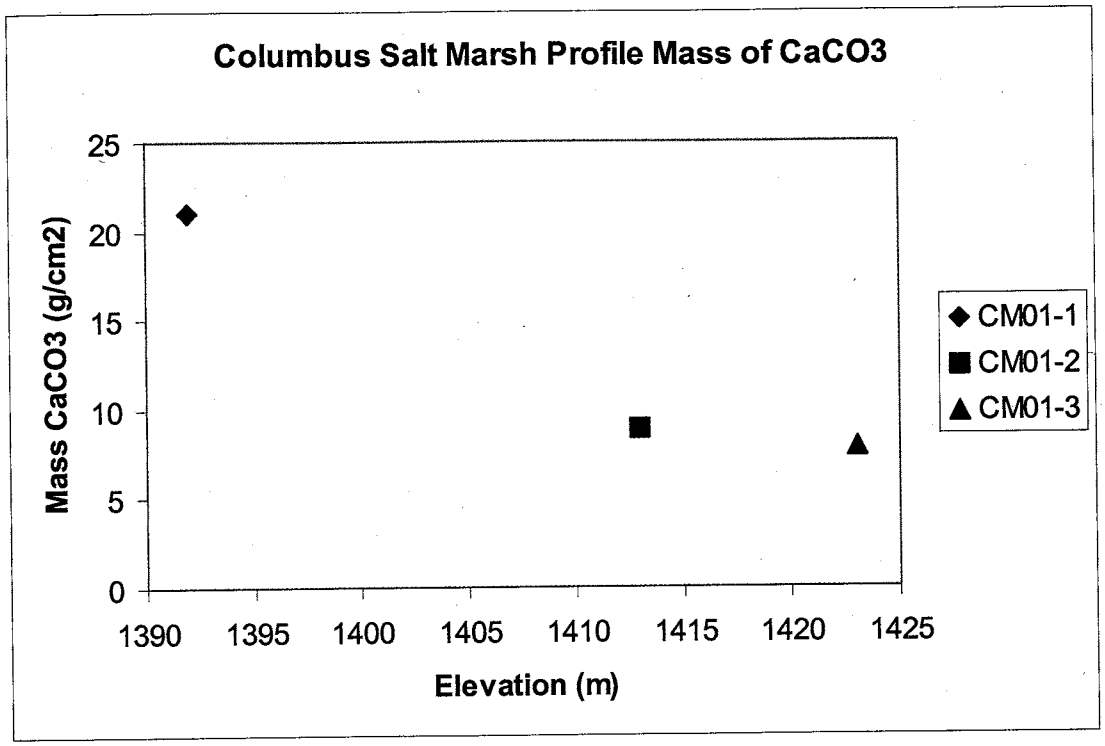

Figure 9.3. Profile masses of carbonate for the Columbus Salt Marsh shorelines.

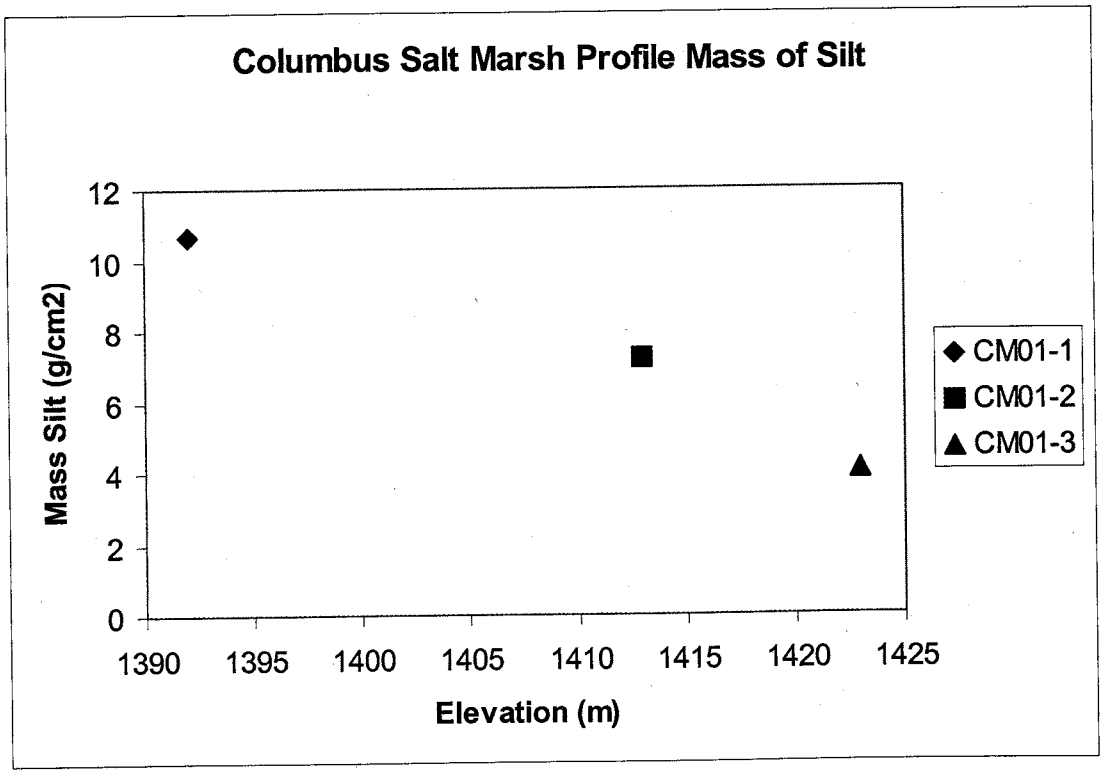

Figure 9.4. Profile masses of silt for the Columbus Salt Marsh shorelines.

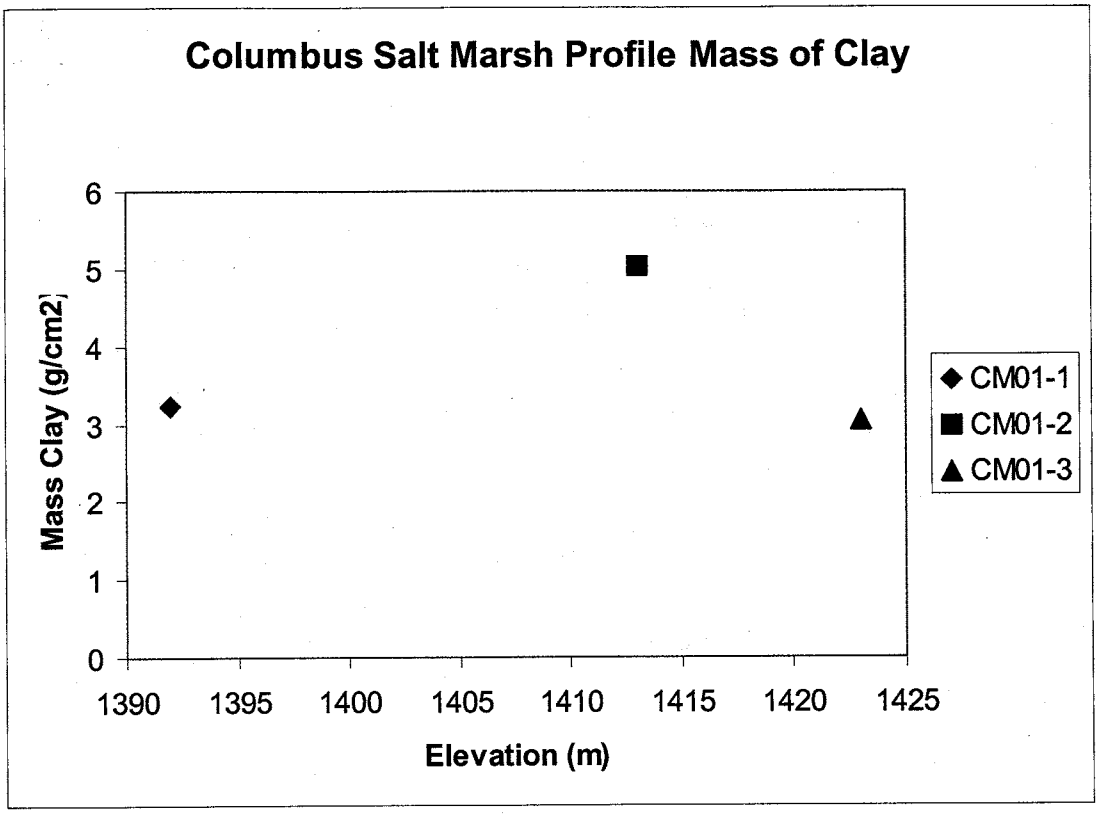

Figure 9.5. Profile masses of clay for the Columbus Salt Marsh shorelines.

such as large storms, and samples at certain levels may not capture the average composition of the profile.

There is a gravel-free silt layer present on this shoreline, which is indicative of eolian inflation. The gentle slope of the shoreline suggests that there has been erosion of the shoreline in addition to inflation. It is possible that the shoreline has undergone both processes, but the morphology suggests that erosion rates have been higher on this shoreline than the three lower Thorne Bar shorelines.

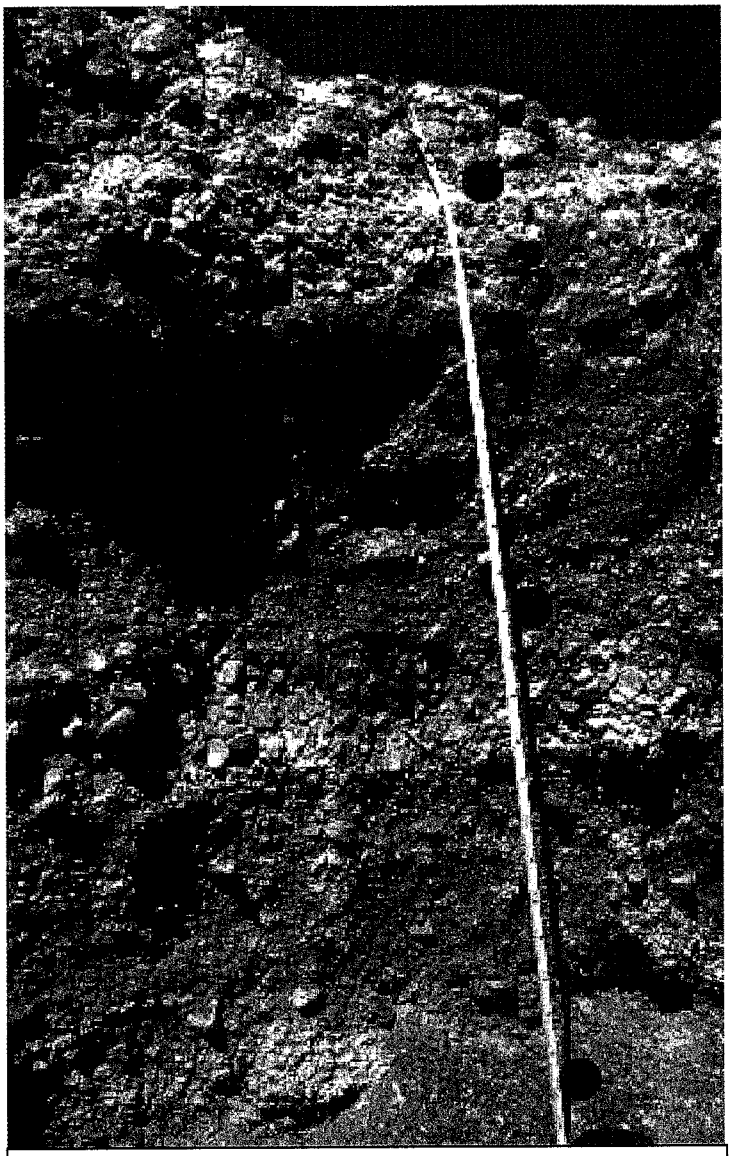

Figure 9.6. Photo of CM01-2, with sample locations indicated by green circles.

The next higher shoreline is CM01-02. Figure 9.6 is a photo of the inside of the trench, in which the good clast sorting and rounding is visible.

The degree of carbonate development in this shoreline relative to CM01-1 is discussed above. The profile mass of silt is lower than that of CM01-1 but the profile mass of clay is higher for this shoreline (Figures 9.4 and 9.5). Therefore, the overall degree of soil development may support this shoreline being older than CM01-1.

The PDI also suggests that this soil is older than CM01-1. The PDI of CM01-2 is 23.8 whereas the PDI of CM01-1 is 12.8. This difference supports an older age for CM01-2 than CM01-1, in spite of the profile mass differences.

A gravel-free silt layer underlying the gravel pavement is present on this shoreline, suggestive of eolian inflation. The shoreline also appears morphologically distinct, possibly because it is protected by a bedrock outcrop. These to factors suggest that erosion rates have been low on this shoreline, and eolian inflation may be a greater influence on the surficial modification than erosion.

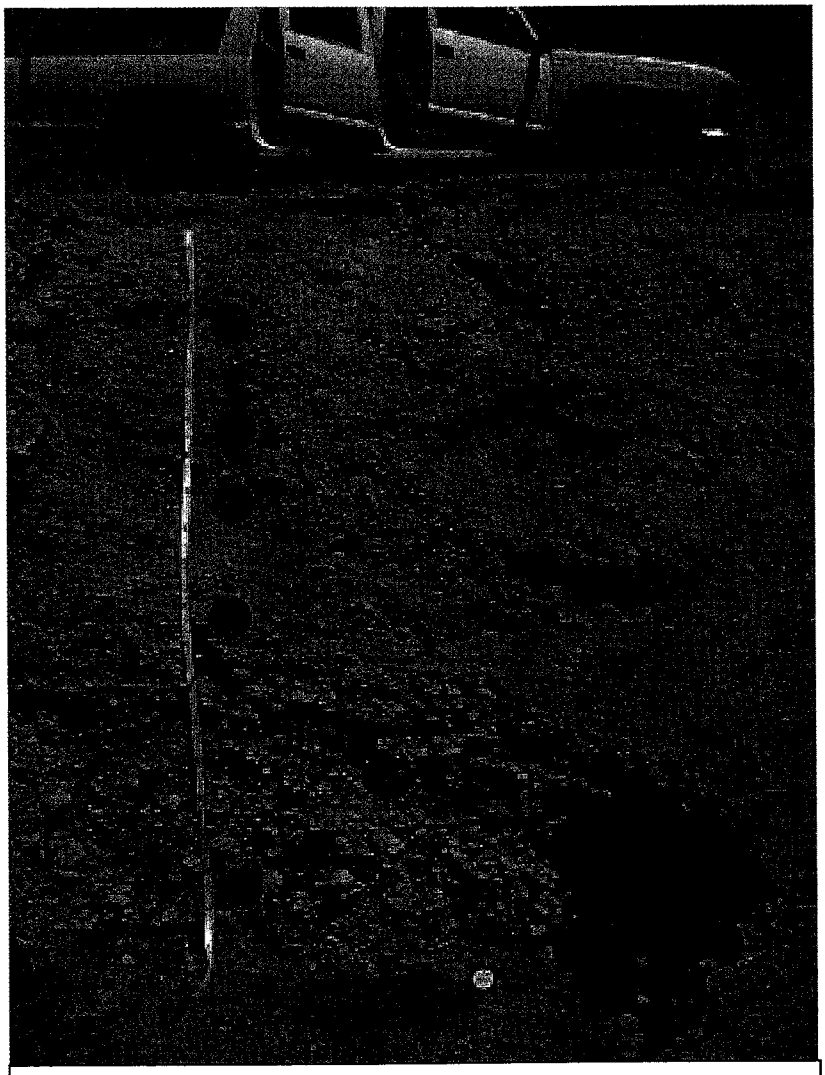

Figure 9.7. Photo of the inside of CM01-3, with sample locations indicated by green circles.

The highest shoreline studied at Columbus Salt Marsh is CM01-03, on the south side of the basin. The morphology of this shoreline appears less distinct than the two lower shorelines. The total thickness of the deposit is about 210 cm and it overlies Tertiary lacustrine clay. The fact that the lacustrine deposit is thin compared to the two lower shorelines suggests that it has undergone more erosion. The higher

elevation and relatively high degree of soil development suggests that this is the oldest of the three shorelines at Columbus Salt Marsh.

A photo of the inside of the pit is presented in Figure 9.7 with the sample points indicated by green circles. The profile masses of silt and clay (Figures 9.4 and 9.5) do not follow the trend of the two lower shorelines, but given that this shoreline is on the opposite end of Columbus Salt Marsh from the other two shorelines, it is not unreasonable to expect variations between these soil properties. The PDI is 22.1 of this shoreline, slightly lower than the PDI of CM01-2. This may also reflect the different locations within the basin. Alternatively, it may reflect relatively higher erosion rates on CM01-3. If erosion rates have been higher on this shoreline, the soil development rates may not have been fast enough to make this shoreline as apparently old as it may be. There is a gravel-free silt layer underlying a gravel pavement at the surface, but if the inflation has been recent (i.e., since the LGM), then there may have been erosion prior to the start of inflation. The thickness of the deposit suggests that erosion rates have been higher on this shoreline than the two lower shorelines.

9.2 Columbus Salt Marsh results

During June of 2001, three backhoe trenches were dug into shorelines, two in the northern part of the basin and one in the southern end. The geographic coordinates, elevations, and determined ages of each shoreline are given in Table 8.1.

9.3 CM01-1, Elevation 1392 m

Figure 9.8 shows the ^{36}Cl data for this shoreline with the modeled age and erosion rate. Figure 9.9 shows a plot of the reduced χ^2 for different ages of this

shoreline. The results of the χ^2 minimizations under different conditions are presented in Table 9.2. As Figure 9.8 shows, the ^{36}Cl data suggests that the shoreline is about 22 ka, or related to OIS 2.

Shoreline	Elevation (m)	Latitude	Longitude	Characteristic Features	Age (ka)	Erosion Rate (mm/kyr)	Average Inheritance (atoms $^{36}Cl/g$)
CM01-1	1392	38.139208 75 °	-117.9606 786°	^{14}C age on tufa gives age of ~14,860 +/- 50 B.P.*	22	0	6.62×10^5
CM01-2	1413	38.134125 15°	-117.9751 571°	^{14}C on tufa gives minimum age of ~38,580 +/- 410 B.P.*	78	0	2.02×10^4
CM01-3	1423	38.025312 16°	-117.8806 23°	Deposit ~2.10 m thick over Tertiary lacustrine clay	173	3	2.18×10^5

Table 9.1. Geographic locations, elevations, as well as modeled ages and erosion rates for the Columbus Salt Marsh suite of shorelines.

The sample point at 2.70 m was regarded as an outlier and not used in the reduced χ^2 analysis. There is a stratigraphic break at a depth of about 2.20 m in the profile, and the samples below this break may not contain the same average composition of the samples above this break. In the photo of the profile, a sand layer above this sample point is visible; the stratigraphy is not continuous between this point and the samples above it. The break in stratigraphy above this sample may be the result of a change in clast source, resulting in a different average inheritance for the lowest sample.

The relationship between shoreline construction and Pleistocene glacial periods was investigated and the results are given in Table 7.2. The reduced χ^2

values increase for deposition to have occurred during oxygen isotope periods other than OIS 2. Therefore, the χ^2 errors are in agreement with shoreline deposition occurring during a Pleistocene cooling period.

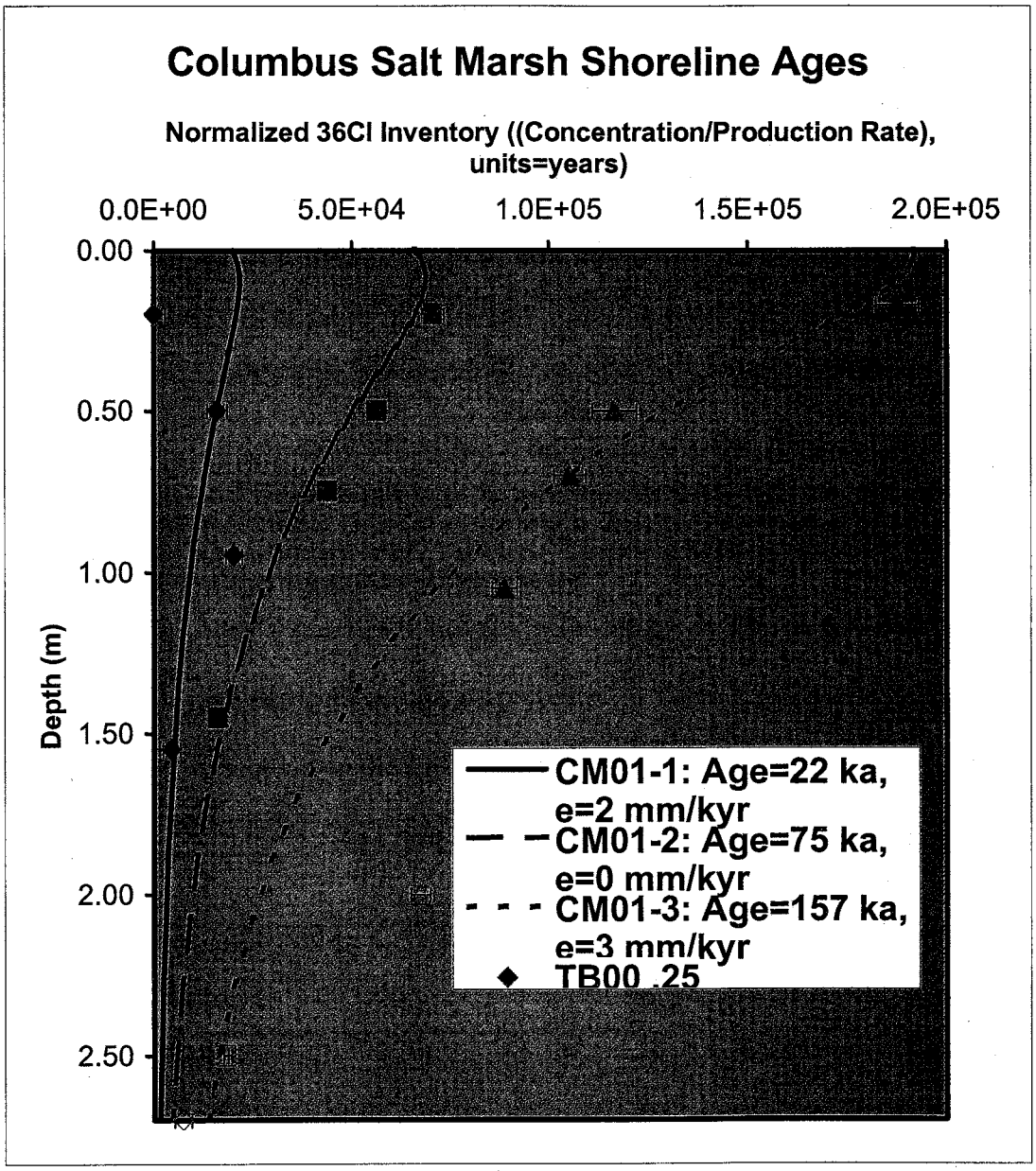

Figure 9.8. Modeled ages and erosion rates of the ^{36}Cl data from the Columbus Salt Marsh shorelines. Hollow symbols indicate outlying samples that were not used in the reduced χ^2 minimization. The sample concentrations and the modeled curves were normalized by the average production rate of each profile and inheritance was subtracted out.

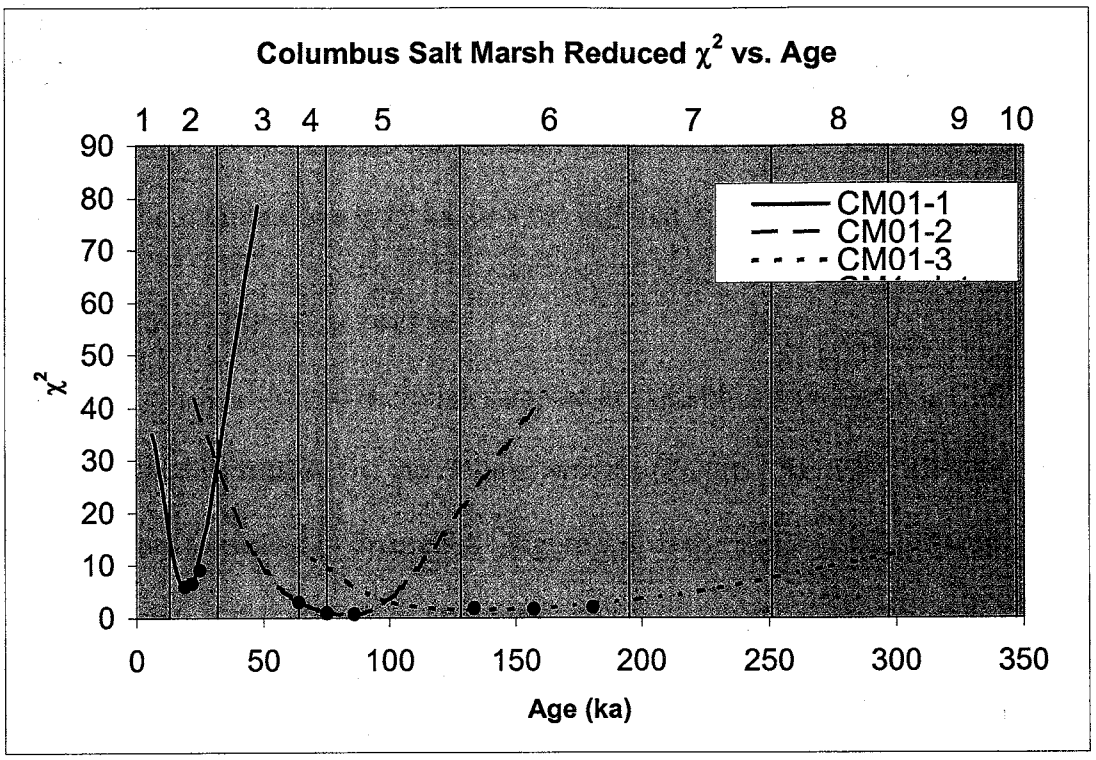

Figure 9.9. Reduced χ^2 versus shoreline age for the Columbus Salt Marsh shorelines. The reduced χ^2 for several different shoreline ages is shown. Black dots correspond to the shoreline age and to fifteen percent uncertainties. The black lines represent marine oxygen isotope stage boundaries and the stages are numbered along the top.

Like the other shorelines in this study, the effects of silt accumulation on the surface were investigated; the results are presented in Table 9.2. First, the effect of a constant silt accumulation on the age was explored by using an accumulation rate of

	Age (ka)	Erosion rate (mm/kyr)	χ^2 Error
^{36}Cl age	22 +/- 3.3	2	6.5
Eolian inflation	20	-4.5	6.5
Recent silt cap deposition (10 cm)	19	2	6.9
Stone production rate	29	0	8.6

Table 9.2. Results of the reduced χ2 minimizations of the ^{36}Cl data for CM01-1.

4.5 mm/kyr to produce a silt cap of approximately 0.10 m in thickness. This scenario suggests that the age is 20 ka. Second, to see the effects of a recently emplaced silt cap, the depths of the samples were changed to 0.10 cm higher. This scenario suggests the shoreline age is 19 ka, or a 9% difference in the age.

9.4 CM01-2, Elevation 1413 m

The second-lowest shoreline sampled at Columbus Salt Marsh is CM01-2, preserved at the north end of the Columbus basin (Figure 2.5). The ^{36}Cl data for this shoreline are presented in Figure 9.8. Figure 9.9 shows a plot of the reduced χ^2 for different ages of this shoreline. The reduced χ^2 minimization yields an age of 75 ka and an erosion rate of 0 mm/kyr, suggesting that this is an OIS 4 shoreline. The lowest sample in the profile, at a depth of 2.50 m, was regarded as an outlier and not included in the reduced χ^2 minimization. There is no buried soil or stratigraphic break above this sample. The sample may be related to a subtle stratigraphic change, or biased by a storm deposit that favored a particular source area; these explanations are possible through they were not apparent during sampling. It is not possible to fit a modeled curve to this sample as well as the samples above it; therefore it may be a statistical outlier.

The possible effects of the silt cap on the shoreline age were investigated, with a focus on the same two scenarios as the shorelines discussed above. The first was a constant accumulation rate of 1.4 mm/kyr, a rate that would result in a silt cap approximately 0.10 m thick. Using this rate of silt accumulation, the reduced χ^2 minimization yielded an age of 71 ka (Table 8.3).

The second case was that the silt cap was deposited very recently in geologic time. The thickness of the silt cap is 0.10 m so in the model, the samples were raised

	Age (ka)	Erosion rate (mm/kyr)	Reduced χ^2
^{36}Cl age	75 +/- 11.3	0	0.9
Eolian inflation	71	-1.4	1.1
Recent silt cap deposition	72	2	1.6
Stone production rate	90	0	0.2

Table 9.3. Results of the reduced χ^2 minimization of the ^{36}Cl data for CM01-2.

0.10 m. Under this scenario, the best-fit modeled age was 72 ka with an erosion rate of 2 mm/kyr. Whether the accumulation was steady or very recent does not appear to affect the relationship between the shoreline deposition and OIS 4, as neither of the scenarios investigated affect the shoreline age greatly.

The strength of the relationship between shoreline construction and OIS 4 (vs. other oxygen isotope stages) was also investigated. For the shoreline to be constructed during an oxygen isotope stage other than OIS 4, the reduced χ^2 values would have to be higher.

9.5 CM01-3, Elevation 1423 m

The highest shoreline sampled at Columbus Salt Marsh is CM01-3, on the south side of the Columbus basin and near Coaldale Junction (Figure 9.1). The sampling pit was dug by hand into an existing roadcut. The ^{36}Cl data for this shoreline is presented in Figure 9.8. Figure 9.9 shows a plot of the reduced χ^2 for different ages of this shoreline. The modeled age and erosion rate that yields the best

minimization is 157 ka with an erosion rate of 3 mm/kyr. This modeled age suggests that a total of 0.47 m has been eroded off of the shoreline, a result consistent with the hypothesis that this shoreline has undergone more erosion than the two lower ones. In performing the analysis, the lowest sample in the profile, at a depth of 2.00 m, was regarded as an outlier and excluded from the minimization. The reason for this may be that there are two breaks in stratigraphy between this sample point and the next higher sample point. The lowest sample appears to correspond to coarser gravels than the upper part of the deposit, suggesting that it may have been left from an earlier lake highstand onto which the OIS 6 shoreline was constructed. The coarse gravels my also signify a different source area than the gravels above. Either (or both) of these factors would result in this sample being an outlier with regard to the other samples in the profile.

As with the other shorelines, the possible effects of the silt cap on the determined shoreline age were also investigated. First, the effects of a constant silt accumulation rate were explored. In order to obtain a silt cap of approximately 0.10 m thick for a shoreline of this age, the silt accumulation rate would have to be approximately 0.6 mm/kyr. The age that yields the lowest minimization is 115 ka with a reduced χ^2 of 1.6, the same value as the modeled fit obtained using erosion instead of accumulation. Although the model produces good fits to the data, because of the thickness of the deposit and less distinct appearance of the shoreline, it is more likely that the surface has been eroding and this solution is not correct.

Second, the scenario of the silt cap being emplaced very recently in geologic time was explored. The silt cap on this shoreline is approximately 0.10 m thick, so in the model, the samples were moved up 0.10 m, to simulate them accumulating ^{36}Cl at

	Age (ka)	Erosion rate (mm/kyr)	Reduced χ^2
^{36}Cl age	157 +/-	3	1.6
Eolian inflation	115	-0.6	1.6
Recent silt cap deposition (10 cm)	104	0	1.7
Stone production rate	132	0	1.6

Table 9.4. Results of the reduced χ^2 minimization of the ^{36}Cl data for the Columbus Salt Marsh shorelines.

a shallower depth before deposition of the silt. This resulted in an age of 104 ka and an erosion rate of 0 mm/kyr, with a reduced χ^2 of 1.6. This is the same reduced χ^2 as initially modeled, but again, it is doubtful that a solution suggesting no erosion is correct.

To explore the relationship between shoreline construction and a global cooling period, the reduced χ^2 was calculated for oxygen isotope periods other than OIS 6 (Table 7.2). The reduced χ^2 for these ages are higher than for OIS 6. These values support a relationship between lake cycles and global cooling periods because they are higher than the value for the OIS 6 age.

9.6 Implications of the Columbus Salt Marsh shoreline ages

The shoreline ages at Columbus Salt Marsh support the data obtained at Thorne Bar and Newark Valley that lakes in the western Great Basin filled more

frequently and to higher levels than previously thought. Specifically, lake cycles occurred in Columbus Salt Marsh during OIS 2, 4, and 6.

The OIS 4 lake cycle in Columbus Salt Marsh is in agreement with the evidence of an OIS 4 lake cycle at the Thorne Bar. This suggests that the existence of an OIS 4 shoreline at Thorne Bar may not be an isolated occurrence. The existence of least two different sites in the western Great Basin with OIS 4 highstands suggests that OIS 4 may have had stronger effects in this region than previous research has suggested.

The shoreline record at Columbus Salt Marsh also supports the apparent trend of drier lake cycles from the middle to late Pleistocene. It is not possible to determine from the shoreline record whether the trend is real or apparent, but this additional evidence suggests that future research into its existence is warranted.

10 DISCUSSION

The ^{36}Cl dates obtained for this work suggest that lakes in the western Great Basin filled more often and to higher levels than previously thought. All three sites investigated for this work have old, high shorelines that are now quantitatively dated. The main goal of this work was to understand the response of the western Great Basin to global cooling periods. The intent was to test two competing hypotheses regarding the Great Basin pluvial cycles: (1) that a lake cycle occurred during OIS 16 and was followed by a long period of aridity until OIS 6 or 2, and (2) that the western Great Basin responded to those cooling periods as well as the intervening glacial periods. In testing these hypotheses, it became possible to make additional interpretations regarding the pluvial cycles in the western Great Basin.

10.1 Quality of the results obtained in this work

This work has resulted in a suite of ^{36}Cl depth profiles from thirteen different surfaces. This large number of depth profiles allows for a comparison of the quality of the modeled fits obtained in this study to the quality of modeled fits to other depth profile studies. In addition, the number of profiles makes it possible to examine the possible causes of larger and smaller χ^2 errors associated with the modeled shoreline ages.

Ayarbe (2000) used a ^{36}Cl depth profile to calculate the age of the control profile in his fault scarp study. Similar to this work, he minimized the χ^2 error to obtain the best-modeled fit to his data. He omitted the top sample in the profile as an outlier and obtained a modeled age by minimizing the reduced χ^2. The exact value of the reduced χ^2 associated with the age of the feature is not stated but all his sample points (excluding the top sample) fall along the modeled curve. His modeled fit to the ^{36}Cl data is apparently consistent with the modeled fits obtained in this work.

Other studies use the cosmogenic nuclides ^{10}Be and ^{26}Al to determine the ages of depositional features. Repka et al. (1997) obtained modeled fits to their ^{10}Be and ^{26}Al data consistent with the results of this study but they dated fewer surfaces (four) than were dated in this work. They also sampled multiple samples at fewer discrete depths (ranging from 2 to 4) than the profiles in this work; these factors make a thorough comparison of the two studies difficult. Hancock et al (1999) obtained good modeled fits to their data for surfaces younger than ~150 ka; they suggested that independent dating methods be used in conjunction with cosmogenic nuclide dating for surfaces older than ~150 ka due to complexities in the histories of older surfaces (e.g., eolian inflation and deflation). Like the work of Repka et al. (1997), they sampled for ^{10}Be and ^{26}Al at several depths, ranging from three to four sample depths per profile. In both of these studies, a least squares approach was used to obtain the best modeled fit.

Because the techniques of obtaining the best modeled fits varied between this work and other studies, it is difficult to quantitatively compare the goodness of the fits. It is possible to compare the modeled fits qualitatively by appearance, and this

comparison suggests that the modeled fits in this work are consistent with those obtained by other researchers.

The calculated shoreline ages using the ^{36}Cl production rates of Stone et al. (1996) do not significantly change the shoreline ages calculated using the production rates of Phillips et al. (1996, 2000). Using the production rates of Stone et al (1996) results in several of the shoreline ages falling outside of global cooling periods, but not into other global cooling periods. The majority of the shoreline ages stay within the previously calculated oxygen isotope stage, suggesting that the use of the Stone et al. (1996) production rates do not significantly affect the conclusions of this work. Both production rates result in shoreline ages consistent with lake cycles during major cooling periods throughout the middle to late Pleistocene.

The factor that appears to have the greatest effect on the amount of χ^2 error associated with the ages of the shorelines is the size of sample collected in the field. Hancock et al. (1999) determined that a minimum of 30 clasts is necessary to obtain the average ^{10}Be concentration and inheritance with depth. Ayarbe (2000) hypothesized that the minimum number of clasts needed to obtain the average ^{36}Cl concentration and inheritance is 150. The results of this work suggest that the minimum number of clasts for ^{36}Cl studies may be higher than 150.

Figure 10.1 is plot of the average sample size collected in the field from the Thorne Bar and Newark Valley shoreline profiles versus the total minimum reduced χ^2 for each profile. The plot includes those samples determined to be outliers and includes only the profiles for which sample mass data is available. The data from three Thorne Bar profiles show consistently low reduced χ^2 values while the data

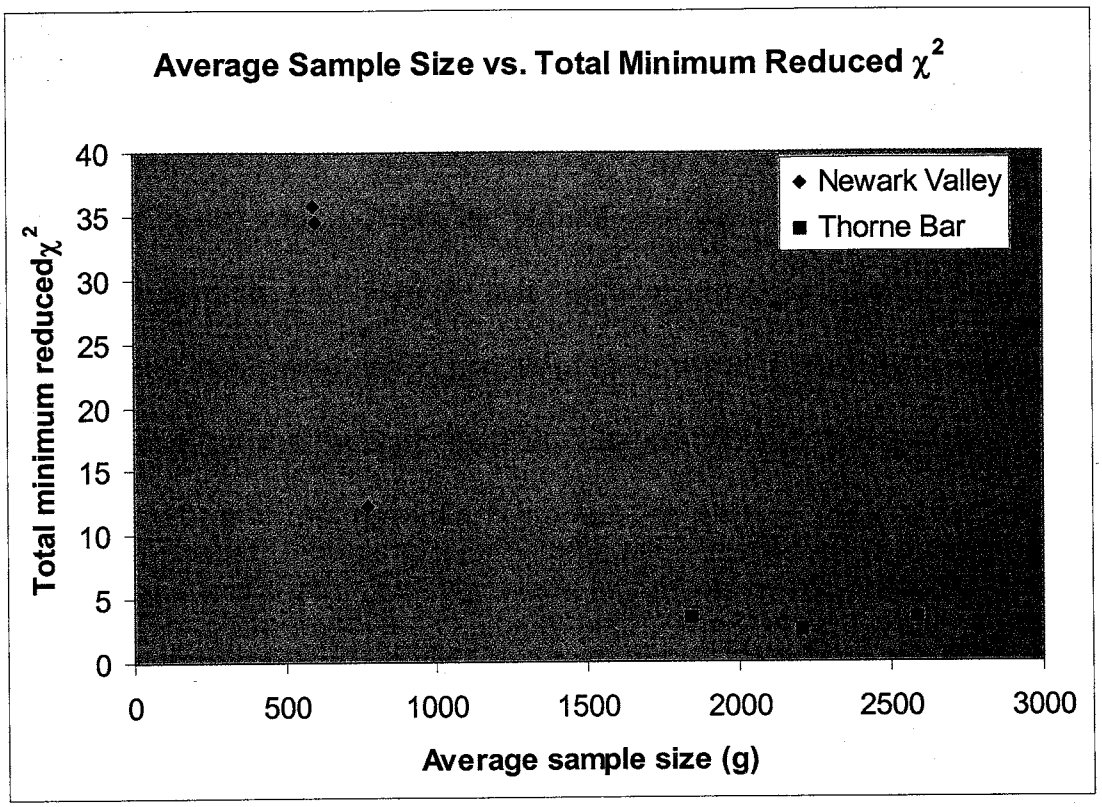

Figure 10.1. Plot of the average sample sizes of the profiles versus the total minimum reduced $\chi 2$ of the profiles for the Newark Valley and Thorne Bar sites.

from Newark Valley shows more variation in the total reduced χ^2. The average Newark Valley sample sizes are less than 1000 g while the average Thorne Bar sample sizes are around 2000 g. The sample size data suggest that sample size may be correlated to the quality of the modeled fit to the ^{36}Cl data and larger sample sizes (>2000 g) may lead to modeled ages with better fits. In order to thoroughly address this subject, more data is needed, but the available data suggests the possibility of a relationship between sample size and reduced χ^2 and that larger sample sizes (>2000 g) may lead to better modeled fits to the data.

For the clast size collected in this work (diameters of ~0.5-2.5 cm), 30 clasts are equal to about 41.8 g and 150 clasts are equal to about 209.0 g. A sample size of 1000 g (as collected, on average, in Newark Valley) consists of about 700 to 950

clasts; a sample size of 2000 g (as collected, on average, at the Thorne Bar) consists of 1400 to 1900 clasts.

The number of clasts needed to constrain the average inheritance and ^{36}Cl concentration with depth is dependent on the source of the material in the feature of interest. If the clasts come from the same source and have similar travel times prior to final deposition, then a smaller number of clasts would be needed to constrain the average inheritance. If the clasts come from several different sources, then more clasts would be needed to constrain the average composition. For example, in dating terraces in a fluvial system, the clasts would be likely to originate from the same material upriver and travel for similar amounts of time. In contrast, the shorelines in this study could have more heterogeneity in their source areas because the clasts come from a larger area and their travel time changes with changes in lake currents or storms. Therefore, the number of clasts required to obtain the average composition with depth depends to some extent on the feature being dated, but the results of this work suggest that, when possible, sample sizes of 1400 to 1900 clasts (~2000 g) may facilitate better results.

10.2 Connection to global climate record

From early on, previous work has supported a connection between western Great Basin lake cycles and Pleistocene cooling periods (e.g., Russell, 1885; Broecker & Orr, 1958; Morrison, 1991). One goal of this research was to further establish the relationship between lake cycles in the western Great Basin and the Pleistocene climate record. Based on the ^{36}Cl data, lake cycles occurred during OIS 2, 4, 6, 8, and possibly 12 or 16. As determined by the χ^2 error minimizations, the

^{36}Cl evidence supports a relationship between western Great Basin lake cycles and Pleistocene glacial/interglacial periods. This work suggests that higher reduced χ^2 values are associated with shoreline age corresponding to interglacial rather than glacial periods. Therefore, this work supports previous interpretations that western Great Basin lake cycles were connected to the Pleistocene global climate record.

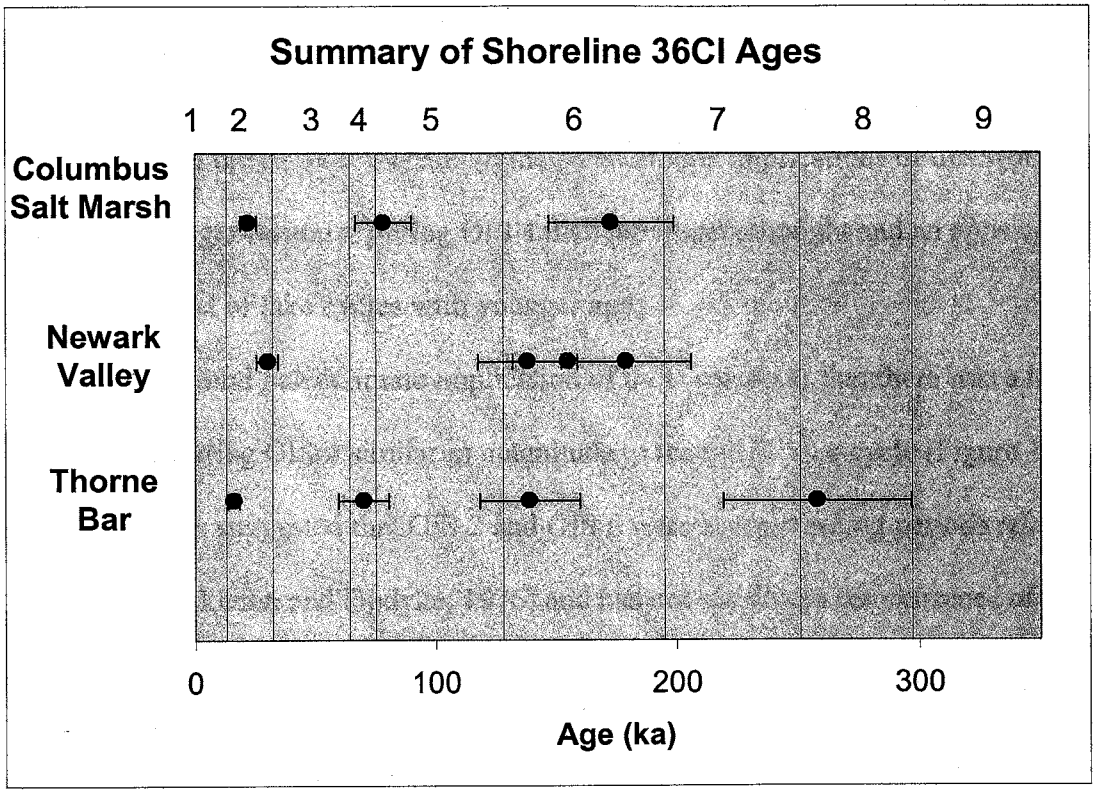

Figure 10.2. Summary plot of the ^{36}Cl shoreline ages for each site. Uncertainty bars represent the 15% age uncertainty. Black lines represent oxygen isotope stages and are numbered along the top.

10.3 Hypothesis testing

The shoreline ages enable interpretations to be made regarding the two hypotheses of the lacustrine history of the western Great Basin. The ^{36}Cl evidence suggests that the Great Basin responded to multiple cooling periods during the middle-to-late Pleistocene, supporting the second hypothesis (Figure 10.2). Under the first hypothesis, the higher shorelines could be recessional features from the OIS

16 highstand. However, the ^{36}Cl data suggests that the shoreline ages correspond to different Pleistocene glacial periods. If the shoreline features were recessional, they would not be expected to correspond to different Pleistocene glacial periods. Furthermore, the shoreline ages are constrained within each glacial period. Therefore, the results of this research support the second hypothesis of the lacustrine history of the western Great Basin.

10.4 Paleoclimate implications

Beyond the hypothesis testing, the paleoclimate implications of this work include a stronger response during OIS 4 than previously thought and an apparent decreasing level of lake cycles with younger age.

The second paleoclimate implication of these results is that there was a lake-filling cycle during OIS 4 similar in magnitude to the OIS 2 lake cycle (Figure 10.2). Other work has suggested that OIS 2 and OIS 6 were strong cooling periods relative to OIS 4 (Shackleton and Opdyke, 1976) and has not supported the existence of a large lake during OIS 4 (e.g., Morrison, 1991). The ^{36}Cl data suggests that this interpretation may require further study. The data suggests that the Lahontan basin responded to OIS 6, 4, and 2 with the OIS 4 highstand being similar in magnitude to the OIS 2 highstand. This is the first time OIS 2 and 4 lake events of similar magnitudes have been quantitatively demonstrated.

The shoreline ages decrease with decreasing elevation, demonstrating an apparent drying trend of pluvial cycles in the western Great Basin. The fact that this is an apparent drying trend and not necessarily an actual drying trend has been discussed in Section 1; it is not possible to discern from the ^{36}Cl evidence obtained in

this work whether the trend is apparent or actual. The possible reasons for this apparent trend (uplift of the Sierra Nevada, changes in the jet stream position, or drainage changes) have also been discussed. The apparent trend of drier pluvial periods over time from the middle-to-late Pleistocene warrants future work to test whether or not it is real and, if so, to determine its causes.

10.5 Comparison with previous interpretations of the lacustrine history of Lake Lahontan

This work presents a revised lacustrine chronology of Pleistocene lakes in the western Great Basin. The results of this study support the occurrence of lake cycles with more frequency and of greater magnitude than previous workers have proposed and therefore contrast with certain earlier works regarding the longer-term history of the basin.

Russell (1885) identified two deep-lake periods, which have been correlated with the Eetza (OIS 6) and Sehoo (OIS 2) Formations (Morrison, 1991). Morrison (1991) also correlated the Rye Patch AF with OIS 16, and identified an older (but within the last 1 Ma), unnamed unit. Other workers have modified Morrison's (1964) lacustrine chronology (e.g., Davis, 1978) or tended to focus on the chronology of the most recent lake cycle in the western Great Basin. Shorelines older and higher than the OIS 2 level have been noted by some workers but attributed to faulting or isostatic rebound in the basin (Mifflin & Wheat, 1979; King,1978). This work presents a lacustrine chronology for a longer-term history of the basin. The ^{36}Cl evidence obtained in this study support more frequent lake cycles of greater magnitudes in the western Great Basin than previously thought.

The results of this study are consistent with the earlier work of Morrison and Frye (1965) who suggested major lake highstands during times correlative to OIS 2 and OIS 4. The shoreline ages obtained in this study extend this interpretation to major highstands during the times of OIS 2, OIS 4, and OIS 6. The timing of the major highstands within OIS 2 has been subject to considerable debate in the literature, and the results of this study suggest large OIS 2highstands at different times at the three sites in the western Great Basin. The OIS 2 highstands at the three different sites are as follows: 1) 16 ka at the Thorne Bar, 2) 30 ka at Newark Valley, and 3) 22 ka at Columbus Salt Marsh. The Thorne Bar highstand age is consistent with a Lake Lahontan highstand approximately 15 ka (Morrison, 1991). The differences in the timing of the OIS 2 highstand may be the result of local variations in climatic factors at each site. Alternatively, the differences may reflect which shorelines are preserved.

In addition, the results of this work suggests that there may be a discrepancy between recognized OIS 2 and OIS 4 shorelines in the western Great Basin and therefore that some studies may need to be revised. Some research has regarded the prominent shoreline with an altitude range of about 1319 to 1337 m (from the edge to the middle of the basin) as representing the OIS 2 highstand throughout the western Great Basin (Adams et al., 1999). The findings of this work support at least one of these shoreline features (at the Thorne Bar), previously thought to be related to OIS 2, being related to OIS 4. Previous work on the soil development of this highstand supported an OIS 2 age of this feature (e.g., Adams & Wesnousky, 1999; Reheis, M., U.S. Geological Survey, personal communication). The ^{36}Cl evidence suggests that

some shorelines previously ascribed to OIS 2 may instead be related to OIS 4, and it may not be possible to differentiate between the two ages using soil development alone. The work of Chadwick and Davis (1990) found that confusion between shorelines of OIS 2 and OIS 6 age is possible. If so, then it follows that differentiating between OIS 2 and OIS 4 shorelines based soil development alone may be even more difficult.

10.6 Contrast with the Lake Bonneville record

The new chronology of lakes in a near the Lahontan Basin differs with that of the Lahontan's contemporary lake, Lake Bonneville. Research on the Lake Bonneville chronology suggests that there were four major highstands over the past ~600 ka, with the most recent being the largest. In contrast, the ^{36}Cl data is consistent with major lake cycles in the western Great Basin during every marine oxygen isotope period over the past 600 ka.

The Bonneville basin deep lake cycles appear correlative with marine oxygen isotope stages 2, 6, 12, and 16 (Oviatt et al., 1999). These correlations do not include OIS 4 or OIS 8, two periods in which the ^{36}Cl data supports lake cycles in the Lahontan basin. Two possible explanations for this difference are variations in climate effects between the basins or differences in the available evidence of lacustrine deposits. The climate controls that produced large lakes that apparently decrease in magnitude with time in the western Great Basin may not have affected the central and eastern Great Basin. Regional Pleistocene climates may have been expressed differently in these different parts of the Great Basin.

Alternatively, it is possible that there were lakes in the Bonneville basin during OIS 4 and OIS 8 but lake cycles were relatively small in magnitude and evidence of them is not preserved. This hypothesis is in agreement with the data from Newark Valley, which underwent highstands during OIS 2, OIS 6, and possibly OIS 16. Newark Valley may have held a lake during OIS 4, but if the level was below the OIS 2 level, the evidence may have been obliterated by the OIS 2 lake cycle. Because the valley is located in east-central Nevada, it may be expected to show a lacustrine record similar to that of Lake Bonneville. The cause of this apparent contrast between the Lahontan and Bonneville records is complex and warrants future study.

11 CONCLUSIONS

The original goal of this study was to test two competing hypotheses regarding the lacustrine history of the western Great Basin. The first hypothesis is that there were two deep-lake cycles: one during the middle Pleistocene and one during the late Pleistocene with a long period of low levels or aridity intervening. The second is that lake cycles in the western Great Basin occurred in predictably in response to glacial periods throughout the Pleistocene. The ^{36}Cl data from this study supports the second hypothesis and suggests that lake cycles in the western Great Basin occurred more frequently and to higher levels than previously thought (Figure 10.2). The shoreline ages also support previous interpretations of a relationship between western Great Basin lake cycles and Pleistocene cooling periods.

The shoreline ages also support a lake cycle during OIS 4 similar in magnitude to the OIS 2 lake cycle. This contrasts with earlier work that generally suggested that the response of the western Great Basin to OIS 4 was weaker in magnitude than OIS 2 or OIS 6. The existence of an OIS 4 highstand similar in magnitude to the OIS 2 highstand also suggests that some studies in this region may have to be revised. Shorelines within the OIS 2 elevation range and displaying what are thought to be OIS 2 soil properties may in fact be related to OIS 4.

The shoreline ages decrease with decreasing elevation, which demonstrates an apparent drying trend of western Great Basin lake cycles from the middle to the late Pleistocene. Whether this trend is real or apparent cannot be determined from this study, but the evidence suggests future study into the actual existence and possible causes of the trend is warranted. Finally, this western Great Basin lacustrine record contrasts with the record of Lake Bonneville, which underwent its greatest highstand during OIS 2 and shows evidence of four highstands during the middle-to-late Pleistocene. The causes of the discrepancy between these two records is complex, but the discrepancy may suggest that different climate factors were at work in the western Great Basin than the central and eastern Great Basin. The possible causes of these regional differences in climate also warrant future investigation.

12 APPENDIX 1. Sample collection, grinding, and leaching (Zreda, 1994; and Ayarbe, 2000)

- Select the flattest parts of the shorelines for the backhoe pits in order to minimize the effects of erosion.
- Collect samples along a vertical transect inside the trench. Samples should be taken as high within the trench and also as deep as possible. The shoreline samples were taken about 15 to 20 cm apart and the area defined by each sample was about 10 cm vertically and about 40 cm horizontally.
- Each sample should be as large as possible, with a minimum of 150 clasts. Before bagging samples in the field, they should be sieved to collect the clasts between 0.5 and 2.5 cm in diameter. This minimizes the size difference among clasts and prevents skewing the sample towards a few larger clasts.
- In the laboratory, rinse the clasts to remove dirt and dry them in the oven.
- Separate all the quartz-rich clasts from the sample, in case ^{10}Be analysis becomes necessary for that sample.
- Grind the clasts to a diameter of <1 mm in a TEMA mill (shatterbox).
- Sieve the ground samples to separate the <150 μm from the >150 μm size fraction.

- The >150 μm size fraction is used for analysis but the <150 μm fraction is kept in reserve for use if needed.
- The TEMA mill was cleaned in between samples by running OTTAWA quartz sand in it for 2-3 minutes.
- The >150 μm size fraction is then leached in 3% HNO_3 for 12 hours to remove meteoric chloride and secondary carbonate material. The HNO_3 solution is added at 3-4 times the sample volume and then the sample is stirred well and covered.
- After ~12 hours, the leachate is decanted and the sample is rinsed in deionized water. During this step, suspended fines are also rinsed off the sample.
- A small amount of 3% HNO_3 is added to the rinsed sample to check for effervescence. If the sample still effervesces, it must go through another leaching in the HNO_3 solution.
- If the sample does not effervesce, add 1% NaOH and stir the sample well. Continue adding NaOH until the pH is between 7 and 9.
- Pour off the NaOH solution and rinse the sample 3 times in deionized water. The pH at this point should be 5-6.
- Dry the samples in the oven at about 105°C

13 APPENDIX 2. Estimation of chloride concentration with a chloride electrode (Ayarbe, 2000)

- To perform this step, about 40 g of the leached sample was ground to a size fraction of <150 μm. A small amount (~3-5 g) of powder was reserved for this total chloride analysis.
- Airtight, Teflon cells containing 2 separate chambers are necessary for this procedure. The purpose of the chambers is to keep the reducing and oxidizing solutions apart. The Teflon cells are referred to as diffusion cells.
- Before the procedure, the diffusion cells must be cleaned according to the following:
    - Prepare a cleaning solution of 375 mL concentrated H_2SO_4 with 13 mL of saturated $K_2Cr_2O_7$.
    - The cleaning solution is heated and then poured into each diffusion cell.
    - Place the lids on the cells, turn them over several times, and let them sit for ~15 minutes.
    - Pour out the cleaning solution and rinse the cell in deionized water.
    - Prepare a second cleaning solution of 300 mL HNO_3 and 50 mL H_2O_2 and heating it.

- Pour the second solution into the cells and clean them the same way as the first solution.

- Prepare standards to make a voltage/concentration log-linear regression. These are needed to convert the voltage reading from the electrode into a chloride concentration. For complete unknowns the following standards were used: 10, 100, 250, and 500 ppm.
- Weigh 0.2 (± 0.0004) g of each standard or powdered sample into the oxidizing cell of each diffusion cell.
- Add 2.5 mL of reducing solution to the reducing chambers. Prepare this solution with 5.8 g of KOH, 0.29 g of Na_2SO_3, and 31 g of deionized water.
- Add 3 mL of oxidizing solution to the oxidizing chambers. This solution is prepared using: 0.4 g $KMnO_4$, 5.6 g deionized water, 1.85 mL of 50% H_2SO_4, and 32 mL HF. Do not let the oxidizing solution come in contact with the standard or sample until all the lids are on the diffusion cells.
- Place the diffusion cells on an orbital shaker for 16-20 hours. During this period, the standards and samples are oxidized, releasing Cl_2, which the reducing solution captures to form Cl^-.
- Use a voltage meter and chloride electrode to take voltage readings of each reducing solution. Rinse the electrode between readings. In this study, a Beckman meter and an Orion model 96-17BN chloride electrode were used.
- During voltage measurements, ensure that the base of the electrode is completely immersed in the solution and carefully rinse the electrode between measurements.

14 APPENDIX 3. Estimation of expected $^{36}Cl/Cl$ ratio

- To perform this estimation, the following must be known: 1) the estimated age of the sample, 2) the sample chemistry (as determined by XRF), and 3) the cosmogenic ^{36}Cl production rate.
- Approximate the age of the landform using the degree of soil development present and/or any other independently known age constraints.
- The rock chemistry is found by XRF analysis and the amount of chloride is estimated using a chloride electrode, as described in Appendix 1.2.
- The cosmogenic ^{36}Cl production rates were calculated using the analytical solution in CHLOE (Phillips and Plummer, 1996). The solution uses the sample chemistry, the effective attenuation coefficients, and the mass depth.
- The following equation was used to estimate the concentration of ^{36}Cl in atoms (g sample^{-1}).

$$N = \frac{P}{\lambda}\left(1 - e^{-t\lambda}\right)$$

In the equation, P is the ^{36}Cl production rate, λ is the ^{36}Cl decay coefficient (ln (2) / half-life of ^{36}Cl, e is the attenuation length, t is the estimated age of the sample, and N is the ^{36}Cl concentration.

- The ^{36}Cl concentration is then divided by the estimated chloride concentration to estimate the $^{36}Cl/Cl$ ratio.

15 APPENDIX 4. Protocol for extracting Cl from rock samples for ^{36}Cl analysis (Zreda, 1994; and Ayarbe, 2000)

- Before performing this extraction, all laboratory ware should be cleaned to remove residual chloride. This was done by acid washing, a procedure that requires rinsing with NH_4OH, heating in HNO_3, and rinsing the labware with deionized water.
- Weigh the crushed, leached sample into a Teflon bottle. The amount of sample to be dissolved is determined using the estimated $^{36}Cl/Cl$ ratio (Appendix 1.3).
- After the sample is in the Teflon bottle, add deionized water to the sample and swirl. The amount of water should be approximately equal to the mass of the sample.
- Weigh out the required amount of ^{35}Cl spike (as determined by the estimated $^{36}Cl/Cl$ ratio, the estimated Cl concentration, the amount of AgCl necessary for AMS, and the amount of sample available) into the Teflon bottle. The goals of using the ^{35}Cl spike are: (1) to make the final $^{35}Cl/^{37}Cl$ ratio of the sample approximately 6.0, (2) to obtain a final mass of AgCl greater than 10 mg, (3) to make the sample large enough to be representative, and 4) to obtain a $^{36}Cl/Cl$ ratio greater than 50×10^{-15}. The spreadsheet model, LABCALCS

(developed by Plummer and Phillips, unpublished), was used to perform these calculations.

- Under the fumehood, add concentrated HNO_3 at a 1:2 ratio to the sample mass to a separatory funnel.
- Add concentrated HF at a 2.5:1 ratio to the sample mass to the separatory funnel.
- Place the Teflon bottle containing the sample under the separatory funnel and slowly drip the acid solution into it. This step must be done slowly to avoid violent reactions with silicates in the sample. If the sample becomes very hot, it can be placed in a cold-water bath to slow the reactions.
- After the acid solution has been added to the sample, loosely cap the bottle and let the sample cool. Then place the sample on a hot plate at a low temperature (~60°C) setting.
- Let the samples dissolve on the hotplate- this may take between 48 and 72 hours.
- After sample dissolution is complete, transfer the sample liquid and remaining solids (rock waste) into a Teflon centrifuge bottle. Balance the centrifuge and centrifuge samples at ~2500 rpm for ~15 minutes to separate the solution from the rock waste.
- Decant the solution into a Teflon beaker and add 10 mL of 0.2 M $AgNO_3$ to precipitate AgCl. Leave the beakers covered and on a hotplate at a warm (~60°C) setting for about 12 hours.

- Transfer the AgCl and the solution to Teflon centrifuge bottles. Centrifuge for 15-20 minutes at ~2500 rpm.
- Decant the solution into a waste container and transfer the AgCl precipitate into a glass test tube.
- Rinse the sample with deionized water, centrifuge, and pour off the water.
- Add enough NH_4OH to dissolve the sample and centrifuge it. Decant the solution and add concentrated HNO_3 to it in order to precipitate AgCl.
- Dissolve the AgCl in NH_4OH again and add 1.0 mL of $Ba(NO_3)_2$ to precipitate $BaSO_4$. This step removes ^{36}S, an isobar of ^{36}Cl that interferes with AMS analysis. Let the solution react for ~24 hours in a dark place, then centrifuge for at least 20 minutes. Use a pipette to transfer the solution to another test tube.
- Precipitate AgCl by adding concentrated HNO_3 and let the solution stand for ~2 hours. Centrifuge the sample, pour off and discard the supernatant, and rinse the sample with deionized water. Centrifuge the sample again, and discard the rinse water.
- Repeat the sulfur-removal steps at least once.
- After removal of sulfur has been performed at least twice, rinse the sample three more times in deionized water, centrifuging and discarding the rinse water between each rinse.
- Use deionized water to transfer the AgCl to a watch glass and remove excess water with a pipette. Cover the watch glass with aluminum foil and dry the sample for ~24 hours in the oven at a temperature of ~60°C.

- The sample is then ready to be packed.
- Weigh the sample, then pack it in folded weighing paper. Wrap the folded weighing paper in parafilm, the use labeling tape to label the sample.
- The sample is ready to be sent for AMS analysis.

16 APPENDIX 5. Procedure for normalization of ^{36}Cl profiles

The ^{36}Cl profiles in this work were normalized to account for small variations in production rates within the profile. The following procedure details how this was performed.

- Subtract the inherited component from all samples in the profile. The inheritance has usually been determined during preliminary age estimations.
- In the output sheets for the profile, sum the thickness-averaged production rates for each sample. Then find the average sum for the profile and determine which sample total is closest to the average. This sample is the sample used for normalization and is referred to as the curve sample (CS). If the CS is known to be an outlier in the ^{36}Cl profile, select the next sample that is closest to the average production rate to be the CS.
- In CHLOE, import the CS. Look in the "Ptotal" column on the "Production vs. Z" page to find production rates at particular depths. Then write down the production rate for each sample depth in the profile.
- Next, find the actual production rates for each sample. First import a new sample sheet in CHLOE. For each sample, find the actual production rate at that sample depth. Repeat this step for all of the samples in the profile.

- Then find the normalization factor for each sample. Divide the CS value by the actual production rate value for each sample depth. Then multiply this normalization factor by the sample concentration (with the inheritance subtracted out). Also multiply the uncertainty by the normalization factor.
- Paste in the normalized sample ^{36}Cl concentrations and uncertainties into the appropriate columns in the "Sample Data" part of the worksheet.
- Now the normalized age can be estimated. Exposure time prior to sediment deposition is now zero.

17 APPENDIX 6. Table of chemical and soil data

Table A1. Chemical compositions of the samples used in this study.

	TB02-00-25	TB02-00-40	TB02-00-60	TB02-00-80	TB02-00-100	TB02-00-120	TB02-00-152	TB00-01-30-40	TB00-01-60-50
Na_2O [%]	4.35	4.52	4.44	4.37	4.37	4.42	4.5	4.53	4.59
MgO [%]	0.86	0.87	0.86	0.81	0.82	0.87	0.85	0.92	0.81
Al_2O_3 [%]	15.32	15.47	15.35	15.19	15.31	15.42	15.46	15.42	15.28
SiO_2 [%]	69.42	69.77	69.83	69.74	69.975	69.13	69.75	70.02	70.65
P_2O_5 [%]	0.05	0.05	0.04	0.05	0.04	0.05	0.05	0.05	0.04
K_2O [%]	3.24	3.32	3.32	3.38	3.45	3.31	3.38	3.54	3.75
CaO [%]	1.99	1.91	1.99	1.72	1.75	1.94	1.88	1.81	1.57
TiO_2 [%]	0.36	0.37	0.35	0.35	0.36	0.37	0.38	0.36	0.33
MnO_2 [%]	0.06	0.06	0.06	0.06	0.06	0.06	0.06	0.06	0.06
Fe_2O_3 [%]	3.03	3	2.91	2.77	2.79	2.99	3.01	2.94	2.72
Li [ppm]	4	3	3	4	3	3	3	4	3
Th [ppm]	12	11	11	9	10	11	10	13	6
B [ppm]	10		9	9	8	5	5	8	6
Cd [ppm]	2		2	2	3	2	2	3	3
Cl [ppm]	107.35	110.75	104.19		99.98		105.87	124.46	153.70

ND= Below the level of detection
Blank box= Not analyzed
Last 2-6 digits refer to sample depth or depth interval

	TB00-01-120-110	TB00-01-150-140	TB00-01-160-170	TB00-01-220-240	TB00-02-45-30	TB00-02-65-50	TB00-02-90-75	TB00-02-120-100	TB00-02-150-135
Na_2O [%]	5.266	4.43	4.54	4.46	4.09	4.05	4.18	4.19	4.074
MgO [%]	1.574	0.88	0.94	0.89	1.39	1.47	1.27	1.29	1.211
Al_2O_3 [%]	16.366	15.32	15.45	15.43	16.29	16.55	16.1	16.17	16.973
SiO_2 [%]	60.380	70.63	69.58	69.52	65.91	65.29	67.29	66.94	58.902
P_2O_5 [%]	0.097	0.04	0.04	0.04	0.06	0.07	0.06	0.08	0.423
K_2O [%]	6.711	3.62	3.51	3.36	3.03	3.1	3.12	3.18	5.626
CaO [%]	2.720	1.75	1.89	1.96	3.36	3.58	3.1	3.36	5.608
TiO_2 [%]	0.748	0.35	0.36	0.36	0.54	0.61	0.54	0.52	1.033
MnO_2 [%]	0.127	0.06	0.06	0.06	0.08	0.08	0.08	0.07	0.120
Fe_2O_3 [%]	6.010	2.79	3	3	4.44	4.64	4.07	3.98	6.009
Li [ppm]		4	3	4	3	4	3	2	
Th [ppm]		12	6	13	11	12	6	12	
B [ppm]	6	8	6	9	11	13	12	11	9
Cd [ppm]	2	2	3	2	3	5	3	2	3
Cl [ppm]	121.67	114.01	131.29	113.89	87.23	90.70	109.67	112.26	91.71

	TB00-01-85-75	TB00-02-240	TB00-03-40-30	TB00-03-60-70	TB03-105-95	TB00-03-115-105	TB00-03-130-120	TB00-03-205-190	TB00-03-260-240
Na_2O [%]	6.001	4.2	5.487	4.49	3.424	4.3	5.281	4.46	5.288
MgO [%]	1.403	1.16	1.663	1.04	0.956	0.99	1.839	0.97	1.661
Al_2O_3 [%]	17.456	16.14	17.642	15.63	15.523	15.58	17.312	15.59	15.997
SiO_2 [%]	58.923	66.36	54.470	69.18	67.728	69.31	56.683	68.96	60.472
P_2O_5 [%]	0.031	0.05	0.135	0.06	0.046	0.05	0.177	0.05	0.125
K_2O [%]	6.894	3.12	6.014	3.11	4.972	3.28	6.240	3.27	6.451
CaO [%]	2.433	3.1	4.817	2.22	2.791	2.17	4.495	2.14	2.997
TiO_2 [%]	0.680	0.5	1.443	0.4	0.689	0.41	0.780	0.4	0.502
MnO_2 [%]	0.085	0.07	0.188	0.06	0.069	0.06	0.166	0.6	0.122
Fe_2O_3 [%]	5.942	3.86	7.533	3.24	3.789	3.18	7.017	3.12	6.344
U [ppm]				3		3		3	
Th [ppm]		13		4		12		4	
B [ppm]	10	11	7	8	53	7	10	8	10
Gd [ppm]	3	3	3	4	1	3	3	3	3
Cl [ppm]	126.24	92.58	109.24	114.46	114.73		133.42	115.03	115.07

ND= Below the level of detection
Blank box= Not analyzed
Last 2-6 digits refer to sample depth or depth interval

	TB00-02-180-165	TB00-04-40-50	TB00-04-80-70	TB00-04-110-90	TB00-04-140-150	TB00-04-175-165	TB00-04-200-190	TB00-04-240-260	P1-40
Na_2O [%]	4.4	4.43	4.06	3.262	4.31	4.2	4.17	4.44	0.32
MgO [%]	1.15	1.07	1.13	1.461	1.23	1.31	1.26	1.08	0.32
Al_2O_3 [%]	16.18	15.79	15.67	17.716	15.89	16.08	15.95	15.69	2.47
SiO_2 [%]	67.35	68.63	68.52	60.161	67.59	66.77	67.66	68.81	93.42
P_2O_5 [%]	0.05	0.07	0.09	0.136	0.08	0.07	0.09	0.07	0.03
K_2O [%]	3.17	3.36	3.45	6.329	3.26	3.21	3.29	3.34	0.59
CaO [%]	3.14	2.3	2.42	3.061	2.56	2.92	2.64	2.13	0.16
TiO_2 [%]	0.49	0.47	0.49	1.071	0.5	0.55	0.51	0.46	0.12
MnO_2 [%]	0.07	0.07	0.07	0.134	0.07	0.07	0.07	0.07	ND
Fe_2O_3 [%]	3.76	3.65	3.64	6.655	3.91	4.2	3.95	3.59	1.51
U [ppm]	2.5	3.5	4		3	3	4	3	3
Th [ppm]	4	6	14		6	5	13	6	ND
B [ppm]	9	12	14	10	12	11	10	10	22
Gd [ppm]	3	4	3	3	3	3	3	2	1
Cl [ppm]	86.03	136.40	131.35		116.68	136.45	110.49	117.19	60.43

	TB00-04-15-10	P1-80-70	P1-110	P1-150	P1-240	N2-35	N2-50	N2-75	N2-95	N2-130	N2-160	N2-205	P2-40	P2-65	P2-85	P2-115	P2-140	P1-65
Na_2O [%]	5.499	0.38	0.35	0.27	0.5	0.53	0.77	0.76	0.72	0.61	0.6	0.64	0.61	0.85	0.61	0.52	0.69	0.31
MgO [%]	1.677	0.33	0.37	0.22	0.27	2.7	3.58	3	2.54	2.86	2.49	2.64	0.43	0.82	0.52	0.44	0.62	0.3
Al_2O_3 [%]	16.709	2.93	2.91	2.62	3.04	9.3	11.27	9.82	8.94	9.84	9.26	9.79	3.41	5.5	3.71	3.09	4.29	2.79
SiO_2 [%]	58.704	92.62	91.69	93.65	92.55	76.16	71.59	75.69	77.6	74.57	77.36	74.7	90.26	83.85	88.95	90.35	87.2	93.04
P_2O_5 [%]	0.133	0.03	0.04	0.03	0.03	0.06	0.049	0.042	0.05	0.063	0.048	0.05	0.05	0.06	0.046	0.054	0.047	0.03
K_2O [%]	6.784	0.7	0.7	0.83	0.84	2.06	2.38	2.1	1.93	1.95	1.9	2.09	0.91	1.41	0.96	0.78	1.09	0.63
CaO [%]	3.673	0.25	0.35	0.08	0.15	1.81	1.61	1.16	1.12	1.86	1.28	1.21	0.84	1.15	0.93	0.95	1.01	0.09
TiO_2 [%]	0.714	0.14	0.13	0.11	0.11	0.46	0.58	0.54	0.51	0.49	0.48	0.53	0.18	0.34	0.23	0.19	0.27	0.14
MnO_2 [%]	0.118	ND	ND	0.01	0.01	0.03	0.039	0.03	0.03	0.032	0.025	0.03	0.01	0.03	0.019	0.014	0.021	ND
Fe_2O_3 [%]	5.962	1.43	1.51	1.07	1.05	3.67	4.79	3.92	3.39	3.68	3.65	4.72	1.7	3.65	2.03	1.69	2.46	1.39
U [ppm]		2	1	3	3	4			4			4	3	4				3
Th [ppm]		ND	2	ND	ND	5			5			5	ND	ND				ND
B [ppm]	10	21	20	19	21	55			50			47	31	36				21
Gd [ppm]	4	1	1	1	1	1			3			1	1	1				1
Cl [ppm]	105.47		66.06	91.61	97.59	42.40	47.00	49.02	47.03	45.75	38.19	48.69	56.75	72.80	93.53		77.52	55.97

ND= Below the level of detection
Blank box= Not analyzed
Last 2-6 digits refer to sample depth or depth interval

	P2-190	P2-230	P2-280	N1-50-60	N1-85-75	N1-100-90	N1-115	N1-140	N1-170	P3-45-35	P3-75-65	P3-105-95	P3-120	P3-150	P3-190	CM01-1-15-25	CM01-1-25-35	CM01-1-45-55
Na_2O [%]	0.59	1.09	0.6	0.59	0.55	0.55	0.4	0.47	0.48	0.6	0.73	0.57	0.65	0.65	1.36	0.69	0.64	0.81
MgO [%]	0.37	0.87	0.56	1.11	2.19	1.58	1.7	1.79	2.07	0.57	0.41	0.39	0.48	0.42	1.07	0.73	0.93	0.97
Al_2O_3 [%]	3.21	6.69	4.03	7.55	8.67	6.76	7.37	7.66	8.13	3.56	3.49	2.87	3.38	3.12	7.87	6.31	6.09	7.33
SiO_2 [%]	91.03	83.02	88.32	81.5	75.62	82.88	80.58	81.86	80.2	88.24	89.67	89.55	89.81	90.43	78.43	85.05	84.95	82.35
P_2O_5 [%]	0.04	0.06	0.04	0.04	0.05	0.05	0.05	0.04	0.04	0.057	0.047	0.069	0.047	0.046	0.09	0.05	0.07	0.08
K_2O [%]	0.89	1.85	1.02	1.6	1.65	1.42	1.52	1.45	1.68	0.91	0.96	0.73	0.88	0.81	1.97	1.47	1.42	1.63
CaO [%]	0.58	1.25	0.68	0.41	0.94	0.66	1.28	0.72	0.69	1.21	0.88	1.41	0.86	0.85	1.97	0.16	0.17	0.24
TiO_2 [%]	0.16	0.38	0.24	0.41	0.41	0.39	0.38	0.4	0.41	0.23	0.2	0.17	0.22	0.2	0.45	0.61	0.59	0.69
MnO_2 [%]	0.01	0.03	0.02	0.01	0.02	0.02	0.02	0.02	0.02	0.021	0.017	0.015	0.019	0.018	0.04	0.02	0.01	0.02
Fe_2O_3 [%]	1.52	3.39	2.86	3.62	6.07	3.03	3.36	3.15	3.5	2.17	1.91	1.78	1.8	1.95	4.34	3.1	2.94	3.67
U [ppm]	3	4	4	2	5	3	5	4	4							2	2	2
Th [ppm]	1	2	ND	6	6	3	4	3	3							4	4	4
B [ppm]	30	24	29		52	46	45	47	53						34		37	41
Gd [ppm]	1	2	1		3	1	1	1	2						2		2	2
Cl [ppm]	106.35		104.42	24.67	33.33	24.08	28.17	29.22	39.37	97.58	89.94	87.78	105.06	94.10	85.38	29.10		45.14

	CM01-1-65-75	CM01-1-90-100	CM01-1-150-160	CM01-1-200-210	CM01-1-265-275	CM01-2-15-25	CM01-2-45-55	CM01-2-70-80	CM01-2-140-150	CM01-2-245-255	CM01-3-15-20	CM01-3-45-55
Na_2O [%]	0.94	0.93	0.66	1.58	0.95	0.18	0.12	0.17	0.14	0.14	1.27	1.05
MgO [%]	1.34	1.12	0.72	1.02	1.07	0.4	0.44	0.46	0.41	0.58	0.99	0.86
Al_2O_3 [%]	8.12	8.41	6.01	7.16	7.08	3.05	3.31	3.27	3.22	4.13	7.32	6.71
SiO_2 [%]	79.1	79.75	84.73	81.75	82.04	92.46	92.38	91.68	92.02	89.86	82.03	84.08
P_2O_5 [%]	0.16	0.08	0.06	0.12	0.09	0.04	0.04	0.04	0.04	0.05	0.07	0.07
K_2O [%]	1.78	1.8	1.38	1.39	1.4	0.84	0.93	0.9	0.89	1.18	1.49	1.48
CaO [%]	0.75	0.24	0.14	0.25	0.22	0.02	0.02	0.03	0.03	0.03	1.49	1.21
TiO_2 [%]	0.77	0.92	0.68	1.03	0.9	0.14	0.16	0.15	0.15	0.17	0.44	0.42
MnO [%]	0.04	0.02	0.02	0.02	0.02	ND	ND	ND	ND	0.01	0.03	0.04
Fe_2O_3 [%]	4.07	4.39	3.39	3.98	3.82	1.5	1.44	1.34	1.39	1.91	2.7	2.65
U [ppm]	3	2	2	2	2	1	2	1	2	2	2	2
Th [ppm]	5	5	4	3	4	1	3	1	ND	2	2	4
B [ppm]	58	52	39		39	26	23	22	24	30	28	32
Gd [ppm]	5	2	2		2	1	2	2	1	2	1	2
Cl [ppm]		41.58	24.05		28.31	8.99	7.49	7.74	10.59	7.10	58.63	74.90

ND= Below the level of detection
Blank box= Not analyzed
Last 2-6 digits refer to sample depth or depth interval

	CM01-3-65-75	CM01-3-100-110	CM01-3-195-205
Na_2O [%]	1.01	1.19	1.02
MgO [%]	0.81	0.96	0.67
Al_2O_3 [%]	6.86	7.23	6.67
SiO_2 [%]	84.28	82.03	84.97
P_2O_5 [%]	0.06	0.08	0.05
K_2O [%]	1.56	1.63	1.57
CaO [%]	1.11	1.31	1.04
TiO_2 [%]	0.39	0.4	0.33
MnO [%]	0.02	0.03	0.02
Fe_2O_3 [%]	2.44	2.86	2.06
U [ppm]	2	2	1
Th [ppm]	4	4	4
B [ppm]	32	36	30
Gd [ppm]	1	3	2
Cl [ppm]	53.67	66.96	34.19

Table A2. Accelerator mass spectrometry results and cosmogenic ^{36}Cl concentrations.

	TB02-00-25	TB02-00-40	TB02-00-60	TB02-00-100	TB02-00-152	TB00-01-30-40	TB00-01-60-50	TB00-01-85-75
Measured atoms $^{35}Cl/10^{15}$ atoms ^{37}Cl	5.39	5.34	5.7	5.55	5.42	5.312 +/- 0.043	5.25 +/- 0.16	5.298 +/- 0.037
Measured atoms $^{36}Cl/10^{15}$ atoms Cl	1036 +/- 18.07	1057 +/- 18.53	1008 +/- 40.72	988 +/- 23.27	966.9 +/- 31.26	1042 +/- 40	980 +/- 100	844 +/- 42
Cosmogenic ^{36}Cl (atoms $^{36}Cl/g$)	2893566	3032450	2878969	2647056	2683596	3325667	3854722	2727213

	TB00-01-120-110	TB00-01-150-140	TB00-01-160-170	TB00-01-220-240	TB00-02-45-30	TB00-02-65-50	TB00-02-90-75	TB00-02-120-100
Measured atoms $^{35}Cl/10^{15}$ atoms ^{37}Cl	5.429 +/- 0.045	5.97 +/- 0.20	4.920 +/- 0.057	5.517 +/- 0.06	6.78 +/- 0.15	5.80 +/- 0.32	5.36 +/- 0.55	5.97 +/- 0.10
Measured atoms $^{36}Cl/10^{15}$ atoms Cl	664 +/- 35	683 +/- 22	663 +/- 16	595 +/- 27	1830 +/- 42	1410 +/- 70	1216 +/-40	754 +/- 54
Cosmogenic ^{36}Cl (atoms $^{36}Cl/g$)	2086831	2194141	2100112	1767563	5147031	3575358	3488891	2410714

	TB00-02-150-135	TB00-02-180-165	TB00-02-240	TB00-03-40-30	TB00-03-60-70	TB03-105-95	TB00-03-130-120	TB00-03-205-190
Measured atoms $^{35}Cl/10^{15}$ atoms ^{37}Cl	5.612 +/- 0.021	5.77 +/- 0.24	6.03 +/- 0.06	5.388 +/- 0.027	5.49 +/- 0.08	5.50 +/-0.08	5.17 +/- 0.11	5.61 +/-0.07
Measured atoms $^{36}Cl/10^{15}$ atoms Cl	620 +/- 25	554 +/- 20	418 +/- 12	2130 +/- 110	1625 +/- 57	1312 +/-53	948 +/- 44	742 +/- 23
Cosmogenic ^{36}Cl (atoms $^{36}Cl/g$)	1544366	1320373	1107700	5978967	4982330	4037757	3188398	2315454

	TB00-03-260-240	TB00-04-15-10	TB00-04-40-50	TB00-04-80-70	TB00-04-140-150	TB00-04-175-165	TB00-04-200-190	TB00-04-240-260
Measured atoms $^{35}Cl/10^{15}$ atoms ^{37}Cl	5.15 +/-0.07	5.809 +/- 0.014	5.512 +/- 0.048	5.57 +/-.010	5.117 +/- 0.039	5.104 +/- 0.59	5.57 +/- 0.17	4.284 +/- 0.056
Measured atoms $^{36}Cl/10^{15}$ atoms Cl	526 +/-19	984 +/- 51	678 +/- 18	559 +/- 21	352 +/- 26	374 +/- 38	328 +/- 12	322 +/- 9
Cosmogenic ^{36}Cl (atoms $^{36}Cl/g$)	1500125	2848075	2456958	1935601	1005054	1252526	930844	787076

	P1-40	P1-65	P1-110	P1-150	P1-240	N2-35	N2-50	N2-75
Measured atoms $^{35}Cl/10^{15}$ atoms ^{37}Cl	5.95	6.18	6.11	5.01 +/- 0.040	4.36 +/-0.06	7.23 +/-0.21	8.83 +/- 0.08	7.24 +/- 0.08
Measured atoms $^{36}Cl/10^{15}$ atoms Cl	1585 +/- 37.30	1554 +/- 32.66	1230 +/-29.25	1060 +/- 40	800 +/-30	1290 +/- 50	925 +/- 47	814 +/- 32
Cosmogenic ^{36}Cl (atoms $^{36}Cl/g$)	2762890	2594100	2401906	2405582	1725313	1876413	1762023	1345856

	N2-95	N2-130	N2-160	N2-205	P2-40	P2-65	P2-85	P2-140
Measured atoms $^{35}Cl/10^{15}$ atoms ^{37}Cl	7.47 +/- 0.2	7.572 +/- 0.044	8.35 +/- 0.12	5.21 +/- 0.05	6.16	5.97	5.735 +/- 0.05	5.64 +/- 0.06
Measured atoms $^{36}Cl/10^{15}$ atoms Cl	980 +/- 50	720 +/- 60	765 +/- 34	1320 +/- 70	2364 +/- 55.56	2488 +/- 53.31	1730 +/- 80	1348 +/- 56
Cosmogenic ^{36}Cl (atoms $^{36}Cl/g$)	1630691	1170625	1123913	1646469	3992188	5242789	4426672	2826760

	P2-190	P2-280	N1-50-60	N1-85-75	N1-100-90	N1-115	N1-140	N1-170	P3-45-35
easured atoms $^{35}Cl/10^{15}$ atoms ^{37}Cl	4.75 +/- 0.08	3.91 +/- 0.05	18.68	11 +/- 0.4	8.6 +/- 0.5	9.2 +/- 0.3	16.5 +/- 1	9.17 +/- 0.26	6.43 +/- 0.09
Measured atoms $^{36}Cl/10^{15}$ atoms Cl	1340 +/- 50	1430 +/- 60	1339 +/- 28.56	1360 +/- 50	1720 +/- 70	1640 +/- 50	680 +/- 30	990 +/- 50	1820 +/- 70
Cosmogenic ^{36}Cl (atoms $^{36}Cl/g$)	3387519	2999720	2827574	2279858	1675610	1965370	1485716	1658267	5390520
	P3-75-65	P3-105-95	P3-120	P3-150	P3-190	CM01-1-15-25	CM01-1-45-55	CM01-1-90-100	CM01-1-150-160
easured atoms $^{35}Cl/10^{15}$ atoms ^{37}Cl	6.68 +/- 0.10	6.82 +/- 0.047	5.45 +/- 0.14	5.73 +/- 0.07	4.76	8.36	6.12	6.39	5.82
Measured atoms $^{36}Cl/10^{15}$ atoms Cl	1289 +/- 53	1044 +/- 41	1035 +/- 40	966 +/- 45	1718 +/-30.54	582.4 +/- 21.48	627.5 +/- 20.03	681.3 +/- 16.00	1022 +/- 24.08
Cosmogenic ^{36}Cl (atoms $^{36}Cl/g$)	3636490	2927804	2851072	2491458	3502556	661993	834629	867675	694633
	CM01-1-265-275	CM2-15-25	CM2-45-55	CM2-70-80	CM2-140-150	CM2-245-255	CM3-15-20	CM3-45-55	CM3-65-75
easured atoms $^{35}Cl/10^{15}$ atoms ^{37}Cl	3.96	21.42	22.42	21.5	18.63	7.68	6.52	5.81	6.88
Measured atoms $^{36}Cl/10^{15}$ atoms Cl	1246 +/-29.29	361.1 +/- 13.6	332.9 +/- 9.24	268.0 +/- 6.88	110.9 +/- 12.8	400.0 +/- 11.0	819.7 +/- 23.5	588.1 +/- 27.9	541.5 +/- 20.4
Cosmogenic ^{36}Cl (atoms $^{36}Cl/g$)	719496	319557	256828	204950	99270	102429	1503838	1237400	948135
	CM3-100-110	CM3-195-205	CM3-100-110	CM3-195-205					
easured atoms $^{35}Cl/10^{15}$ atoms ^{37}Cl	6.16	5.51	6.16	5.51					
Measured atoms $^{36}Cl/10^{15}$ atoms Cl	438.1 +/- 15.1	499.6 +/- 18.3	438.1 +/- 15.1	499.6 +/- 18.3					
Cosmogenic ^{36}Cl (atoms $^{36}Cl/g$)	865540	458812	865540	458812					

Table A3. Soil horizons and laboratory data.												
Trench ID		Thickness	Bulk Density		Profile	% Soluble		Lab				Lab
	Depth (cm)	(cm)	(g/cm2)	%CaCO3	Mass	Salt	% Gypsum	Gravel %	% Sand	% Silt	% Clay	Texture
TB00-01												
Av	0-7	7	1.29	5.72	0.52	0.051	0.002	19	74.52	19.04	6.44	SL-
Bw	7-20	13	1.56	5.35	1.08	0.060	0.002	64	56.74	31.34	11.92	SL
2Bwk1	20-32	12	2.20	6.14	1.62	0.079	0.002	73	80.68	13.44	5.88	LS
2Bwk2	32-51	19	2.20	6.75	2.82	0.213	0.002	72	81.85	14.23	3.92	LS
2Bk1	51-78	27	1.74	8.85	4.17	1.311	0.008	78	81.27	13.89	4.84	LS
2Bk2	78-114	36	2.05	4.24	3.12	0.917	0.009	87	51.31	39.75	8.94	L-
2C	114-200	86	2.01	9.28	16.05	0.315	0.003	81	47.20	45.30	7.50	SL
TB00-02												
Av	0-11	11	1.60	2.74	0.48	0.057	0.002	15	70.99	20.85	8.16	SL
Btk	11-30	19	1.43	3.16	0.86	0.083	0.002	34	79.64	14.38	5.98	LS
2Bk	30-85	55	1.69	6.73	6.26	0.304	0.002	47	58.75	37.00	4.25	SL-
2/3Bk	85-125	40	1.89	3.87	2.93	0.400	0.003	57	24.38	66.83	8.79	SiL
3Btjk	125-156	31	2.07	3.70	2.38	0.341	0.002	71	27.86	58.66	13.48	SiL
3Btj	156-200	44	2.25	4.37	4.33	0.674	0.007	76	72.28	19.13	8.59	SL
TB00-03												
Av	0-8	8	1.59	2.95	0.38	0.145	0.003	12	83.03	13.08	3.89	LS
Av/Bw	8-19	11	1.42	3.59	0.56	0.108	0.002	9	51.30	31.94	16.76	L-
Btk	19-30	11	1.43	4.38	0.69	0.400	0.003	45	61.63	28.87	9.50	SL
2Btky	30-48	18		4.39	0.00	0.547	0.004	65	64.62	29.42	5.96	SL
2Bkm	48-60	12	1.63	5.89	1.15	0.457	0.003	79	43.59	35.09	21.32	L
3Bk	60-162	102	1.79	6.07	11.09	0.411	0.003	81	45.56	46.68	7.76	SL+
4C	162-210	48	2.15	2.92	3.01	0.193	0.003	83	45.89	33.63	20.48	L
TB00-04												
Av	0-7	7	1.68	2.65	0.31	0.264	0.007	27	23.08	50.96	25.96	SiL+
Btk1	7-15	8	1.74	4.15	0.58	1.153	0.008	67	10.80	62.23	26.97	SiL
Btky2	15-31	16		3.00	0.00	1.831	0.217	72	7.02	76.56	16.42	SiL
Btky3	31-49	18		8.77	0.00	0.685	0.008	62	44.77	46.64	8.59	L-
2Bk	49-67	18		4.42	0.00	1.363	0.004	1	48.65	45.95	5.41	SL
3Btk	67-108	41	1.53	4.20	2.63	0.951	0.003	76	5.83	80.01	14.16	SiL
4Bk	108-151	43	1.70	5.29	3.87	0.764	0.002	23	56.91	38.15	4.94	SL
5Bk	151-230	79	2.19	3.12	5.38	0.669	0.002	93	76.65	19.20	4.16	LS+

Table A3 (continued)												
Trench ID		Thickness	Bulk Density		Profile	% Soluble		Lab				Lab
	Depth (cm)	(cm)	(g/cm2)	%CaCO3	Mass	Salt	% Gypsum	Gravel %	% Sand	% Silt	% Clay	Texture
P1												
Av	0-15	15	1.54	3	0.60			5	72	16	12	SL
Btk	15-48	33	1.42	1	0.66			14	67	12	21	SCL
2Bkm	48-94	46	1.91	30	26.14			86	72	16	11	SL
2Btkq	94-117	23	*1.86*	27	11.41			78	46	29	25	L
2Ckq	117-230+	113	1.86	12	24.44			93	63	19	18	SL
N2												
Av	0-8	8	1.92	6	0.89			16	25	52	22	SiL
Bwk1	8-25	17	1.64	13	3.50			22	36	47	18	L
Bwk2	25-33	8	1.51	25	2.97			57	58	28	14	SL
2Bk	33-50	17	2.08	51	18.01			70	87	7	6	S
2Ckq	50-150+	100	1.46	46	67.32			87	89	7	4	S
P2												
Av	0-12	12	1.49	15	2.64			17	55	31	14	SL
Btk	12-29	17	1.55	19	4.87			18	55	27	18	SL
Bk	29-59	30	1.71	25	12.74			21	72	17	11	SL
2Bkm	59-88	29	1.85	29	15.59			47	87	6	7	S
2Cox	88-192	37	1.51	25	14.09			75	90	2	7	S
(subsplit)	(125-192)	67	1.45	20	19.72			33	93	2	6	S
3Ck	192-238	46	1.37	40	25.13			12	42	29	29	CL
4Ck(b?)	238-263+	25	1.45	24	8.54			78	72	18	10	SL
N1												
Av	0-9	9	1.54	5	0.66			12	16	60	24	SiL
Bwk1	9-19	10	1.97	6	1.26			14	28	52	19	SiL
Bwk2	19-26	7	1.71	9	1.02			15	17	60	23	SiL
Bwk3	26-43	17	1.63	39	10.93			21	18	59	23	SiL
2Bkmq	43-92	49	1.91	43	39.84			83	44	37	19	L
2Ckq	92-155	63		44	0.00			88	70	19	11	SL
(subsplit)	95-130				0.00							
(subsplit)	130-155				0.00							
3Ck	155-158	3	1.85	61	3.39			81	79	11	11	SL
4Ck	158-162	4	1.24	52	2.56			9	54	32	14	SL
5Ck	162-163	1	1.24	46	0.57			19	0	66	34	SiCL
6Ckq	163-190+	27	1.45		0.00							

Table A3 (continued)												
Trench ID		Thickness	Bulk Density		Profile	% Soluble		Lab				Lab
	Depth (cm)	(cm)	(g/cm2)	%CaCO3	Mass	Salt	% Gypsum	Gravel %	% Sand	% Silt	% Clay	Texture
P3												
Av	0-13	13	1.44	14	2.60			34	37	49	14	L
Btk1	13-30	17	1.34	19	4.27			25	42	41	17	L
Btk2	30-51	21	1.48	27	8.36			34	42	44	15	L
2Bkm	51-67	16	1.77	39	10.99			63	41	32	27	CL,L
2Bky	67-95	28	1.51	30	12.86			70	74	11	15	SL
2Cky	95-156	61	1.45	31	27.11			77	68	18	14	SL
(subsplit)	100-120				0.00							
2C1	156-185	29	1.46	18	7.58			2	73	15	13	SL
(subsplit)	171-182				0.00							
2C2	185-230+	45	1.46	28	18.66			21	81	8	12	SL,LS
CM01-1												
Av	0-12	12	1.63	16.72	3.27	0.69	0.008	21	49.17	35.70	15.13	S
Bwkz	12-25	13	1.79	10.03	2.33	1.60	0.239	78	97.73	2.01	0.26	S
2Bk1	25-40	15	1.57	8.58	2.02	1.14	0.246	75	98.70	1.20	0.09	S
2Bk2	40-75	35		9.75	0.00	0.72	0.016	70	98.31	1.53	0.17	S
2Bk3	75-122	47		11.06	0.00	0.33	0.006	71	99.41	0.52	0.07	S
3C	122-150	28	1.36	7.03	2.68	0.41	0.004	36	99.05	0.67	0.29	S
4C	150-218	68		8.84	0.00	0.02	0.003	80	98.54	1.14	0.32	S
5Btkb	218-233	15	1.57	12.49	2.94	0.54	0.007	60	97.35	2.15	0.50	S
5Bwkb	233-280	47		17.48	0.00	0.41	0.008	90	95.60	3.85	0.54	S
CM01-2												
Av	0-9	9	1.60	6.14	0.88	4.27	0.042	15	58.04	32.80	9.15	LS
Btk1	9-16	7	1.39	4.00	0.39	1.57	0.017	45	61.26	29.44	9.30	LS
Btk2	16-43	27	1.74	3.36	1.58	1.37	0.009	55	63.84	32.08	4.08	S
Bwk	43-60	17	1.88	4.07	1.30	0.90	0.017	53	94.16	5.09	0.75	S
Bk1	60-89	29		2.03	0.00	0.55	0.010	71	98.58	0.78	0.64	S
Bk2	89-125	36	2.16	4.16	3.24	0.03	0.008	63	99.10	0.57	0.33	S
2C	125-220	95		1.66	0.00	0.05	0.002	76	99.58	0.25	0.18	S
CM01-3												
Av	0-10	10	1.37	6.08	0.83	1.30	0.042	24	63.10	27.48	9.42	SL
Bwkz	10-26	16		6.34	0.00	3.01	0.607	66	83.49	14.91	1.60	S
Bkz1	26-43	17		3.70	0.00	1.46	0.014	59	95.92	3.40	0.68	S
Bk2	43-85	42		2.45	0.00	1.59	0.015	55	95.57	3.16	1.27	S
Bk3	85-123	38		1.84	0.00	1.45	0.020	54	95.19	4.00	0.82	S
2Bk4	123-210	87		1.80	0.00	0.32	0.004	60	97.66	2.27	0.07	S
3C -R-	210-230	20	1.36		0.00							

18 REFERENCES CITED

Adams, K. D., and Wesnousky, S. G., 1999, The Lake Lahontan highstand: age, surficial characteristics, soil development, and regional shoreline correlation: Geomorphology, v. 30, p. 357-392.

Adams, K. D., Wesnousky, S. G., and Bills, B. G., 1999, Isostatic rebound, active faulting, and potential geomorphic effects in the Lake Lahontan basin, Nevada and California: GSA Bulletin, v. 111, no. 12, p. 1739-1756.

Anderson, K., Wells, S., and Graham, R., 2002, Pedogenesis of vesicular horizons, Cima Volcanic Field, Mojave Desert, California: Soil Science Society of America Journal, v. 66, p. 878-887.

Anderson, R. S., Repka, J. L., and Dick, G. S., 1996, Explicit treatment of inheritance in dating depositional surfaces using in situ ^{10}Be and ^{26}Al: Geology, v. 24, no. 1, p. 47-51.

Ayarbe, J. P., 2000, Coupling a Fault-Scarp Diffusion Model with Cosmogenic ^{36}Cl: Rupture Chronology of the Socorro Canyon Fault, New Mexico [M.S. thesis]: New Mexico Institute of Mining and Technology, 71 p.

Benson, L., and Thompson, R. S., 1987, The physical record of lakes in the Great Basin, *in* Ruddiman, W. F. W., H.E., Jr., ed., North America and adjacent oceans during the last deglaciation: The Geology of North America: Boulder, CO, Geological Society of America, p. 241-260.

Bentley, H. W., Phillips, F. M., and Davis, S. N., 1986, Chlorine-36 in the terrestrial environment, *in* Fritz, P., and Fontes, J.-C., eds., Handbook of Environmental Isotope Geochemistry, Vol. 2, The Terrestrial Environment: New York, Elsevier, p. 427-480.

Birkeland, P. W., 1999, Soils and Geomorphology: New York, Oxford University Press, Inc., 430 p.

Broecker, W. S., and Orr, P. C., 1958, Radiocarbon chronology of Lake Lahontan and Lake Bonneville: Bulletin of the Geological Society of America, v. 69, p. 1009-1032.

Broecker, W. S., and Kaufman, A., 1965, Radiocarbon chronology of Lake Lahontan and Lake Bonneville II, Great Basin: Geological Society of America Bulletin, v. 76, p. 537-566.

Cerling, T. E., and Craig, H., 1994, Geomorphology and in situ cosmogenic isotopes: Annual Review of Earth and Planetary Science, v. 22, p. 273-317.

Chadwick, O. A., and Davis, J. O., 1990, Soil-forming intervals caused by eolian sediment pulses in the Lahontan basin, northwestern Nevada: Geology, v. 18, p. 243-246.

Davis, J. O., 1978, Quaternary tephrochronology of the Lake Lahontan area, Nevada and California: Nevada Archeological Survey, Research Paper 7.

-, 1983, Level of Lake Lahontan during deposition of the Trego Hot Springs Tephra about 23,400 years ago: Quaternary Research, v. 19, p. 312-324.

Demsey, K., 1987, Holocene faulting and tectonic geomorphology along the Wassuk Range, west-central Nevada [M.S. thesis]: University of Arizona, 64 p.

Elmore, D., and Phillips, F. M., 1987, Accelerator mass spectrometry for measurement of long-lived radioisotopes: Science, v. 236, p. 543-550.

Gilbert, G. K., 1890, Lake Bonneville: U. S. Geological Survey Monograph 1.

Gosse, J. C., and Phillips, F. M., 2001, Terrestrial in situ cosmogenic nuclides: theory and application: Quaternary Science Reviews, v. 20, no. 14, p. 1475-1560.

Hancock, G. S., Anderson, R. S., Chadwick, O. A., and Finkel, R. C., 1999, Dating fluvial terraces with ^{10}Be and ^{26}Al profiles: application to the Wind River, Wyoming: Geomorphology, v. 27, p. 41-60.

Hubbs, C. L., and Miller, R. R., 1948, The Great Basin, with emphasis on glacial and postglacial times: The zoological evidence: Bulletin of the University of Utah, v. 38, no. 20, p. 17-166.

King, C., 1878, Systematic geology: U.S. geological exploration of the fortieth parallel from the Sierra Nevada to the eastern slope of the Rocky Mountains.

King, G. Q., 1978, The Late Quaternary History of Adrian Valley, Lyon County, Nevada [M.S. thesis]: University of Utah, 88 p.

-, 1993, Late Quaternary history of the lower Walker River and its implications for the Lahontan paleolake system: Physical Geography, v. 14, no. 1, p. 81-96.

Lal, D., 1991, Cosmic ray labeling of erosion surfaces: *in situ* nuclide production rates and erosion models: Earth and Planetary Science Letters, v. 104, p. 424-439.

McFadden, L. D., Wells, S. G., Jercinovich, M. J., 1987, Influences of eolian and pedogenic processes on the origin and evolution of desert pavements: Geology, v. 15, p. 504-508.

Mifflin, M. D., and Wheat, M. M., 1979, Pluvial Lakes and Estimated Pluvial Climates of Nevada, Nevada Bureau of Mines and Geology: Reno, NV, Mackay School of Mines, University of Nevada, Reno, Bulletin 94, p. 57.

Morrison, R. B., 1964, Lake Lahontan: Geology of the Southern Carson Desert, Nevada: U.S. Geological Survey, 401.

-, 1991, Quaternary stratigraphic, hydrologic, and climatic history of the Great Basin, with emphasis on Lakes Lahontan, Bonneville, and Tecopa, *in* Morrison, R. B., ed., Quaternary Nonglacial Geology: Conterminous U.S.: The Decade of North American Geology Project: Boulder, CO, The Geological Society of America, Inc., p. 283-320.

Morrison, R. B., and Frye, J. C., 1965, Correlation of the middle and late Quaternary successions of the Lake Lahontan, Lake Bonneville, Rocky Mountain (Wasatch Range), Southern Great Plains, and Eastern Midwest areas: Nevada Bureau of Mines, Report 9.

Oviatt, C. G., and Currey, D. R., 1987, Pre-Bonneville Quaternary Lakes in the Bonneville Basin, Utah, Cenozoic Geology of Western Utah- Sites for Precious Metal and Hydrocarbon Accumulation, Utah Geological Association, p. 257-263.

Oviatt, C. G., Thompson, R. S., Kaufman, D. S., Bright, J., and Forester, R. M., 1999, Reinterpretation of the Burmester Core, Bonneville Basin, Utah: Quaternary Research, v. 52, p. 180-184.

Phillips, F. M., Leavy, B. D., Jannik, N. O., Elmore, D., and Kubik, P. W., 1986, The accumulation of cosmogenic chlorine-36 in rocks: a method for surface exposure dating: Science, v. 231, p. 41-43.

Phillips, F. M., and Plummer, M. A., 1996, CHLOE: A program for interpreting *in-situ* cosmogenic nuclide data for surface exposure dating and erosion studies, (Abstr.) 7th International Conference - Accelerator Mass Spectrometry, p. 98-99.

Phillips, F. M., Stone, W. D., and Fabryka-Martin, J. T., 2001, An improved approach to calculating low-energy cosmic-ray neutron fluxes near the land/atmosphere interface: Chemical Geology, v. 175, p. 689-701.

Phillips, F. M., Zreda, M. G., Elmore, D., Sharma, P., 1996, A reevaluation of cosmogenic ^{36}Cl production rates in terrestrial rocks: Geophysical Research Letters, v. 23, n. 9, p. 949-952.

Phillips, F. M., Zreda, M., Smith, S. S., Elmore, D., Kubik, W., and Sharma, P., 1990, Cosmogenic chlorine-36 chronology for glacial deposits at Bloody Canyon, Eastern Sierra: Science, v. 248, p. 1529-1531.

Redwine, J., 2003, *in progress*, Investigation of the Quaternary Pluvial History and Paleoclimate Implications of Newark Valley, East-Central, Nevada; Including Geologic Mapping of Surficial Units and Geomorphic Features [M.S. thesis]: Humboldt State University.

Reheis, M., 1999, Highest pluvial-lake shorelines and Pleistocene climate of the western Great Basin: Quaternary Research, v. 52, p. 196-205.

Reheis, M., Adams, K., Stine, S., Redwine, J., and Negrini, R., *in press*, Pliocene to Holocene Lakes in the Western Great Basin, USA: New Perspectives on Paleoclimate, Landscape Dynamics, Tectonics, and Paleodistribution of Aquatic Species: INQUA Fieldtrip guidebook.

Reheis, M. C., and Morrison, R., 1997, High, Old Pluvial Lakes of Western Nevada: BYU Geology Studies, v. 42, no. Part I, p. 459-492.

Reheis, M. C., Sarna-Wojcicki, A. M., Reynolds, R. L., Repenning, C. A., and Mifflin, M. D., 2003, Pliocene to middle Pleistocene lakes in the western Great Basin: Ages and connections, *in* Hershler, R., Currey, D., and Madsen, D., eds., Great Basin Aquatic Systems History: Washington, D.C., Smithsonian Institution, p. 53-108.

Reheis, M. C., Slate, J. L., Sarna-Wojcicki, A. M., and Meyer, C. E., 1993, A late Pliocene to middle Pleistocene pluvial lake in Fish Lake Valley, Nevada and California: Geological Society of America Bulletin, v. 105, p. 953-967.

Repka, J. L., Anderson, R. S., and Finkel, R. C., 1997, Cosmogenic dating of fluvial terraces, Fremont River, Utah: Earth and Planetary Science Letters, v. 152, p. 59-73.

Russell, I. C., 1885, Geological History of Lake Lahontan, a Quaternary Lake of Northwestern Nevada: U.S. Geological Survey Monograph 11.

Shackleton, N. J., and Opdyke, N. D., 1976, Oxygen-isotope paleomagnetic stratigraphy of Pacific Core V28-239 late Pliocene to Latest Pleistocene: Geological Society of America, Memoir 145, p. 449-464.

Small, E. E., and Anderson, R. S., 1995, Geomorphically driven Late Cenozoic rock uplift in the Sierra Nevada, California: Science, v. 270, p. 277-280.

Stone, J. O., Evans, J., Fifield, K., Cresswell, R., Allan, G., 1996, Cosmogenic chlorine-36 production rates from calcium and potassium: Radiocarbon, v. 38, n. 1, p. 170-171.

Stuiver, M. and Reimer, 1993, CALIB Radiocarbon Calibration (version 4.1), http://depts.washington.edu/qil/calib/

Thompson, R. S., Benson, L., and Hattori, E. M., 1986, A revised chronology for the last Pleistocene lake cycle in the central Lahontan basin: Quaternary Research, v. 25, p. 1-9.

Thompson, R. S., Whitlock, C., Bartlein, P. J., Harrison, S. P., and Spaulding, W. G., 1993, Climatic changes in the western United States since 18,000 yr B.P., *in* Wright, H. E. J., Kutzbach, J. E., Webb, T., Ruddiman, W. F., Street-Perrott, F. A., and Bartlein, P. J., eds., Global Climates Since the Last Glacial Maximum: Minneapolis, University of Minnesota Press, p. 468-513.

Wells, S. G., McFadden, L. D., Poths, J., and Olinger, C. T., 1995, Cosmogenic ^{3}He surface-exposure dating of stone pavements: Implications for landscape evolution in deserts: Geology, v. 23, p. 613-616.

Winograd, I. J., Szabo, B. J., Coplen, T. B., Riggs, A. C., and Kolesar, P. T., 1985, Two-million-year record of deuterium depletion in Great Basin watersq: Science, v. 227, p. 519-522.

Zreda, M. G., 1994, Development and Calibration of Cosmogenic ^{36}Cl Surface Exposure Dating Method and Its Application to the Chronology of Late Quaternary Glaciations [PhD. thesis]: New Mexico Institute of Mining and Technology, 318 p.